COMBINED NATURAL KILLER T CELL IMMUNOTHERAPY WITH RECOMBINANT VESICULAR STOMATITIS ONCOLYTIC VIRUS IN OVARIAN CANCER

by

Rushit Madeka

Submitted in partial fulfilment of the requirements
for the degree of Master of Science

at

Dalhousie University
Halifax, Nova Scotia
May 2022

Dalhousie University is located in Mi'kma'ki, the
ancestral and unceded territory of the Mi'kmaq.
We are all Treaty people.

TABLE OF CONTENTS

LIST OF TABLES

LIST OF FIGURES

ABSTRACT

Despite good initial response rates to first-line therapies, high relapse rates and limited secondary treatment options make ovarian cancers the leading cause of gynecologic cancer-related deaths in women worldwide. Therefore, development of novel therapeutics with long-lasting outcomes are needed. Natural Killer T (NKT) cells are a rare population of lipid-reactive T-cells, and their infiltration is implicated to improve survival outcomes in several human cancers. Here, we sought to enhance therapeutic benefits of NKT cell activation in the ID8 model of ovarian cancer by incorporating it with recombinant vesicular stomatitis virus (VSV-ΔM51) constructs expressing p14 FAST protein or IL-15. A VSV-ΔM51 construct expressing IL-12 was also engineered to enhance local NKT cell activation. NKT cell therapy significantly prolonged survival and increased tumor immune infiltration whereas the combination therapy with VSV-GFP further enhanced survival. Mice that survived initial tumor challenge exhibited increased cytotoxicity, and proinflammatory IFNγ production and remained tumor-free following tumor re-challenge, demonstrating formation of immune memory. Technical challenges associated with VSV-p14 treatments, including a reduction in its oncolytic potency, prevented complete therapeutic evaluation. Treatments with VSV-IL-15 and VSV-IL-12 did not improve the therapeutic efficacy of standalone VSV-ΔM51, and instead resulted into increased episodes of hind-limb impediments. However, room remains to optimize therapeutic application of these agents; and this study outlines suggestions that might help mitigate this risk potential. Additional studies are therefore needed before concluding ineffectiveness of these recombinant viruses in the ID8 tumor model.

LIST OF ABBREVIATIONS

α-GalCer	α-galactosylceramide
ADP	adenosine diphosphate
ANOVA	analysis of variance
APC	antigen-presenting cell
ATP	adenosine triphosphate
BRCA 1/2	breast cancer gene 1 and 2
CRT	calreticulin
CTL	cytotoxic T lymphocyte
CTLA-4	cytotoxic T-lymphocyte-associated protein 4
CXCL	CXC chemokine ligand
CXCR	CXC chemokine receptor
DAMP	damage associated molecular patterns
DC	dendritic cells
DIP	defective interfering particles
DMEM	Dulbecco's modified eagle medium
DMSO	dimethyl sulfoxide
DNA	deoxyribonucleic acid
EDTA	ethylenediaminetetraacetic acid
ELISA	enzyme-linked immunosorbent assay
EOC	epithelial ovarian cancer
FasL	Fas ligand
FAST	fusion associated small transmembrane protein
FBS	fetal bovine serum
FOXO1	forkhead box protein O1
FOXP3	forkhead box protein P3

FTE	fallopian tube epithelium
GATA3	GATA binding protein 3
GFP	green fluorescent protein
GM-CSF	granulocyte-macrophage colony-stimulating factor
HEPES	4-(2-hydroxyethyl)-1-piperazineethanesulfonic acid
HGSC	high-grade serous carcinoma
HIF-1	hypoxia-inducible factor 1
HLA	human leukocyte antigen
HMGB1	high-mobility group box 1
HSV	herpes simplex virus
ICB	immune checkpoint blockade
ICD	immunogenic cell death
ICOS	inducible T cell costimulator
IDO	indoleamine-2,3-dioxygenase
IFN	interferon
IL	interleukin
IRES	internal ribosome entry site
KRAS	Kirsten rat sarcoma virus
LAG3	lymphocyte activation gene 3
LDL	low-density lipoprotein
LGSC	low-grade serous carcinoma
M-CSF	macrophage colony-stimulating factor
MDSC	myeloid-derived suppressor cell
MEM	minimum essential media
MHC	major histocompatibility complex
MICA	MHC class I polypeptide–related sequence A

MMP	matrix metalloproteinases
MOI	multiplicity of infection
MTT	(3-(4,5-dimethylthiazol-2-yl)-2,5-diphenyl tetrazolium bromide
MVA	modified vaccinia virus Ankara
NK	natural killer cell
NKG2D	natural killer group 2D receptor
NKT	natural killer T cell
NOS	nitic oxide synthase
Nup-98	nuclear pore complex protien-98
ORF	open reading frame
OSE	ovarian surface epithelium
OV	oncolytic virus
OX40	tumor necrosis factor receptor superfamily-4
PARPi	poly (ADP-ribose) polymerase inhibitor
PBS	phosphate buffered saline
PCR	polymerase chain reaction
PD-1	programmed cell death protein-1
PD-L1	programmed death ligand-1
PFU	plaque forming unit
PRR	pattern recognition receptor
RAE-1	ribonucleic acid export 1
RAS	rat sarcoma virus
RdRp	RNA-dependent RNA polymerase
RNA	ribonucleic acid
RNP	ribonucleoprotein
ROR-Y-T	retinoic acid-related orphan receptor γ T

STAT-4	signal transducer and activator of transcription-4
STIC	serous tubal intraepithelial carcinoma
T-VEC	talimogene laherparepvec
TAA	tumor-associated antigens
TAE	Tris-acetate-EDTA
TAM	tumor-associated macrophages
TAN	tumor-associated neutrophils
TCR	T cell receptor
TGF	tumor growth factor
TME	tumor microenvironment
TNF	tumor necrosis factor
TP53	tumor protein p53
TRAIL	TNF-related apoptosis inducing ligand
Treg	T regulatory cell
TSA	tumor-specific antigens
VCAM-1	vascular cell adhesion protein-1
VEGF	vascular endothelial growth factor
VSV	vesicular stomatitis virus

ACKNOWLEDGEMENTS

I would first like to thank my supervisor, Dr. Brent Johnston, for giving me the opportunity to be a part of such a wonderful lab, and for providing me with valuable mentorship throughout my graduate degree. I would also like to thank my committee members Dr. Andrew Makrigiannis and Dr. Shashi Gujar for all their guidance. I would like to extend my special thanks to Nichole McMullen for providing extensive guidance and technical assistance with the VSV-IL-12 project. In addition, I would also like to thank Alexander Edgar for sharing reagents and expertise concerning VSV-IL-12 project. I am thankful to Derek Rowter and Tatjana Brauer-Chapin for their assistance with flow cytometry and also to Carleton Animal Care Facility for all the help with animal studies.

I would also like to thank current and past members of the Johnston lab, Dr. Adam Nelson, Dr. Dihia Meghnem, Jordan Lukacs, Rhea Nickerson, Terry LeVatte, Natasha Osborne, Laura Korycinska, and Emily Pritchard for their assistance with experiments, and for all the good conversations that leave me with a memorable lab experience. Thanks to all the past and current members of Marshall lab, Boudreau lab, Bezhuly lab and Micro Dept. for all the support.

My final thanks go to my father, and my wife Manya, for their unwavering support and patience during my degree. Thanks to all the members of my extended family and friends for your support.

CHAPTER 1: INTRODUCTION

1.1 Ovarian cancer

Ovarian cancer is the most lethal gynecological malignancy and the 5th leading cause of cancer-associated mortality in women worldwide [1]. Each year, an estimated 300,000 women are diagnosed with ovarian cancer, and incidence is projected to increase 47% by 2040, especially in developed countries [1,2]. Ovarian cancer largely manifests as an asymptomatic disease and is usually diagnosed at advanced stages, when the disease has already metastasized outside the pelvis and disseminated into the peritoneum – leading to build up of ascites fluid in the abdomen [3]. Despite good initial response rates to first-line therapies, the 5-year survival rate (35-45%) has remained stable between the periods 1995-99 and 2010-14 [1,4]. In addition, high relapse rates and limited secondary treatment options necessitate the development of novel therapeutics with long-lasting outcomes [1,5]. In recent years, significant attempts have been made to stimulate enhanced immune responses against cancer by incorporating immunotherapies (targeted antibodies, adoptive cell transfers, vaccines, etc.) into conventional cancer treatment regimens [6–9].

1.1.1 Pathogenesis and histopathological classification

Ovarian cancers were initially thought to originate from the ovaries, and that all tumor subtypes shared a common site of pathogenesis in the ovarian surface epithelium (OSE) [3,10–12]. The theory behind this idea asserts that repetitive ovulatory cycles inflict physical trauma on the exterior of the ovaries, requiring OSE cells to constantly undergo DNA damage repair processes - predisposing OSE cells to transform into malignant cells [11,13]. The theory, however, fails to explain the morphological and genetic differences observed between various histological subtypes [11].

It is now clear that ovarian tumors are heterogenous in nature with distinct histological subtypes differing in their pathogenesis, gene expression, disease progression and overall prognosis [14–17]. Ovarian tumors are primarily classified based on their cellular origin: epithelial ovarian carcinoma (EOC), ovarian germ cell tumour or sex cord-stromal tumour. EOC remains the most lethal form of malignancy and accounts for 95% of ovarian cancer [18]. Depending on the morphology and tissue architecture, EOC is further

subdivided into 5 well-defined histoypes: high-grade serous carcinoma (HGSC), low-grade serous carcinoma (LGSC), mucinous, endometroid and clear cell carcinoma; of these, HGSC tumors are the predominant type and have the lowest survival rates [19,20].

Classification of EOC subtypes based on histological differences alone was recently replaced by a two-pathway model that, in addition to the morphological differences, also integrates genetic and molecular alterations - making the latter more applicable under clinical settings [11]. The dualistic model broadly categorises EOC as Type I and Type II tumors [21]. Type I tumors comprise LGSC, endometroid (G1 and G2), mucinous and clear cell carcinoma, and usually get diagnosed as benign cystic tumors that largely remain confined in the ovaries. Genetic mutations in Kirsten murine sarcoma virus 2 (KRAS) and V-RAF murine sarcoma viral oncogene homolog B-1 (BRAF) are most often associated with Type I EOC tumors [21]. Type II ovarian tumors constitute HGSC, endometroid (G3) and carcinosarcoma. These tumors frequently harbor genetic mutations in tumor protein 53 (TP53) and breast cancer gene 1 and 2 (BRCA 1/2), and rapidly evolve into an aggressive malignancy [21,22]. Although, the two-pathway model integrates the site of tumorigenesis for type I tumors, it does not do the same for type II, especially HGSC, tumors.

1.1.2 Fallopian tube: origin of pathogenesis and dissemination

Cellular origin and pathogenesis of type II tumors is not well-described. Recent findings, however, have suggested an extra-ovarian origin of type II ovarian tumors; and that early cancerous lesions such as stromal tubal intraepithelial carcinomas (STIC), are most notably found in the fimbriae of the distal fallopian tube [10,23–29]. It has been postulated that fimbria's close proximity to the ovary, exposes it to similar genotoxic stressors such as inflammatory cytokines and reactive oxygen species that are known to induce malignancy in ovaries following ovulation [11,21].

Fallopian tube epithelium (FTE) is composed of two cell types: secretory and ciliated cells. In 2004, Piek et. al reported that FTE associated neoplastic cells exhibited a shift towards secretory phenotype with an increased proliferative capacity [29]. Upon tumor progression, these malignant cells exfoliate and implant onto ovaries or traverse through visceral fluid to the peritoneum cavity and rapidly grow into secondary tumor nodules

[26,30]. Although there are no anatomical barriers in the peritoneum that prevent HGSC spread, HGSC tumor cells reportedly exhibit particular predilection for the omentum [30,31]. In their study, Neiman et al show that adipocytes in the omentum secrete immunomodulators such as interleukin (IL)-8 that facilitate homing and migration of tumor cells [31]. In addition, adipocytes serve as an energy reservoir for these cancer cells by inducing fatty acid catabolism in tumor cells and lipolysis in adipocytes [31,32].

Although these findings improve our understanding of the disease heterogeneity and pathogenesis, recent studies also identify intratumor heterogeneity as a major cause of treatment failures and poor prognosis; and have advocated for the development of better treatment strategies optimized for the local tumor microenvironment, that are specific to each well-defined EOC histotype [15,33].

1.1.3 Current treatment strategies

Conventional treatment for ovarian cancer includes a combination of cytoreductive surgery followed by a platinum and taxane-based chemotherapy [34,35]. Maximal surgical resection of tumor has been associated as the strongest determinant in improving the overall survival in comparison to other available modalities [35]. Removal of pelvic and para-aortal lymph nodes is common during early stages (stage I and II); advanced stage disease additionally requires removal of relevant peritoneal organs [36]. Current standard of chemotherapy includes systemic administration of paclitaxel and carboplatin, and in recent years, addition of the angiogenesis inhibitor bevacizumab, a monoclonal antibody against vascular growth endothelial factor (VEGF), that has improved overall prognosis [35,37].

High initial response rates (60-80%) with complete clinical remission are prevalent, nevertheless, 75% of advanced EOC cases experience disease relapse within 3-years and present with chemoresistance [35]. Recent introduction of poly ADP ribose polymerase inhibitors (PARPi), a class of drugs that inhibit DNA repair in neoplastic cells, improves tumor-free survival and are used as maintenance therapies in front-line and recurrence settings [38–40]. However, only women that have BRCA1/2 mutations are candidates for this targeted therapy; and amongst these, only 60% respond to PARPi

therapy [39]. In addition, prolonged treatment with olaparib, a PARPi, has been associated with acquired drug-resistance and increased incidence for myelodysplastic syndrome [39,41].

A significant heterogeneity in resistance mechanisms is reported for both platinum- and PARPi-based treatments [39]. While the precise mechanisms remain multifactorial and elusive, recent studies have identified intratumor heterogeneity as a major cause of treatment failures and poor prognosis [14,15,17,39]. Despite an extensive heterogeneity observed in EOC, the standard line of care remains the same for most patients; and limited secondary options necessitates the development of targeted therapies that are optimized for the local tumor microenvironment, and that are specific to each well-defined EOC histotype.

1.2 Cancer and tumor microenvironment

The tumor microenvironment (TME) represents a dynamic crosstalk between cancer cells, local immune cells and the surrounding stroma [42]. The tumor stroma represents the non-immune components of the TME that enable tumor progression and evasion. These include extracellular matrix, fibroblasts and mesenchymal stromal cells that collectively establish an immunosuppressive axis. During cancer development, fibroblasts change their expression profiles to become cancer associated fibroblasts and secrete dense extracellular matrix and pro-tumorigenic growth factors in addition to immune inhibitory and anti-apoptotic proteins [43,44]. The immune context within the TME consists of innate and adaptive cells, and a myriad of soluble factors, including cytokines and chemokines [42]. Similar to many solid tumors, ovarian cancers are immunogenic and elicit varying levels of immune responses depending upon the tumor site and its clonal heterogeneity [42,45–47]. Failure to achieve a favorable immune homeostasis between activation and suppression components leads to evasion and tumor proliferation [15].

1.2.1 Cancer immunoediting

In 1909, Paul Ehrlich was the first to postulate the “immune surveillance” theory that predicted the immune system’s role in maintaining host defence against nascent tumor cells [48]. Subsequent studies were thus aimed towards designing experimental models that could test this hypothesis; and with the advent of immunodeficient mice

models and discovery of cytokines, interferon- γ (IFN-γ) and IL-2, the confidence in the theory received critical support [49]. Specifically, it was demonstrated that lymphocyte deficient mice exhibited a significantly higher incidence for developing tumors compared to wild type mice [50].

In 2002, Schreiber et. al. later elaborated on the immunosurveillance concept to develop a unifying framework that also accounts for immune mechanisms that aid cancer progression [49]. This dynamic interaction between cancer and immune cells is defined as cancer immunoediting, and depending on the stage of tumor progression, it is sub-divided into 3 phases: elimination, equilibrium and escape [51]. The *elimination* phase is a redefined version of the classical immune surveillance concept wherein both the innate and adaptive components of immune system actively mediate recognition and elimination of the nascent tumor cells. During the *equilibrium* phase, the immune system applies a selective evolutionary pressure on remaining tumor cells leading to acquisition of genomic changes that enable immunogenic sculpting and early development of an immunosuppressive network. Failure to achieve a favorable immune homeostasis eventually leads to tumor *escape* and proliferation [49].

1.2.2 Elimination

A robust DNA damage and repair system is central in maintaining genomic integrity for normal cell survival and reproduction [52,53]. Continuous exposure to exogenous, as well as endogenous, genotoxic stressors can overwhelm the DNA damage repair machinery - resulting in frequent error prone repairs that may or may not induce cell cycle arrest [54]. Severe DNA damage that is beyond the system's restorative capacity eventually leads to induction of processes that mediate programmed cell death or apoptosis [53]. Nascent cancer cells, however, are able to circumvent these cell-intrinsic mechanisms owing to defective DNA repair mechanisms coupled with acquired resistance to apoptosis; requiring external support from the immune system to prevent tumor initiation [54].

In the elimination phase, both the cellular (innate and adaptive cells) and soluble (antibodies, cytokines, chemokines and growth factors) components of the immune system mount an anti-tumor response [55]. Cells of the innate immune system act as first

responders against developing tumors, but are usually unable to provide long-lasting protective immunity [55]. In order to drive an effective tumor-antigen-specific adaptive immune response, strong signals of immunogenic cell death (ICD) are required to activate dendritic cells (DCs), who play a vital role in initiating adaptive immunity [55].

Cancer cells are characterized by their surface expression of stress-induced ligands such as MICA/B (human) and RAE-1 (mouse), that upon recognition by innate effectors cells such as, natural killer (NK) and natural killer-T (NKT) cells via germline encoded receptors (e.g. NKG2D), release perforin and granzyme to lyse cancer cells [56,57]. In addition, cancer cells also express calreticulin that serve as phagocytic signal for macrophages [58]. This results in release of damage associated molecular patters (DAMPs), tumor associated antigens (TAAs) and tumor specific antigens (TSAs) that are captured by DCs, leading to amplified production of cytokines and chemokines that recruit more immune cells [55]. Activated DCs migrate to secondary/tertiary lymphoid organs wherein naïve T-cells are primed and activated [55]. At this stage, the nature of immune response is determined since naïve T-cells could either mature into T-effector or T-regulatory lineage, the former being associated with strong anti-tumor immunity, while the latter are known for their immunosuppressive effects [55]. In the TME, $CD8^+$ T-effector cells recognize TSAs presented via major histocompatibility complex-I (MHC-I) on tumor cells through their T-cell receptors (TCRs) and exert cytotoxic activity by releasing perforin and granzyme [55,59]. Subsequent tumor lysis results in increased release of tumour antigens, and further amplifies ICD in a cyclic series of events as explained above [55].

1.2.3 Natural Killer Cells

NK cells are innate members of the lymphoid lineage and are involved in recognition and elimination of virus-infected and nascent tumor cells [60–62]. Human NK cells are broadly classified according to surface expression of CD56 and CD16 antigens: $CD56^{dim}CD16^+$ and $CD56^{bright}CD16^-$ NK cells sub populations, with the former expressing higher levels of cytolytic molecules, while the latter are associated with secretion of pro-inflammatory cytokines [62]. Mice NK cells are classified based on surface expression of CD27 as $CD27^{hi}$ and $CD27^{lo}$ and are functionally analogous to human $CD56^{bright}$ and $CD56^{dim}$ subsets respectively [63]. In humans and mice, NK cell activation

and effector functions are largely determined by net integration of signals from activating and inhibitory receptors, in addition to other factors including: prior sensitization, maturation and cytokine stimulation [45,64–68].

Cancer cells upregulate stress-ligands that mediate enhanced immune recognition and ICD [69]. Many cancer cells also downregulate MHC-I expression in order to evade from T-cell mediated immune responses [70–74]. Cytolytic NK cells exploit this evasive mechanism of MHC-I negative tumors, since they are equipped with germline encoded inhibitory receptors that are able to sense loss of MHC-I, allowing them to mount an anti-tumor response [71,72,75]. Activated NK cells exhibit lytic function via degranulation of granzyme and perforins, or alternatively, through binding of tumor necrosis factor-alpha-related apoptosis-inducing ligand (TRAIL) or Fas Ligand (FasL) to their cognate receptors on cancer cells. Several studies have attempted to harness NK-mediated tumor cytotoxicity [60,75]. Sun et. al. [76] show enhanced NK cytotoxicity *in-vitro* when co-cultured with cancer cells derived from ovarian cancer patients. Similarly, adaptive transfer of expanded NK cells from ovarian cancer patients generated significant cytotoxicity against autologous tumors in patient-derived xenograft mouse models [77].

In the context of ovarian cancers, NK cell infiltration into the TME is associated with improved survival[68,71,78]. Some studies have associated improved prognosis with increased co-infiltration of cytotoxic T-cells, suggesting that NK activation in TME may play a crucial role in sustaining long-lasting adaptive response [79,80]. Additionally, immunosuppressive cytokines and pro-angiogenic factors in ovarian tumors lead to dampened NK responses [81–87]. For instance, overexpression of macrophage inhibiting factor has been associated with poor clinical outcomes due to its ability to downregulate activating receptor NKG2D on NK cells [88]. Higher NK cell concentrations have been reported in ascitic fluids than peripheral blood, but reprogramming of stromal cells to overproduce TGF-beta consequently leads to NK cell suppression [81].

1.2.4 CD8+ T cells

1.2.4.1 Priming and activation

CD8+ T-lymphocytes play a central role in eliminating intracellular infections and malignant cells [89]. Principally, TCRs on CD8+ T cells recognize peptide epitopes

(antigens) bound to MHC-I molecules on target cells and mediate their effector functions either by killing cancer cells directly with lytic granules or by producing pro-inflammatory cytokines (TNF, IFN-γ) that enhance immune surveillance. Priming and activation of naïve CD8+ T cells is primarily regulated by activated DCs, and it occurs in three successive stages [90]. In phase I, activated DCs cross-present tumour associated ligands through MHC-I to TCRs on naïve $CD44^{low}$ $CD62L^{hi}$ CD8+ T cells in the regional lymph nodes. Depending upon the TCR affinity to the peptides, this phase could last anywhere between 2-8 hours and is characterized by surface expression of the early activation markers CD69, and upregulation of CD44 on naïve CD8+ T cells [90–92]. Complete activation, however, is dependent upon other costimulatory signals and their absence may induce T cell death, anergy, or conversion to regulatory phenotype. Phase II lasts for 8-24 hours after original DC stimulation, during which stable TCR-peptide/MHC-I conjugation takes place [90]. At this stage, CD28 and CD40L on activated CD8+ T cells bind to CD80/86 and CD40 ligands, respectively, on mature DCs that promote differentiation and expansion of CD8+ T [90,93]. The CD28 mediated co-stimulation of activated T cells leads to IL-2 secretion by T cells and results in surface expression of IL-2 receptor, CD25, and other co-stimulatory molecules including CD40L, ICOS, 41BB, and OX40 [90,94]. Binding of these receptors to their complementary ligands on DCs enhances CD8+ T proliferation [90,95]. Rapid division, however, is observed during phase III. Phase III begins 24 hours post antigen exposure, and here, dividing CD8+ T cells differentiate into $CD44^{hi}$ effector cytotoxic T lymphocytes (CTLs) or long-lived memory subpopulations. Effector CTLs shed CD62L adhesion molecules which prevents re-entry into lymph nodes [90,96]

Upon antigen recognition, CTLs form an immunological synapse with the target cell and release cytolytic molecules like perforins and granzymes, resulting into direct cell lysis [97,98]. Perforins form pores in the target cells, for the entry of granzymes, which subsequently initiates caspase mediated cell apoptosis [99]. Additionally, CTLs could also induce apoptosis upon binding of its FAS-L to FAS on the target cells [100].

Following pathogen clearance, 90-95% of expanded T cells undergo apoptosis, with the remaining cells becoming memory T cells that are identified by increased expression of FOXO1 transcription factor [101,102]. FOXO1 represses CTL associated

effector functions by downregulating a master transcription factor T-bet, necessary for Th1 development and IFN-γ production [103]. In contrast, FOXO1 induces upregulation of EOMES transcription factor that has been shown to promote development of memory phenotype [101].

Memory cells are mainly categorised into central memory cells (T_{CM}) or effector memory cells (T_{EM}). T_{CM} cells ($CD44^{hi}$ $CD62L^{hi}$) primarily reside in the lymph nodes and provide long term memory, whereas T_{EM} cells ($CD44^{hi}$ $CD6L^{lo}$) are effector cells found in peripheral circulation and tissues [102]. In recent years, another major CD8+ T cell memory subset T memory stem cells (T_{SCM}), have also been identified for its enhanced self-renewal and long-term effector functions, and are actively studied as immunotherapeutic targets [104–106]. These cells present with naïve like $CD44^{low}$ $CD62L^{hi}$ phenotype and express memory markers including interleukin-2 receptor (IL2R) β and chemokine CXCR3 together with stem cell antigen–1 (Sca-1) [106].

1.2.4.2 Immunosuppressive axis and CD8+ T-cells

Accumulation of cytotoxic CD8+ tumor infiltrating lymphocytes in the TME mediates tumor clearance and has been associated with improved prognosis in several cancers, including EOC, but the anti-tumor effects are often neutralized by a complex immunosuppressive network that limits T-cell priming and homing to the tumor core [79,80,107–113]. Cancer cells inhibit CTL-infiltration in several ways. First, activation of oncogenic WNT/β-catenin and KRAS signaling leads to production of immunosuppressive factors such as VEGF, TGF-β and Indoleamine 2,3-dioxygenase (IDO) that collectively mediate development of aberrant vasculature surrounding the tumor islet [114–121]. In particular, VEGF decreases expression of VCAM-1 on stromal endothelial cells, an adhesion molecule necessary for CTL trafficking, which results into reduced CTL infiltration into the tumor core [116,122]. Second, insufficient blood supply and increased vascular permeability in the tumor bed results in a hypoxic TME [114,122–124]. Hypoxia triggers activation of HIF-1, a key transcription factor that induces recruitment of immunosuppressive cells including MDSCs, Tregs, tumor associated macrophages (TAMs), and limits CTL infiltration [124,125]. Third, stromal reprogramming of fibroblasts by cancer cells to produce a dense extracellular matrix surrounding the tumor islet, which

together with tumor vasculature serves as a nest for immunosuppressive cells while restricting CTLs from reaching the tumor bed [126–128]. Such TMEs are histologically characterized as "infiltrated-excluded" or "non-inflamed/cold" tumors [114,129]. Non-inflamed tumors have been associated with melanoma, colon cancer and pancreatic ductal adenocarcinoma [129–132].

In contrast, "infiltrated-inflamed" or "inflamed/hot" tumors are characterized by relatively lower levels of stromal barriers and higher CTL-infiltration in the tumor bed [129]. However, chronic antigen stimulation polarizes CTLs to increase expression of certain inhibitory receptors (PD-1/CTLA-4/LAG-3/TIM-3) that upon binding to their corresponding ligands on the tumor cells promotes an exhausted phenotype [133,134]. Exhausted or hyporesponsive T-cells often lose their effector functions and contribute towards immune evasion. In recent years, therapeutic blockade of CTL exhaustion pathways has significantly improved survival outcomes in several cancers, and the concept is termed immune checkpoint blockade (ICB) [114,129,135]. In recent years, various therapeutic strategies including ICBs, both alone and in combination with other ICBs, and in combination with soluble mediators such as IL-2 have been shown to reinvigorate exhausted T-cells [136,137].

1.2.5 Natural Killer T cells

NKT cells are a distinct subset of T-lymphocytes that co-express a lipid-reactive TCR and markers associated with NK cells (NK1.1, Ly49, CD16) [138–140]. Unlike conventional T-cells that recognizes peptide antigens on MHC class I or II molecules, NKT TCRs are restricted to lipid and glycolipid antigens that are presented by the MHC class I-like molecule CD1d [139]. Type I or invariant NKT (iNKT) cells express a restricted TCR-α chain rearrangement (Vα14Jα18 in mice or Vα24Jα18 in humans) and are stimulated by glycolipid antigens such as α-Galactosylceramide (α-GalCer) [141,142]. Type II NKT cells exhibit a more diverse TCR-repertoire that do not recognize α-GalCer, but recognize different lipid antigens (e.g. sulfatides) [143–145]. Additionally, these 2 NKT cell subtypes distinctively modulate immune responses and cross-regulate each other [146,147]. In the TME, type I NKTs promote anti-tumor immunity whereas type II NKTs generally facilitate immune suppression [146,147]. Due to our interest in exploring anti-tumor potential

of NKT cells, the thesis will focus exclusively on type I iNKT cells; hereafter referred as NKT cells.

1.2.5.1 NKT cell activation and anti-tumor effector functions

NKT cells mediate tumor clearance via both TCR-dependent and TCR-independent mechanisms [138,141,148]. In contrast to conventional peptide-restricted T cells that complete development before exiting the thymus, most NKT cells leave thymus partially matured and complete maturation in the periphery, where they upregulate NK1.1 and cytokine production capacity [149]. They exhibit a memory phenotype (ie. $CD44^{hi}$) and preformed cytokine transcripts that enable them to exert their innate-like effector functions rapidly upon stimulation [150,151]. NKT cells recognize tumor-associated and stress-induced glycolipid antigens presented via CD1d molecules [152,153], and mediate direct tumor lysis by release of perforin/granzyme-B or through TRAIL and FasL surface receptors [154]. Additionally, activated NKT cells produce immunomodulatory cytokines (e.g. TNF, IFN-γ) [155,156] that mediate increased infiltration and activation of neutrophils [157–159], macrophages [160–164], NK [154,165–167], T [165,166,168,169] and B cells [170,171]. Specifically, CD40:CD40L interaction between NKT and DC leads to DC maturation and increased production of IL-12 [7,168]. This IL-12, subsequently stimulates NK and NKT cells to produce more IFN-γ for activation of cytotoxic NK and T-cells [141,172]. NK cell activation enables clearance of MHC-negative tumor cells, whereas DC maturation and IL-12 production provides stimulus for sustained T-cell immunity [141,168]. Cancer cells can evade NKT cell mediated immune surveillance by downregulating CD1d molecules to avoid glycolipid antigen presentation [153,173]. However, NKT cells can also target CD1d-negative tumors by transactivating NK and CD8+ T cells downstream of exogenous glycolipid stimulation [173]. As a result, NKT cell activation serves as an effective therapeutic tool for targeting heterogeneous tumors [173].

1.2.5.2 NKT cell development and distribution

Invariant NKT cells originate from CD4+CD8+ double positive precursor thymocytes that are positively selected for invariant TCR expression [151,174]. These NKT precursors are selected by self-lipid antigens that are presented via CD1d molecules on

other double positive thymocytes, [151]. NKT cells were initially thought to undergo a linear model of development in which NKT precursors transition through 4 stages of development from the most immature S0 to final S3 stage [151,175]. In this model, NKT cell development is defined to progress in stages: S0 ($CD24^{hi}CD44^{lo}NK1.1^{lo}$), S1 ($CD24^{lo}CD44^{lo}NK1.1^{lo}$), S2 ($CD24^{lo}CD44^{hi}NK1.1^{lo}$) to S3 ($CD24^{lo}CD44^{hi}NK1.1^{hi}$) [151,175]. Immature NKT cells from S0 lose CD24 expression to enter S1, followed by CD44 upregulation in S2 and finally differentiate into S3 with NK1.1 expression [151,175]. Recent studies, however, have challenged this model as it fails to explain early maturation of certain NKT subsets, NKT-2 and NKT-17, that express Gata3 and ROR-y-t, respectively at stage 2. Some NKT precursors are now thought to undergo maturation and become thymic resident NKT cells, while the remaining ones migrate to periphery and complete maturation [151,175]. Depending upon the nature of antigen-TCR signal (strength and duration) and type of cytokine stimulation, immature NKT cells can differentiate into: NKT-1, NKT-2, NKT-10 and NKT17 effector subtypes that mirror cytokine profiles of Th1, Th2, Th10, Th17 subsets of conventional T-cells respectively [151,176,177]. For instance, increased TCR signaling intensity has been associated with increased differentiation into NKT-2 and NKT-17 subsets [178]. Additionally, cytokines such as IL-15, IL-25 and IL-7 have also been implicated in survival and differentiation of NKT-1, NKT-2 and NKT-17, respectively [151].

After thymic or peripheral development, mature NKT subpopulations are broadly divided into CD4- and CD4+ subsets [179,180]. In humans, CD4+ NKT cells generally express Th2 and Th1 cytokines, whereas CD4- subsets (CD4-CD8+ and CD4-CD8-) exhibit a cytotoxic phenotype and predominantly secrete Th1-related cytokines [151,181]. Th1-like NKT cells predominantly reside with liver (12-30% of lymphocytes) and spleen (1-3%), and feature greater anti-tumor potential [154,182–184]. Th2-like NKT populations are enriched in the lungs (5-10%) and intestine (0.05-0.6%), although lungs also contain Th-17 producing NKTs [151,182].

1.2.5.3 NKT cell agonists

NKT cell maturation and activation is facilitated by endogenous and exogenous lipid antigens that each have the potential to skew NKT cell cytokine responses [185]. This

unique ability of NKT cells also predisposes them as promising therapeutic targets, and in this area of research, various efforts have been directed towards either screening for novel NKT cell ligands or development of synthetic NKT cell stimulators for desired therapeutic manipulation [148,150]. One such NKT ligand α-Galactosylceramide (αGalCer), was originally extracted from a marine sponge *Agelas mauritianus* during a screening for novel anti-cancer therapeutics, and has been extensively studied for inducing potent anti-tumor responses [165,166,186–189]. α-GalCer is essentially a sphingolipid composed of a galactose moiety that is covalently linked to sphingosine and fatty acyl chains (Fig. 2) [186]. Its synthetic analog, KRN7000, is a commonly used NKT cell stimulator that induces rapid production of Th1 and Th2 cytokines and downstream transactivation of other immune cells in mice, rats, humans, and macaques [190–193]. αGalCer administration has been found to prevent metastasis and prolong survival in pre-clinical tumor models, but clinical translation of this compound's anti-tumor efficacy in humans, as noted from over 30 clinical trials, has yielded suboptimal results [7,194,195]. Some of the major challenges include: secretion of both regulatory and anti-inflammatory cytokines, induction of anergy, and immune suppression by TME [7,194].

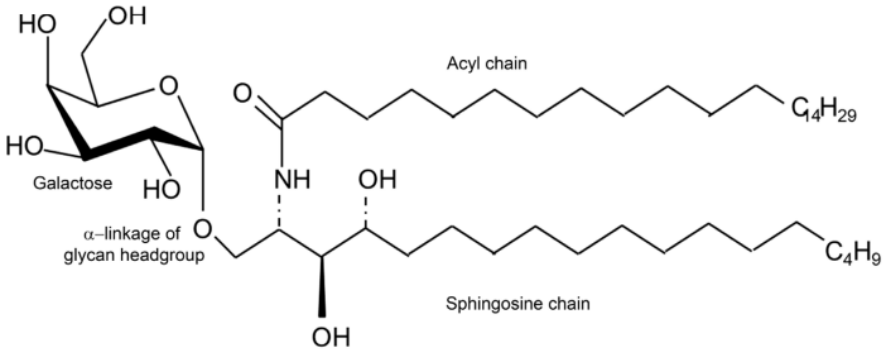

Figure 1 Chemical structure of α-GalCer. (2S,3S,4R)-1-O-(α-dgalactosyl)-N-hexacosanoyl-2-amino-1,3,4-octadecanetriol. α-GalCer is α-GalCer contains galactose head moiety linked to a sphingosine ceramide lipid chain. The lipid portion is further attached to fatty acyl chain which interacts with the antigen-binding groove of CD1d, and galactose moiety binds to α-chain of the invariant TCR of NKT.

α-GalCer treatment polarizes NKT cells to secrete IL-4 within first 2 hours of injection, followed by delayed release of IFN-γ, leading to conflicting immune effects [194,196,197]. Consequently, various derivates of α-GalCer such as OCH and α-C-GalCer

have been designed by making modifications to the glycoside linkages that alter NKT cell signaling [198]. For instance, α-C-GalCer-induced NKT cell activation predominantly drives Th1 responses and provides superior anti-tumor protection in comparison to α-GalCer [199]. In contrast, OCH, an α-GalCer analog with a truncated sphingosine chain, skews NKT cell activation toward a Th2 bias [200]. C20:2 and PBS-25 are other such Th2 biased analogues that have been implicated in controlling autoimmune diseases [201,202].

In addition to these exogenous ligands, a variety of self-lipid antigens such as isoglobotrihexosylceramide 3 (iGb3) [203], β-glucosylceramide(β-GlcCer) [204], α-glycosylceramides [205], lysophosphatidylethanolamine (pLPE) and lysophosphatidic acid (eLPA) [206] have also been identified, but are generally unable to overcome activation threshold necessary for eliciting strong NKT cell activation in the absence of other inflammatory stimulators such as IL-12 or IL-18 [138]. Based on these observations, an affinity threshold model had been proposed that predicted that high affinity TCR-CD1d interactions induce durable IFNγ production whereas weaker agonists drive NKT polarization towards Th2 response [200,207]. However, some studies have argued against establishing TCR affinity-based threshold model as the principle mechanism for driving selective NKT stimulation [208]. For instance, even though α-C-GalCer has weaker TCR interaction than OCH, it exhibits longer half-life interaction with CD1d complex and induces Th1 response [208,209]. Thus, precise mechanisms by which structural variants of αGalCer could be altered for specific iNKT cell functions are not clearly understood [208].

A single dose of free α-GalCer treatment provides superior anti-tumor protection than multiple doses [210]. The latter has been associated with anergy induction in NKT cells wherein constant glycolipid stimulus disrupts normal DC maturation, and leads to accumulation of tolerogenic or regulatory DCs which induce 'hypo-responsiveness' in NKT cells in an IL-10 dependent manner [209,210]. An alternate strategy to overcome NKT cell anergy is to utilize α-GalCer loaded DCs. This has been shown to elicit stronger and more durable NKT cell responses than free α-GalCer injections while avoiding anergy induction [211–213]. αGalCer presentation by non-DCs has been shown to inhibit IFN-y secretion from NKT cells, and induce anergy or a Th2 response [194,214].

1.2.6 Dendritic cells

DCs constitute a uniquely potent subset of antigen presenting cells (APCs) that play a central role in bridging innate and adaptive immunity [215]. Immature DCs constitute the majority of the peripheral DC population and exhibit high endocytic and antigen processing capacity [216,217]. Danger signals such as DAMPs and pathogen-associated molecular patterns serve as maturation signals for DCs [218]. Mature DCs downregulate endocytic activity, migrate to secondary lymphoid organs and upregulate surface expression of MHC (class I and class II) molecules, costimulatory molecules (CD80, CD86, CD40) and proinflammatory cytokines [219]. These 3 stimuli are essential for optimal T cell activation, and hence, DCs are also termed as professional APCs [220]. DCs are unique among APCs in their ability to cross-present extracellular antigens on MHC-I, which is generally reserved for endogenous antigens, and stimulate CD8+T cells. This ability to cross-present antigens by DCs make them central in priming anti-tumour T-cell immunity. Processed antigens are loaded onto MHC-I and MHC-II molecules, and presented to CD8+ and CD4+ T cells respectively [215]. These antigen-specific T cells migrate to TME and target MHC-positive tumor cells. Mature DCs produce chemokines including CXCL9 and CXCL10 which promote infiltration of CD8+T cells, NK and NKT cells [215].

1.2.7 Myeloid derived suppressor cells

In ovarian cancers, myeloid-derived suppressor cells (MDSCs) are associated with increased tumor proliferation, vascularization, immune suppression and an overall poor prognosis [221–226]. The TME is enriched with cytokines and growth factors such as tumor necrosis factor (TNF-α), macrophage colony-stimulating factor (M-CSF), granulocyte colony-stimulating factor (G-CSF), granulocyte monocyte colony-stimulating factor (GM-CSF), VEGF, prostaglandin E2 (PGE2), and interleukins (IL-1β, IL-10, IL-18, and IL-6) that collectively disrupt the differentiation of myeloid precursors – leading into accumulation of a heterogenous population of immature myeloid cells that have immunosuppressive functions [221,227]. MDSCs are CD11b+ and, and can be classified into monocytic ($Ly6C^{high}Ly6G-$) and granulocytic ($Ly6C^{low}Ly6G+$) subpopulations in mice [227,228]. There are no specific markers for MDSCs, and they have to be defined by

functional suppressive activities. In ovarian cancer patients, monocytic MDSCs are more prevalent than granulocytic MDSCs, and are also suggested to be a reliable prognostic biomarker [221,226,229–231].

MDSCs exert their immunosuppressive effects by several mechanisms. MDSCs produce arginase-1 (Arg-1) and Indoleamine 2,3-dioxygenase (IDO), that cause downstream depletion of amino acids, L-arginine, L-tryptophan, and L-cysteine, vital for T-cell proliferation and activation [232–234]. Reactive oxygen species and nitric oxide released by MDSCs stimulate apoptosis in T cells, in addition to diminishing their proliferation and effector functions cells [233,235,236]. Recently, MDSC-derived nitric oxide has also been shown to inhibit the function of Fc receptors on NK cells, to inhibit tumor clearance via antibody-dependant cellular cytotoxicity [234]. MDSCs mediate tumor angiogenesis and metastasis by upregulating expression of VEGF and matrix metalloproteinase (MMP)-9 [237,238]. MDSCs also support tumor immune evasion by upregulating molecules that induce tolerance in T-cells (e.g. programmed death ligand-1 (PD-L1)) [239].

1.3 Immune checkpoint blockade

In past 5 years, therapeutic blockade of T-cell exhaustion pathways has significantly improved survival outcomes in several cancers, and has become current standard of care for the treatments of metastatic melanoma and non-small-cell lung carcinoma [240–246]. Exhausted T-cells exhibit impaired secretion of pro-inflammatory cytokines, such as IL-2 and IFN-γ, that are crucial for T-cell proliferation, cytotoxicity and recruitment [128,135,247,248]. Checkpoint blockade uses antagonistic antibodies to reinvigorate and rescue exhausted T-cells by blocking signalling of T-cell inhibitory receptors such as anti-PD-1 (Pembrolizumab and Nivolumab) and anti-CTLA-4 (Ipilimumab) [247].

Although Ipilimumab (anti-CTLA-4) became the first FDA approved checkpoint inhibitor for treating advanced melanoma, and yielded disease-free survival in 20% of the patients, PD-1 blocking antibody (Nivolumab) exhibited significantly longer recurrence-free survival and improved safety profile in the subsequent studies [249,250]. Since then anti-PD-1/PD-L1 checkpoint inhibitors have expanded to treat several cancers including lung

carcinoma, head and neck squamous-cell carcinoma, Hodgkin's lymphoma, renal clear carcinoma, colorectal cancer, and gastrointestinal cancers [114,242–245,250].

In the context of EOCs, objective response rates range between 6–15% in studies using single-agent anti-PD-1 or anti-CTLA-4 blockades, whereas the combination therapy with anti-PD-1 and anti-CTLA-4 blockades significantly improved overall response rates to 34% [79,80,251,252]. Nevertheless, lack of response to immune checkpoint blockade remains a major challenge in the majority of patients [253,254]. Tumor heterogeneity, PD-L1 expression, tumor mutational burden, and T-cell infiltration levels are some of the determining factors that have been suggested to predict treatment outcomes [131,255,256]. In lung and urothelial cancers, high PD-L1 expression on tumor cells have been positively correlated with better clinical response to ICB [243,251]. In contrast, Hamanishi et. al. [257,258] demonstrated poor prognosis in EOC patients with higher PD-L1 expression when treated with ICB, questioning the predictive validity of PD-L1 expression. In another pre-clinical murine ovarian cancer model, PD-L1 knockdown in ID8 or HM-1 cancer cell lines increased survival times, suggesting the importance of PD-1/PD-L1 regulatory pathway for immune evasion in ovarian cancers [259].

Inflamed tumors with significant T-cell infiltration are consistently associated with better responses to PD-1/PD-L1 blockades, whereas infiltrated-excluded or cold tumors rarely respond to monotherapy [114,129]. To maximize ICB potential, several strategies aimed towards disrupting the stroma-tumor barrier and boost CTL infiltration have been explored [114,251]. These approaches include use of immune modulators such as anti-angiogenic therapies, PARP inhibitors, and inducers of immunogenic cell death in combination with ICBs [114,260].

1.4 Oncolytic viruses

The relationship between naturally acquired viral infections and cancer were first reported in mid 1800s, when patients with hematological malignancies exhibited short-term tumor regression upon contracting measles virus [261]. Similar incidents were later reported in 1904 and 1912 in patients infected with influenza and chicken pox viruses, respectively [262,263]. Although these anecdotal reports motivated early research in understanding the virus biology, the oncolytic potential of viruses wasn't truly explored

until the 1950s with the advent of murine cancer models and cell-culture systems [263,264]. Complete tumor regression was evident from pre-clinical tumor studies; however, the results could not be translated into human clinical trials largely due to uncontrolled virulence [265]. The advent of recombinant DNA technology enabled researchers to genetically engineer wild type viruses with attenuated host pathogenicity and enhanced cancer specificity and potency [263]. Since then, various DNA and RNA based oncolytic agents have been studied including herpes simplex virus, vaccinia, adenovirus, reovirus, measles virus, Myxoma virus and vesicular stomatitis virus (VSV) [266]. In recent years, oncolytic viruses (OVs) have been modified to express immunomodulatory factors such as cytokines, chemokines, and antibodies that enable localized delivery of therapeutic immunomodulators while reducing systemic toxicities [264]. In 2015, United States approved talimogene laherparepvec (T-Vec) for aggressive melanoma, a herpes simplex virus-1 engineered to express the myelopoiesis-stimulating cytokine GM-CSF[267].

1.4.1 General mechanism of action

OVs represent an emerging class of immunotherapeutic agents that preferentially infect and lyse cancer cells with minimal pathogenicity towards healthy cells [264]. Oncolytic viruses selectively replicate in tumor cells due to dysregulated metabolism and signaling pathways (e.g. IFN or RAS) enabling targeted killing by OVs [268–270]. For example, the protein kinase R (PKR) is an intracellular protein that recognizes double-stranded viral RNA [6]. In normal cells, activation of PKR through viral elements impairs protein synthesis triggering IFN production and apoptosis, thus reducing viral replication [6,271]. Cancer cells are often deficient in PKR activity, resulting in increased viral replication [6]. OVs mediate their anti-tumor activities through two mechanisms, direct viral lysis of infected tumor cells and stimulation of anti-tumor immunity that results from release of tumor antigens and inflammatory recruitment of immune cells [265]. Following OV infection and replication, tumor cells undergo lysis to release thousands of virions that infect surrounding cancer cells to mediate tumor killing via ICD [265,266]; a pathway that results in the release of tumor antigens, pro-inflammatory cytokines (TNFα, IFNγ, IL-12) and DAMPs (HMGB1, ATP, CRT) that promote recruitment, activation and maturation of DCs [114,272–275]. Mature DCs cross-present tumor antigens to

T-cells in lymph nodes and stimulate cancer specific adaptive immunity [276]. Additionally, viral oncolysis facilitates disruption of physical barriers surrounding TME in several ways including, collapse of blood vessels feeding tumors, extracellular matrix degradation, reprogramming of TAMs from a pro-tumorigenic M2 phenotype to pro-inflammatory M1 phenotype, decreasing recruitment and differentiation of Tregs, and upregulation of MHC-I on tumor cells [277–279]. These factors collectively alter TME and regulate intratumoral infiltration of T-cells [278].

1.4.2 Synergy with checkpoint blockade therapy

In response to OV infection, various pre-clinical and clinical studies have reported upregulated expression of PD-1 and PD-L1 on immune and tumor cells respectively [280,281]. Combination therapy of anti-PD-1 checkpoint blockade and T-VEC OV has been shown to induce superior CD8+ T infiltration, and increased IFN-γ expression compared to individual treatments in patients with advanced melanoma [277,282]. This synergistic effect is also evident with combination therapy of coxsackievirus and anti-PD-1 blockade, and helps to overcome immunosuppression while simultaneously driving T-cell infiltration into the TME [283,284].

1.4.3 Vesicular stomatitis virus (VSV) overview

VSV is a single-stranded negative sense RNA virus of the *Rhabdoviridae* family [285,286]. Wild type VSV of the Indiana or New Jersey serotypes primarily infects cattle, horses, sheep, and insect vectors. VSV infections are rarely lethal and cause oral lesions in livestock [286]. In humans, VSV infections manifest as an acute flu-like illness, and are limited to laboratory and agricultural workers [287,288].

The VSV oncolytic platform is promising for several reasons [288]. First, the small VSV RNA backbone replicates quickly, efficiently lysing tumor cells with the release of thousands of virions within 6 hours post infection [288]. This is in contrast to large DNA virus backbones such as adenovirus or vaccinia virus that offer greater room for engineered genetic material but are slower to replicate and produce low virus yields [289]. Second, the VSV genome is amenable to manipulation, and in recent years various recombinant VSVs have been genetically engineered for improved potency, and

transgene expression that synergizes with host immunity or combination therapies for greater anti-tumor benefits [288]. Third, VSV cell-receptors, including the low-density lipoprotein (LDL) receptor, sialoglycolipids, heparan sulfate and phosphatidylserine, are ubiquitously expressed on tumor cells, whereas some OVs are dependent on differential receptor expression profiles, specific to the virus itself [289]. Fourth, cytosolic replication ensures no risk of host cell transformation [289]. Fifth, lack of pre-existing immunity against VSV in the global human population makes it an ideal candidate to be translated for therapeutic use in clinical settings [289].

1.4.3.1 VSV structure

VSV is a bullet shaped virus and has a relatively short non-segmented genome of 11 kb that encodes 5 viral proteins: glycoprotein (G), matrix (M), nucleocapsid (N), phosphoprotein (P), and large RNA polymerase (L) [290]. G and M are involved in viral assembly and budding during the early infection phase and facilitate downregulation of host anti-viral machinery, whereas N, P and L form the ribonucleoprotein core and regulate virus transcription, replication and amplification (Figure 2) [291]. Briefly, the VSV RNA is encapsulated by multiple copies of N protein to form a nuclease resistant N-RNA complex that serves as a template for mRNA synthesis and genomic RNA replication [292]. This complex is also fused with viral RNA-dependent RNA polymerase (RdRP), a complex of L and P proteins, and collectively form a ribonucleoprotein (RNP) core that is surrounded by the internal matrix protein [292]. In addition to virus budding, the matrix protein plays an important role in wild-type VSV infection by suppressing transcription of host cell's antiviral machinery [293]. This enables unhindered VSV replication in infected cells. The transmembrane glycoprotein binds to members of the LDL receptor family receptors and mediates viral entry via endocytosis [294].

1.4.3.2 VSV transcription, replication and budding

The VSV life cycle is initiated upon binding of the G protein to LDL cell surface receptors, causing clathrin mediated endocytosis (Figure 2) [291,294]. Internalized VSV is then transported to endosomal compartments wherein the low pH induces a confirmation

change in the G-protein and triggers fusion of viral envelope with endosomal membrane - leading to release of virion content into the cytoplasm [294,295].

In the cytosol, the RdRP complex initiates primary transcription by recognizing a specific single-entry start site in the leader sequence at the 3' end, and sequentially transcribes the RNA genome in the following order: 3'-N>P>M>G>L-5' [296]. Once the RdRP complex arrives at the intergenic regions, which contain the sequences for poly adenylation and transcriptional start/stop sites, the probability of complex-template disassociation become higher [297–299]. This leads to a gradient production of viral proteins since VSV template transcription is polar, meaning transcription of each successive gene depends on complete transcription and termination of the gene upstream. Consequently, a 30% reduced expression of each successive mRNA, relative to the gene upstream, is observed with the N protein being the most abundant, followed by decreasing gradients in the order given: P, M, G and L proteins [298]. Capped and polyadenylated viral mRNAs are translated by host ribosomes to produce viral proteins [298,300].

Once adequate levels of N and P proteins have been produced, the RdRP complex begins transcribing the VSV negative sense RNA strand to synthesize positive sense anti-genomes [292,300]. This anti-genome serves as template strand for RdRP complex, which acquires replicase function, and generates complementary full length, negative sense molecules [292,300]. The nascent RNA genome is encapsulated by soluble N and P proteins to become RNP core and packaged into virions during assembly [300]. The M protein facilitates the assembly and packaging of the nascent RNP cores, and strongly binds to the 'anchor' regions of transmembrane G protein for the release of mature infectious particles from the host cell in a process called budding [301]

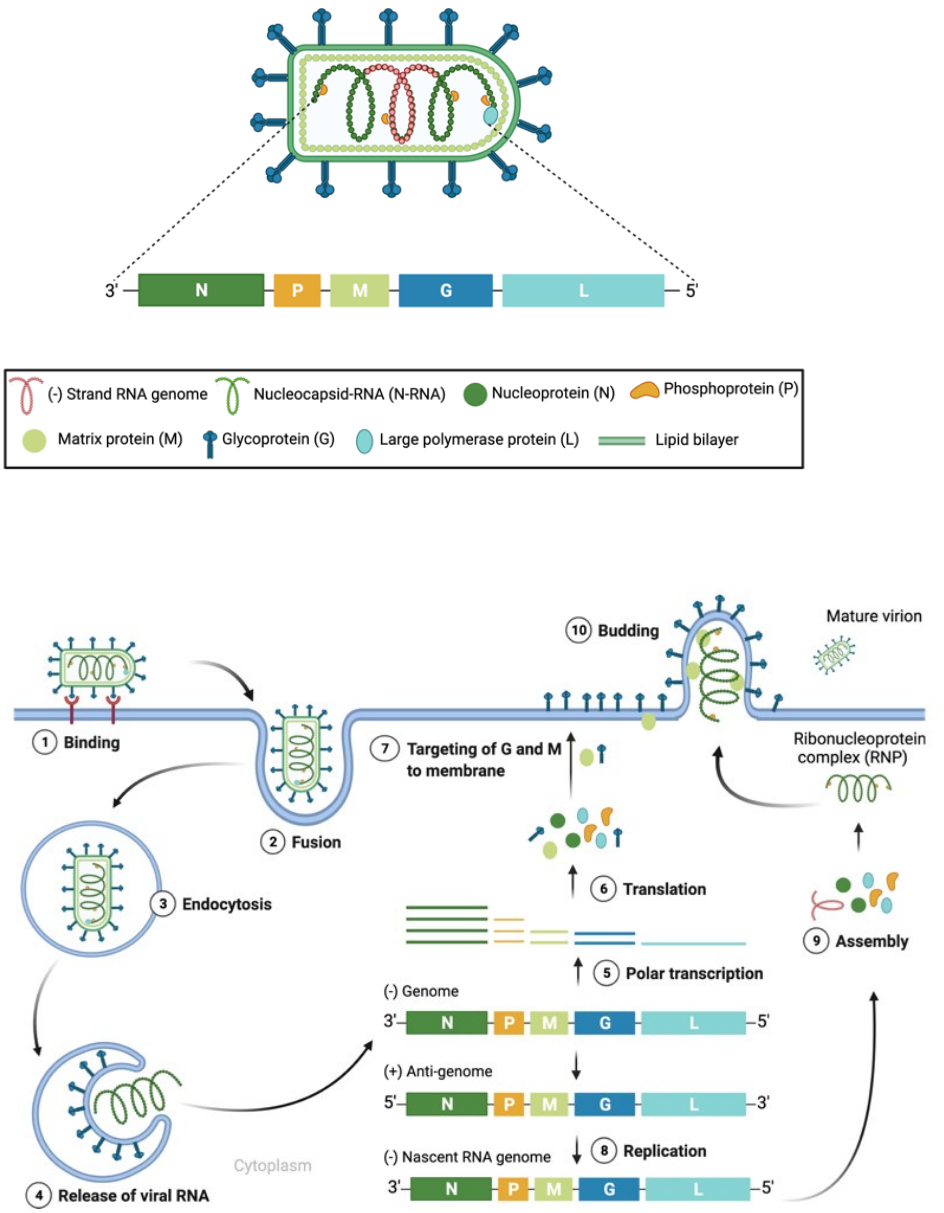

Figure 2 VSV structure and life cycle. VSV virion is a bullet shaped Rhabdovirus that encapsulates a negative-sense single-stranded RNA genome in complex with nucleoprotein (N), phosphoprotein (P) and large polymerase (L); collectively forming a ribonucleoprotein complex. The matrix protein (M) and glycoprotein (G) enable virion budding. VSV enters host cells via receptor-mediated endocytosis and are transported to cytoplasm by endosomes. Release of viral contents including RNA genome, N, L and P proteins trigger transcription and translation in cytoplasm. M proteins facilitate inhibition of host translation machinery. VSV RNA genome undergoes polar transcription followed by translation of polyadenylated mRNAs into viral proteins. VSV replication is induced upon adequate production of N, L and P proteins that upon assembly acquire replicase function and enable synthesis and encapsulation of nascent negative sense RNA genome. G and M proteins are targeted to cell-membrane for facilitating virion budding. The figure was created with BioRender.com.

1.4.3.3 VSV oncoselectivity and IFN sensitivity

VSV is a promising candidate for oncolytic virotherapy due to its natural tropism towards diverse cancer cell lines [302]. This oncoselectivity primarily stems from diminished type I IFN-signaling in malignant cells [302–304]. In contrast, normal cells are equipped with intact IFN-signaling that, upon secretion, activate IFN stimulated genes leading to upregulation of antigen processing machinery and downstream activation of immune cells for viral clearance [303]. To evade host anti-viral response, VSV encodes a matrix protein that binds to two nuclear pore proteins, Rae-1 and Nup98, at the nuclear membrane and prevents host mRNA export into cytosol [293,305]. Additionally, the M protein also inhibits the host RNA polymerase II activity [306,307]. This technique of hijacking the host machinery induces translation host shut off, and eventually leads to apoptosis of malignant, as well as normal cells [308]. In rodents and non-human primates, VSV rapidly replicates in nasal epithelium followed by viral propagation to olfactory neurons and eventually to brain, where they cause severe neuropathogenesis [289,309–311]. To address safety concerns and improve VSV oncoselectivity, Stojdl et al. generated a recombinant VSV-ΔM51 carrying a deleted methionine residue 51 in the M protein; and thus, preventing VSV-M induced masking of host anti-viral responses in normal cells [312]. The VSV-ΔM51 oncolytic platform has been used in many studies and has been engineered to express molecules that improve viral oncoselectivity or modulate anti-tumor immune responses [288,313,314].

1.4.4 Recombinant VSV-IL-12

1.4.4.1 Interleukin-12 general biology

IL-12 is a potent pro-inflammatory cytokine that plays a central role in inducting T, NK and NKT-cell mediated immune responses [315,316]. This 70 kDa heterodimeric protein is composed of two subunits, p35 and p40, that are linked by disulfide bonds to form the bioactive IL-12p70 cytokine [317]. In response to bacterial and viral infections, DCs, B-cells, monocytes, macrophages and neutrophils produce IL-12, which exerts its functions directly on IL-12 receptor expressing immune populations including NK cells,

NKT cells, T cells and Innate Lymphoid cells [318,319]. Upon ligand binding, IL-12 induces transphosphorylation of Janus kinases-2 and specific tyrosine residues on the IL-12 receptor, that serve as docking sites for phosphorylation and dimerization of STAT-4 molecules [320,321]. STAT-4 homodimers translocate to nucleus and mediate transcription of specific genes that promote increased cytolytic functions and clonal expansion of T and NK cells [319,322], polarization of Th1-type immune responses [323,324] and reprogramming of immunosuppressive cells to acquire a pro-inflammatory immune profile [325–327]. Specifically, IL-12 signaling in NK cells, CD4+ and CD8+ T cells induces production of a major effector cytokine - IFN-γ, which is critical for coordinating anti-tumor defense [315,324,328].

Naïve CD4+ T cells differentiate to Th1 phenotype upon stimulation with IL-12 and IFN-γ, and CD8+T cells differentiate into CTLs [324]. IL-12-mediated IFN- γ production has diverse immune stimulatory properties including: upregulation of cytotoxic (perforins, granzyme and Fas Ligand (FasL)) [319] and chemotactic molecules (CXCL9 and CXCL10) leading to increased recruitment of NK, NKT, and effector T cells [329,330]; whereas increased MHC expression on tumor cells facilitate increased cell-mediated tumor lysis [331,332]. Additionally, IL-12 also targets the immunosuppressive axis by downregulating secretion of angiogenic factors (MMP-9, CXCL12 and VEGF) [328,330,333,334] and reprogramming anti-inflammatory M2 macrophages into anti-tumor M1 macrophages [325]. For instance, VEGF has been associated with hindering DC maturation, recruitment of Tregs, and induction of T-cell exhaustion [335–337]. Thus, IFN- γ is a central mediator of IL-12-induced responses, which in turn acts on APCs to increase IL-12 secretion in a positive feedback loop that further maximizes Th1 immunity [338].

1.4.4.2 IL-12 immunotherapy

Therapeutic benefits of IL-12 have been studied in pre-clinical mouse cancer models, but severe dose-limiting toxicities associated with systemic IL-12 administration, as evident from numerous clinical trials, has prevented clinical application [339,340]. Besides toxicity, low immune response rates to intravenous IL-12 treatment is reported in patients with metastatic renal carcinoma, melanoma, colon carcinoma, recurrent ovarian cancer, and neck and head carcinoma [315,339,341]. IL-12 is a potent pleiotropic cytokine and its

systemic administration induces rapid release of pro-inflammatory cytokines (IFN-γ, TNF-α, IL-6), even from non-targeted circulating lymphocytes, which leads to rapid depletion of peripheral leukocytes [342,343]. Repeated IL-12 treatments also evoke production of IL-10 and TGF-beta, cytokines that negatively regulate IL-12 activity and instead neutralize the anti-cancer effects of IL-12 therapy [343,344]. In contrast, localized delivery of IL-12 leads to improved clinical benefits with minimal toxicities in melanoma and other hematological malignancies [345,346]. In recent years, methods to intratumorally deliver IL-12 are being actively explored to optimize efficacy and enhance the safety profile [342]. Some of the methods include: adoptive transfer of lymphocytes that are genetically engineered to express IL-12 under inducible promoter [347], electroporation of IL-12 encoding inducible plasmids [345] or IL-12 encoding oncolytic viral vectors that provide controlled IL-12 expression in the TME [348].

1.4.4.3 VSV-IL-12

Various OVs expressing IL-12 have been developed and studied in pre-clinical mouse models including herpes simplex virus (HSV), adenoviruses, measles virus, maraba virus, Newcastle disease virus, Semliki forest virus, and VSV [348]. Amongst these, IL-12 expressing HSV strains have been extensively studied by several and demonstrate improved anti-tumor efficacies, particularly in pre-clinical glioblastoma and neuroblastoma tumor models [348]. M032, a second-generation IL-12 expressing HSV strain, previously shown to improve survival outcomes without adverse toxicity in non-human primate glioblastoma models, is currently undergoing clinical trials in patients with recurrent glioblastoma [349,350]. IL-12 expressing adenoviruses have also been shown to drastically improve survival outcomes in pre-clinical models and are clinically investigated in melanoma, prostate, pancreatic and breast cancers [351–354]. For instance, IL-12 encoding adenovirus resulted in complete eradication of pancreatic tumors in hamsters and elicited significant accumulation of CD8+ T cells in spleen [351]. In the context of this study, we sought to genetically engineer the oncolytic VSV-ΔM51 platform to express cytokine IL-12, and to examine the anti-tumor response when this virus is used in combination with NKT cell immunotherapy in an ovarian cancer mouse model.

1.4.5 IL-15 immunotherapy

IL-15 is a potent cytokine that is mainly secreted by DCs, monocytes and macrophages and exhibits numerous immunological functions on innate and adaptive cells through its broad pleiotropic activity [355,356]. IL-15 needs to complex with both the IL-15 specific receptor α chain (IL-15Rα) and the βγ common chain (βγc) to execute its biological activity [356]. Some of the major IL-15 induced responses include: increased proliferation and secretion of immunoglobulins from B cells, and enhanced survival and cytotoxic activation of NK, NKT and CD8+ T-lymphocytes [357–359]. IL-15 has also been implicated in accumulation and survival of both NK and memory T-cell populations after infection clearance [355,360,361]. Additionally, IL-15 secretion also inhibits differentiation and proliferation of immunosuppressive CD4+ Tregs [362]. Several preclinical studies have demonstrated metastasis reduction, tumor regression, and increased survival in solid-tumor-bearing mice tumor upon IL-15 treatment [363]. Furthermore, some IL-15 treated mice continued to remain tumor-free upon re-challenge, and elicit a long-term anti-tumor immune response [355,364]. IL-15, thus, presents as an ideal cancer therapeutic agent given its potential to activate effector immune cells without inducing adverse toxicities [365].

1.4.5.1 VSV-IL-15

Targeted delivery of IL-15 in TME using viral vectors such as VSV has previously been shown to enhance anti-tumor activity in the mouse CT26 colon cancer model [313]. Localized delivery mediates superior anti-tumour effects over systemic IL-15 delivery [366]. Developed by Stephenson et. al. [366], VSV-IL-15 is a potent OV engineered to express human (h)IL-15 on a VSVΔM51 platform. This will be used to examine anti-tumor responses in an ID8 ovarian cancer mouse model.

1.4.6 VSV-p14

The reptilian reovirus p14 is a 375 bp Fusion-Associated Small Transmembrane (FAST) protein that enhances lateral viral dissemination through its ability to induce cell-cell fusion [367,368]. Several studies have associated FAST protein-induced syncytia formation in tumor cells with increased apoptosis in the fused tumor cells [369]. In an effort to take advantage of syncytia induced tumor cell death, various oncolytic viruses have

been engineered to express fusogenic proteins including adenovirus and paramyxovirus [369–371]. Our laboratory previously showed improved survival in metastatic 4T1 breast and primary CT26 colon cancer mouse models using a VSVΔM51 vector expressing the p14 FAST protein [314].

1.5 Scope of thesis research

Although conventional treatments for ovarian cancer, including surgical reduction and chemotherapy, provide good clinical outcomes when diagnosed early, a high relapse rate and detection during later stages when the cancer has metastasized highlight the need for the development of novel therapeutic approaches [40]. NKT cell therapy in several pre-clinical tumor models has been shown to elicit anti-tumor immune response and prolong survival [153,166,167,195]. However, clinical translation of the therapy has resulted into modest outcomes and present a need for further optimization [153]. *I hypothesize that VSV constructs expressing IL-12, IL-15, or p14 administered in combination with NKT cell immunotherapy and anti-PD-1 checkpoint blockade will enhance NKT cell recruitment and antitumor activity, resulting in improved survival outcomes in the ID8 mouse model of ovarian cancer. The underlying immunological responses elicited by oncolytic VSV and NKT cell activation therapies were also examined.*

1.5.1 Objective 1: To evaluate the impact of VSV expressing GFP, IL-15 or p14 FAST constructs in combined oncolytic-NKT cell immunotherapy

Our lab has previously demonstrated that NKT cell activation therapy combined with control VSV-GFP prolongs survival in the ID8 model of ovarian peritoneal carcinomatosis [166]. This thesis examined the survival effects of VSV constructs expressing IL-15 or p14 alone and in combination with NKT activation therapy and anti-PD-1 checkpoint blockade. Immune cell infiltration, activation, and proliferation (flow cytometry) following treatment with VSV-p14 in combination therapy were also examined. The induction and magnitude of ID8-specific antitumor activity (cytotoxicity and cytokine production [IFN-γ, IL-4]) was also assessed in ID8-splenocyte co-culture assays. Therapeutic activation of NKT cells using α-GalCer loaded DCs resulted into improved survival outcomes over control. In addition, the treatment led to a significant

increase in NKT, NK, and T cell populations in ascites and reduced number of Tregs in the spleen. Combination therapy with VSV-GFP further prolonged survival. Technical challenges, such as reduced oncolytic activity with VSV-p14, presumably due to accumulation of defective interfering particles, as well as episodes of hind-limb impediments following VSV-IL-15 treatments, made it difficult to determine if these recombinant viruses could be of therapeutic benefit in ID8 model.

1.5.2 Objective 2: Generate a recombinant VSV construct expressing cytokine IL-12

A bioactive and expression ready mouse IL-12 gene construct, with elastin linker between p40 and p35 subunits (Invitrogen) was cloned into the pVSV-ΔM51-XN2 virus plasmid. Reverse genetic techniques were used to generate functional VSV-ΔM51-IL-12-XN2 viruses. To enhance the magnitude of IL-12 production, another recombinant virus construct was generated with an internal ribosome entry site sequence preceding the mIL-12 gene. In our preliminary survival study, VSV-IL-12 treated mice also developed hind limb impairments, and thus had to be sacrificed early during the study. While standalone VSV-IL-12 treatments did not exhibit a superior survival benefit over VSV-GFP, combination with NKT cell therapy showed an early survival benefit, however, the mice eventually succumbed to hind limb impediments.

CHAPTER 2: MATERIALS AND METHODS

2.1 Cell lines

ID8 ovarian cancer cells (generated by Dr. K Roby, University of Arkansas and obtained from Dr. J. Marshall, Dalhousie University), B16-F10 melanoma cells (ATCC), Lewis lung carcinoma cells (ATCC), 4T1 mammary carcinoma cells (ATCC), Pan02 pancreatic cancer cells (generated by Dr T.H. Corbett, Wayne State University and obtained from Dr. J. Bell, University of Ottawa), Vero (African green monkey kidney epithelial) cells (ATCC) and QM5 (RRID:CVCL_M211) cells were cultured in a humidified incubator (37 °C; 5% CO_2) in Dulbecco's Modified Eagle Medium (DMEM; 4.5 g/L glucose, L-glutamine; Corning Life Sciences) supplemented with 10% fetal bovine serum (FBS; Fisher-HyClone), penicillin/streptomycin (100 units/ml - 100µg/ml;

HyClone) and buffered with HEPES (25 mM; GIBCO). Cells were harvested at 90% confluency using trypsin-EDTA (ethylenediamine-tetra-acetic acid; 0.25% Invitrogen) and re-suspended in phosphate buffered saline (PBS) for *in vivo* experiments.

2.2 Mice

Wild-type female C57BL/6 mice were purchased from Charles River Laboratories (Saint-Constant, QC) and were housed in the Carleton Animal Care Facility at the Dalhousie University and used in experiments at 8-12 weeks of age. Experimental procedures were approved by the University Committee on Laboratory Animals in accordance with the guidelines of the Canadian Council on Animal Care.

2.3 α-GalCer reconstitution

A stock concentration of 0.2 mg/mL α-GalCer (KRN7000; DiagnoCine LLC) was prepared in sterile 1X PBS containing 0.5% tween-20 vehicle. The solution was sonicated for 4 hours in a 60°C water bath, aliquoted and stored at -20°C. Prior to use, aliquots were thawed and sonicated for another 20 minutes in a 60°C water bath.

2.4 Cloning of viruses

2.4.1 Generation of a VSVΔM51-IL-12 plasmid construct containing a glycine-serine linker sequence

I designed an *in-silico* gene construct encoding the 1.9-kb single-chain murine IL-12 expression ready cassette (pORF-p40-$(G_4S)_3$-p35; Addgene plasmid # 108665) in which the p40 and p35 IL-12 subunits are linked by a glycine-serine sequence. The sequence of the parent plasmid was engineered to eliminate an internal *NheI* cut site and be repositioned at 3' site of the IL-12 gene. The construct was synthesized, and subcloned into *PspOMI* and *EcoRI* sites of the pUC57 vector by Bio Basic Inc. to generate a pUC57-p40p35 donor plasmid. The transgene was then PCR amplified (Table 1), and subcloned into *XhoI* and *NheI* sites of the pVSVΔM51-XN backbone using Quick Ligation™ Kit (NEB) generating pVSVΔM51-XN-p40-$(G_4S)_3$-p35 (referred as V1; Figure 3). The resulting sequence was validated by PCR, and Sanger sequenced (Table 2). An attempt to rescue V1 virus was made, however, it was unsuccessful.

2.4.2 Generation of a VSVΔM51-IL-12 plasmid construct containing an elastin linker sequence

A murine IL-12 transgene, bearing p40 and p35 subunits linked by $(VPGVG)_2$ elastin linker was PCR amplified (Table 1) from pORF-p40-$(VPGVG)_2$-p35 (InvivoGen). A a *XhoI* 5' restriction site was added to facilitate its cloning into *XhoI* and *NheI* sites of the pVSVΔM51-XN backbone. Assembly and orientation of the IL-12 transgene in pVSVΔM51-XN backbone (referred as V2; Figure 3) was validated by PCR and Sanger sequencing (Table 2). An attempt to rescue the pVSVΔM51-XN-p40-$(VPGVG)_2$-p35 virus was made, however, it was unsuccessful. In particular, no cytopathic effect was observed upon infecting Vero cells with the supernatant obtained after clearing MVA virus.

2.4.3 Generation of a VSVΔM51-IL-12 plasmid construct containing an IRES sequence

An *in-silico* gene construct was designed with a 5' *XhoI*-IRES sequence inserted in frame with a 1.6-kb single-chain murine IL-12 expression ready cassette (pORF-p40-$(VPGVG)_2$-p35 (InvivoGen) that flanked 3' *NheI* site. The construct was synthesized, and subcloned by Bio Basic Inc. into *XhoI* and *ApaI* sites of the pcDNA3 mammalian expression vector (Invitrogen) to generate a pcDNA3-IRES-p40-$(VPGVG)_2$-p35 donor plasmid. The transgene was then PCR amplified using amplification primers (Table 1), and subcloned into *XhoI* and *NheI* sites of the pVSVΔM51-XN backbone using an In-Fusion® HD Cloning Kit (Takara Bio, USA) to generate pVSVΔM51-XN-IRES-p40-$(VPGVG)_2$-p35 (referred to as V3, VSV-IRES-mIL-12 or simply VSV-IL-12; Figure 3). The resulting consensus sequence was validated by PCR, and Sanger sequencing (Table 1, 2).

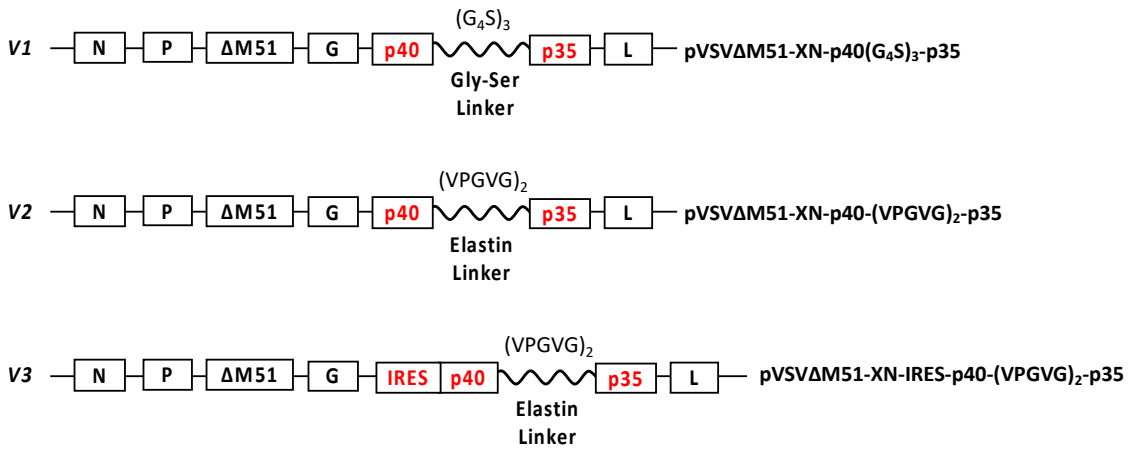

Figure 3 VSV plasmid constructs. Schematic diagram showing the genome organisation with inserted transgenes of the recombinant VSV plasmid constructs. (V1) The construct encodes the p40 and p35 mIL-12 subunits linked by glycine serine linker. (V2) The IL-12 subunits are linked by elastin linker. (V3) The construct encodes IRES sequence in frame with single-chain IL-12 subunits linked by an elastin linker. N – nucleocapsid, P – phosphoprotein, M – matrix protein, G – glycoprotein, L – large polymerase protein, $(G_4S)_3$ – glycine-serine linker, $(VPGVG)_2$ – elastin linker, IRES – internal ribosome entry site.

Table 1: List of primers used to amplify gene constructs

Gene of Interest	Primer Orientation	Restriction Site Added	Primer Sequence
IRES-mIL-12	Forward	*XhoI*	AGATATCACGCTCGAGACTATCCCCTCTCCC TCCCC
	Reverse	*NheI*	GAAGAATCTGGCTAGCTTTAGGCGGAGCTC AGATAGCC
mIL-12	Forward	*XhoI*	TAAGCACTCGAGATGTGTCCTCAGAAGCTA ACCAT
	Reverse	*NheI*	TAAGCATCTGGCCAGCTAGCTTTAGGC
p40p35	Forward	*XhoI*	ATCACGCTCGAGACTATCATGGG
	Reverse	*NheI*	GCAATCTGGCTAGCCTAAATTCAGGC

Table 2: List of primers used for Sanger sequencing

Gene of Interest	Primer Orientation	Primer sequences used for Sanger sequencing
IRES-mIL-12	Forward	1. CTGCAAAGGCGGCACAAC 2. GCAGTAGCAGTTCCCCTGAC 3. TCATACCGGTCTCTGGACCT
	Reverse	1. CCCCTTGTTGAATACGCTTG 2. CCTGGCAGGACACTGAATACT 3. CATCTGTGGTCTTCAGCAGG
mIL-12	Forward	1. GCAGTAGCAGTTCCCCTGAC 2. TCATACCGGTCTCTGGACCT
	Reverse	1. CCTGGCAGGACACTGAATACT 2. CATCTGTGGTCTTCAGCAGG
p40p35	Forward	1. GCAGTAGCAGTTCCCCTGAC 2. GCCCTCCTAAACCACCTCAG
	Reverse	1. CCTGGCAGGACACTGAATACT 2. CATCTGTGGTCTTCAGCAGG

2.4.3.1 Rescue of recombinant VSV-mIL-12

Recombinant VSV-mIL-12 was rescued as described previously [372]. Only the V3 construct could be successfully rescued. Briefly, QM5 cells were infected with the modified vaccinia virus Ankara strain encoding T7 RNA polymerase (MVA-T7). Two hours post infection, MVA-T7 was removed and QM5 cells were transfected with V3 genome plasmid along with the helper plasmids pBS-N, pBS-P, and pBS-L at a ratio of 2:2:1.25:0.25 µg, respectively, using Lipofectamine 2000 (Invitrogen). The transfection mix was replaced by fresh medium 6 hours post incubation. Two days later, the cell culture supernatant was harvested and filtered through 0.22 µm filter to obtain MVA-T7 free supernatant containing the rescued VSV-IRES-mIL-12 virus. This supernatant was then passaged on Vero cells, amplified and plaque purified thrice to obtain recombinant VSV particles.

To confirm the recovery of VSV-IRES-mIL-12, viral plaques were propagated on Vero cells and 24 hours post infection cell culture supernatant was analysed for mIL-12 by ELISA (Invitrogen). Vero cells were harvested for RNA extraction using RNeasy Plus Mini kit (Qiagen). One µg of total RNA was used to prepare cDNA using advanced

cDNA synthesis kit (Wisent Bio). Primers complimentary to the insert were used to generate cDNA amplicons by PCR, and were later Sanger sequenced (Table 2).

2.5 PCR Conditions

PCR reactions were performed using Phusion Hot Start II DNA Polymerase (Thermo Scientifc) as per manufacturer's instructions. PCR amplified products were analysed using DNA agarose gel (1% agarose; 1X TAE buffer; 90 V; 45 min; RedSafe DNA dye (ABM)). Experiments involving extractions of amplified DNA products from gel followed similar conditions, except a 0.8% agarose gel was used, and amplified products were visualized using a UV transilluminator. DNA bands were excised using a scalpel blade and extractions were performed using NucleoSpin® Gel and PCR Clean-Up gel extraction kit (Takara Bio, USA).

2.6 Production of VSV-GFP, VSV-p14, VSV-IL-15, VSV-IL-12 and MVA-T7

Vero cells were grown to 90% confluence in in T-175 flasks and infected with VSV viruses at a multiplicity of infection (MOI) of 1. Two days later, the supernatant containing amplified VSV virus was harvested and centrifuged (500*xg*, 10 minutes, 4 °C) to pellet cell debris. Infected cells were scrapped, resuspended in sterile PBS, lysed with 3 cycles of freeze-thaw cycles and pelleted (500*xg*, 10 minutes, 4 °C) to obtain virus supernatant. Cleared supernatant and virus suspension were combined, filtered through 0.22 µm filter and layered onto 20% sucrose solution in sterile PBS. The virus was then pelleted by ultracentrifugation (36,000 rpm, 1.5 hrs, 4 °C) and resuspended in 15% glucose, aliquoted and stored at -80°C.

Amplification and purification of MVA-T7 viruses was similar to the VSV production system, as described above, with certain differences accounted below. Firstly, MVA-T7 viruses were propagated in QM5 cells. Secondly, virus suspension was layered onto a 36% sucrose solution in PBS. Thirdly, pelleted virus was resuspended in sterile 1mM Tris pH9.0 buffer.

2.7 Plaque assay

In a 12-well cell culture plate, $2x10^5$ Vero cells were seeded per well and cultured into confluent monolayers. Next day, 10-fold serial dilutions (10^{-7} to 10^{-11}) of the virus

stock in cold serum-free DMEM were prepared and 200 µL of each dilution was used to infect Vero cells for 2 hours in duplicates with gentle shaking every 15 minutes. Post infection, virus was removed, and cells were overlayed with 1mL of 1% agarose solution (3.75 mL of 4% agarose in DMEM, 750 µL of FBS, and 10.5 mL of DMEM). The overlayed plate was inverted upon agarose solidification and incubated undisturbed for 2 days. To fix the cells, 1 mL of 10% formaldehyde was added to each well. After 1 hour, agar plugs were gently removed, and cells were stained with 1% crystal violet (Sigma Aldrich). Viral titer determined by multiplying the average number of plaques at a given dilution with the inverse of total dilution factor using the below formula.

$$\text{Virus Titer (PFU/mL)} = \frac{\text{Average number of plaques at a given dilution}}{\text{Inoculum volume (mL)} \times \text{given dilution}}$$

2.8 Bone marrow derived dendritic cells

Wild type C57BL/6 mice were anesthetized using 2-3% inhaled isoflurane and euthanized by cervical dislocation. Under sterile conditions, femur and tibia were harvested after stripping off the skin and muscle tissue. A 30 mL syringe containing DC medium (RPMI 1640 supplemented with 10% FBS, 2-mercaptoethanol (20 µM), sodium pyruvate (1 mM; Gibco), MEM non-essential amino acids (1x; Corning Life Sciences) and penicillin/streptomycin (100 units/ml - 100µg/ml; HyClone)) and a 30-gauge needle was used to flush bone marrow through a 40-micron nylon cell strainer to collect cell suspension in a 50 mL conical tube. The cell suspension was then pelleted by centrifugation (300 x g, 8 minutes, room temperature) and resuspended in 5 mL of cold ammonium chloride buffer for 30 seconds to lyse the red blood cells, followed by neutralization with 5 mL of DC medium. The cell suspension was again pelleted and resuspended in 15 mL DC medium supplemented with GM-CSF (40 ng/mL; PeproTech) and IL-4 (10 ng/mL; PeproTech). The cell suspension was then evenly distributed into 3 wells of a 6-well cell culture plate and incubated in a humidified incubator (37 °C; 5% CO_2) for 3 days. On day 3, fresh DC medium (5 ml) supplemented with GM-CSF (40 ng/mL) and IL-4 (10 ng/mL) was added to each well. On day 5, non-adherent cells were harvested, resuspended into 15 mL DC-medium supplemented with 20 ng/ml GM-CSF and cultured into new wells. On day 6, an additional 1 mL of DC medium supplemented

with DCs 20 ng/ml GM-CSF were added to the cells. On day 7, DCs were loaded overnight with α-GalCer (0.4 μg/ml; DiagnoCine LLC) and harvested the following day for *in-vivo* NKT activation experiments.

2.9 ID8 tumor model

C57BL/6 mice were inoculated (i.p.) with $3x10^6$ ID8 ovarian cancer cells at day 0, and at days 9, 11, and 13, mice were injected (i.p.) with VSV-GFP, VSV-p14, VSV-IL-15 or VSV-IRES-mIL-12 (5×10^8 PFU/mouse). On day 14, mice received 6×10^5 (i.p.) α-GalCer-loaded DCs for NKT cell activation; followed by 3 injections (i.p.) of α-PD-1 or isotype IgG (300 μg) on days 17, 24 and 30. Ascites development was monitored for survival experiments. For immune phenotyping experiments, ascitic and spleen tissues were harvested and analysed 7 days post NKT cell activation.

2.10 Immune phenotyping

C57BL/6 mice were inoculated ip. with 3×10^6 ID8 cells and treated with either NKT activation therapy alone or in combination with VSV-GFP or VSV-p14. Twenty-one days post implantation, ascites and disaggregated spleen cells were harvested and resuspended in cold RBC lysis buffer (150 mM NH_4Cl; Sigma-Aldrich) for 5 minutes, neutralized with equal volume of FACS (2% FBS in PBS) buffer and pelleted by centrifugation (300xg, 10 minutes, 4 °C). Ascitic and splenic cells were resuspended into 0.5 mL and 5 mL of the FACS buffer, respectively, and counted using a hemocytometer. Cells were processed for flow cytometry.

2.11 Flow cytometry

Prior to staining, cells were pre-incubated with anti-CD16/32 for 20 minutes to block non-specific binding, followed by a 20 min incubation with Brilliant Violet-421 (BV) conjugated-fixable viability dye (FVD; Clone HMN1-12; eBioscience) to distinguish live from dead cells. The following antibodies were purchased from eBioscience (San Diego, CA), BioLegend (San Diego, CA), or BD Biosciences (Mississauga, ON): BV510-anti-CD45.2 (Clone 30-F11); BV605-anti-CD8α (Clone 53-6.7); BV785-anti-PD-1 (Clone 29F.1A12); Fluorescein isothiocyanate (FITC) conjugated-NK1.1 (Clone 29F.1A12); phycoerythrin (PE)-conjugated CD44 (Clone

IM7); Peridinin chlorophyll protein-Cyanine5.5 (PerCP-Cy5.5) conjugated-TCRβ (Clone H57-597); Alexa Fluor 700 (AF700) conjugated CD4 (Clone RPA-T4); APC-eFluor780-anti-CD69; FITC-anti-Ly-6C (Clone AL-21); PE-anti-CD86 (Clone GL-1); PerCP-Cy5.5-anti-CD19 (Clone 1D3); Phycoerythrin-Cyanine7 (PE-Cy7) conjugated-CD11b (Clone M1/70); Allophycocyanin (APC) conjugated-Ly-6G (Clone RB6-8C5); AF700-anti-MHC-II (Clone M5/114.15.2); APCe-Fluor780-anti-CD11c (Clone N418); PerCP-Cy5.5-anti-CD25 (Clone 3C7); BV650-anti-IFNγ (Clone XMG1.2); PE-anti-Foxp3 (Clone FJK-16s); APC-anti-CD62L (Clone MEL-14); BV785-anti-CD44 (IM7); FITC-anti-TCRβ (Clone H57-597). NKT cells were identified using APC conjugated CD1d tetramer loaded with the α-GalCer analog PBS57 (National Institute of Allergy and Infectious Disease Tetramer facility, Emory University Vaccine Centre at Yerkes, Atlanta, GA). Intracellular staining of IFN-γ and Foxp3 molecules was performed using the Cytofix/Cytoperm Plus kit (eBioscience, San Diego CA). Flow cytometry data acquisition was performed using a 3 laser BD FACS Celesta with BD FACSDiva software. Flow cytometry data was analyzed using FlowJo V10 software.

2.12 Immune function assays

To evaluate whether VSV-GFP treatment alone and in combination with NKT cells activation could induce a long-term adaptive response, mice were re-challenged with ID8 cells and monitored for tumor growth. Fifty days later, mice were euthanized and splenocytes harvested as described above. ID8-specific cytolytic activity was examined by co-culturing $1.5x10^4$ splenocytes in a 1:1 ratio with CellTrace Violet (Invitrogen)-labelled ID8 cells in a complete RPMI medium for 18 hours. Following incubation, cells were stained with APC-Annexin V and 7-amino-actinomycin D (7-AAD; Invitrogen) and immediately analyzed using flow cytometry to determine apoptotic ID8 cells.

To further characterize immune activation associated with the above splenocyte-ID8 co-culture assay, cytokine levels were measured by an enzyme- linked immunosorbent assay (ELISA) using murine IFNγ (eBioscience) and IL-4 (Invitrogen) kits as per the manufacturer's instructions. To do this, 1 million splenocytes from above experiment were co-cultured in a 1:1 ratio with ID8 cells in a complete RPMI medium.

Supernatants were collected at 12-, 24-, 36- and 48-hours, centrifuged (300*xg*, 10 minutes) to remove cell debris. Cleared supernatants were aliquoted, stored at -80°C and later analysed for IFNγ and IL-4 cytokine levels.

2.13 Murine IL-12 detection

To determine the production and concentration of mIL-12 secretion after infecting Vero and ID8 cells with VSV-IRES-mIL-12, a murine IL-12 ELISA kit (Invitrogen) was used as per the manufacturer's instructions.

2.14 Apoptosis assay

ID8, B16, LLC, 4T1 and Pan02 cancer cells were seeded (5×10^3 cells/100 µL medium/well) in 96-well plates and incubated overnight. Next day, cells were infected with 100 µL of virus at an MOI for 1 for 24 hours. Cells were stained with APC-Annexin V and 7-AAD (Invitrogen) and immediately analyzed using flow cytometry.

2.15 Cell viability assay

To evaluate the cytolytic effects of VSV variants on different cancer cell lines, MTT assays (Life Technologies) were performed. MTT compound consists of tetrazolium rings that are cleaved by mitochondrial dehydrogenase from viable cells resulting in the formation of purple formazan crystals, that could be quantified photometrically. ID8, B16, LLC, 4T1 and Pan02 cancer cells were seeded (5×10^3 cells/100 µL medium/well) in 96-well plates and incubated overnight. Next day, cells were infected with 100 µL of virus at varying MOI for 24 and 48 hours. Two hours prior to the endpoint, 20 µL of MTT solution (5 mg/mL) was added to each well. Post incubation, cells were pelleted by centrifugation (1400xg, 5 minutes, 4 °C) and supernatant was discarded. Formazan crystals were dissolved upon addition of 100 µL of DMSO to each well and left on the orbital shaker for 10 minutes. Formazan concentration was determined at an optical density of 570 nm using an Epoch microplate spectrophotometer (BioTek). Assays were performed in triplicate wells for each condition and the mean of the control was standardised to 100% cell viability. Cell viability was calculated using the equation below.

$$\text{Viable cells (\%)} = \frac{\text{Experimental absorbance value at 570 nm}}{\text{Control absorbance value at 570 nm}} \times 100$$

2.16 Statistical analysis

Data in this body of work is expressed as mean ± standard error of the mean and statistical significance was set at $p < 0.05$. Survival data was analyzed by log-rank (Mantel–Cox) test. A non-parametric two-tailed Mann-Whitney U test was used to compare between two data groups. Comparisons between more than two data groups were made using a Kruskal-Wallis non-parametric ANOVA with Dunn's post-test. Statistical analyses were carried out using GraphPad Prism 8.

CHAPTER 3: RESULTS

3.1 Combining VSV-p14 or VSV-GFP with NKT cell activation therapy to target ID8 ovarian carcinoma

Our laboratory has previously established that NKT cell activation and VSV-GFP oncolytic virotherapy as standalone treatments improve survival outcomes in the mouse model of ID8 ovarian cancer [166]. Combination of these two treatments further enhanced survival [166]. In this study, I sought to investigate whether VSVΔM51 engineered to express the p14 FAST protein from reptilian reovirus could provide superior tumor protection either as a standalone treatment, or in combination with the NKT cell activation therapy and anti-PD-1 checkpoint blockade.

In-vitro infection of Vero cells with VSV-p14 has been previously shown to increase viral spread and induce superior cytolytic activity than VSV-GFP [314]. In addition, our laboratory has also reported improved survival outcomes in primary metastatic 4T1 breast and CT26 colon cancer mouse models using VSV-p14 [314]. We hypothesized that VSV-p14 would also elicit increased survival efficacy over VSV-GFP in the murine ID8 ovarian cancer model.

In our preliminary study, monotherapy treatments with VSV-GFP, VSV-p14, α-GalCer-loaded DCs or anti-PD-1 significantly increased the overall survival of the mice compared with untreated mice (Figure 4A, B). Although VSV-p14 performed slightly better than the VSV-GFP as a standalone treatment, survival outcomes significantly improved in mice treated using VSV-p14 in combination with NKT cell activation therapy. Additional treatments with anti-PD-1 blockade in mice previously treated with the VSV-p14 and NKT activation combination therapy further enhanced overall survival. Interestingly, VSV-GFP treated mice did not reach the survival threshold as established in ID8 tumor model in our previous report, in which at least 50% of the mice survived until day 50 [166]. Additionally, survival outcomes obtained for NKT cell therapy treated mice remained similar to the combined VSV and NKT cell therapy, indicating reduced efficacy of VSV-GFP. To address this inconsistency, VSV-GFP and VSV-p14 viral stocks used for this study were examined by plaque assays and titer loss was observed with long-term storage of viruses (>2 years). Recalculated viral titers of VSV-GFP and

VSV-p14 delivered were found to be suboptimal 1.1×10^5 PFU and 3×10^5 PFU, respectively. Interestingly, even at suboptimal doses VSV-p14 yielded superior survival protection over VSV-GFP. It is possible that increased replication kinetics of VSV-p14 may have compensated for reduced virus dose.

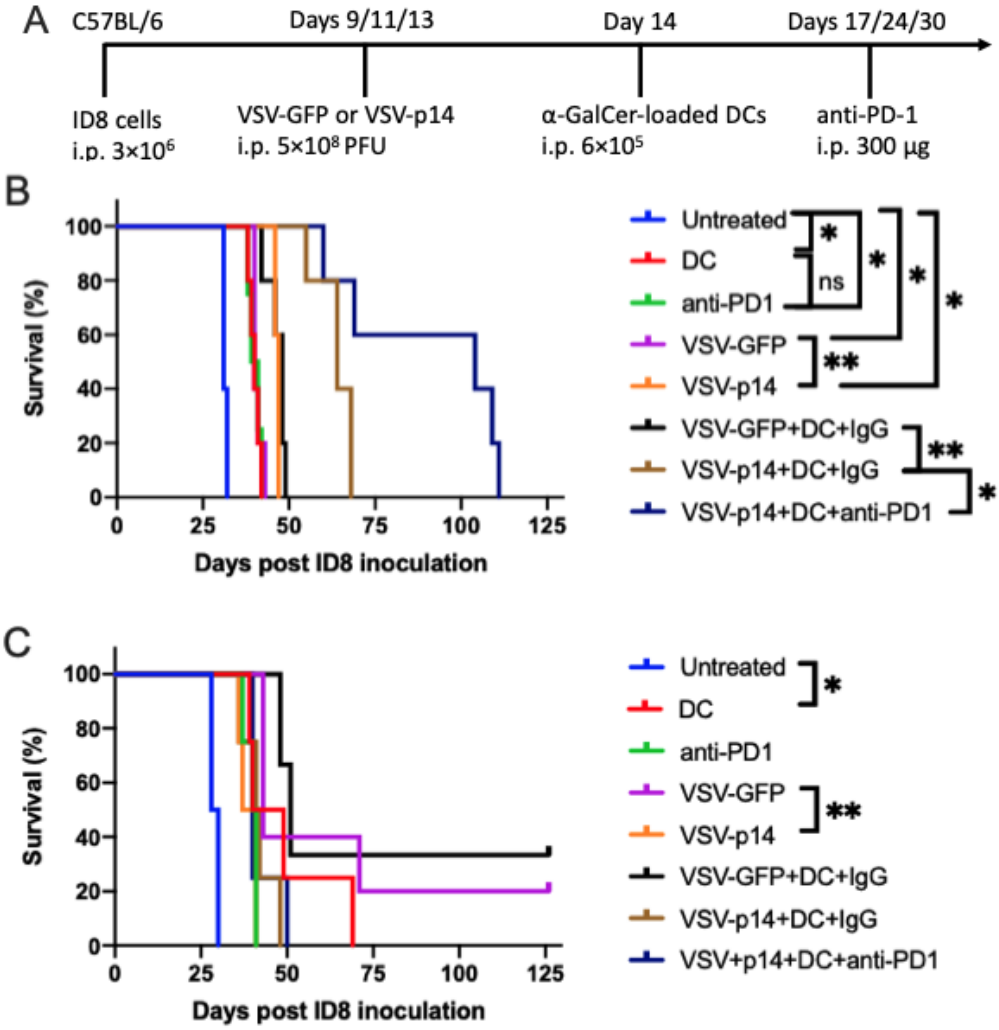

Figure 4 Targeting ovarian cancer with combined NKT cell activation therapy and VSV-p14 or VSV-GFP oncolytic virotherapy. (A) Schematic of treatments delivered in ID8 ovarian cancer mice model. Mice were intraperitoneally (i.p.) inoculated with 3 x 10^6 ID8 ovarian carcinoma cells. Mice received i.p. injection of either VSVMΔ51-GFP or VSVMΔ51-p14 (5 x 10^8 pfu) on days 9, 11 and 13. A single dose of α-GalCer loaded DC's (6 x 10^5 cells, i.p.) was delivered on day 14 for NKT cell-activation. Three doses of anti-PD-1 treatments was given on days 17, 24 and 31 (100 µg, i.p.). (B) and (C) reflect independent survival studies that were performed using different batches of viruses. Kaplan Meier curves were generated to assess survival curve using Log-rank (Mantel-Cox) test following treatments with α-GalCer-loaded DC's or α-PD-1 alone or in combination with VSVMΔ51-GFP or VSVMΔ51-p14 (n = 5). ns = non-significant, *P<0.05, **P<0.01.

To address above inaccuracies in our preliminary study, a similar survival experiment was conducted using the new viral stocks (Figure 4A, C). Survival outcomes obtained for mice treated with anti-PD-1 or NKT activation monotherapies were found to be consistent with our previous observation (Figure 4B, C). However, VSV-GFP individual treatments and in combination with NKT immunotherapy were found to perform better than VSV-p14 (Figure 4C). These observations were surprising given that VSV-p14 has been shown to be effective against many types of tumors. At this point, therapeutic efficacy of VSV-p14 in ID8 model yet remained elusive, and we suspected that the virus might have lost its oncolytic potency over repeated passages likely due to presence of an evolved VSV-p14 serotype with suboptimal fitness.

In addition to discrepancies observed with VSV-p14 treatments, survival outcomes observed for α-GalCer loaded DC treatments were also found to vary in these studies (Figure 4B, C). In the second survival study (Figure 4C), ~25% of mice treated with standalone NKT cell activation exhibited longer survival than the first study, where similar treatments resulted in mortality around day 40. It is speculated that differences in culture conditions (e.g. variability in GM-CSF or IL-4 potency) might have influenced development of bone marrow derived DCs in either of these cases, leading to differing survival outcomes when used therapeutically for NKT cell activation. Additionally, GM-CSF could drive differentiation of mouse bone marrow monocytes into dendritic cells (DCs) or macrophages; and while DCs in suspension could easily be isolated from adherent macrophage population, factors such as age of mouse, serum, and experimental time setup for the DC generation could also influence purity and maturation of DCs [373]. In order to ensure equivalency across repeated BMDC cultures, flow cytometric immunophenotyping can be used to quantify the purity and maturation status of generated DCs.

3.2 VSV-IL-15 did not improve survival outcomes in the ID8 ovarian cancer model

Given that the targeted delivery of hIL-15 using an oncolytic VSV vector enhances VSV efficacy in the CT26 lung metastases model [313], we tested whether VSV-IL-15 improves VSV therapy in the ID8 ovarian carcinoma model either as a monotherapy, or

in combination with the NKT cell immunotherapy and anti-PD-1 checkpoint blockade (Figure 5A, B).

Monotherapy treatments with VSV-GFP, VSV-IL-15, α-GalCer-loaded DCs or anti-PD-1 significantly increased the overall survival compared to the control (Figure 5B). Approximately 70% of the mice treated with VSV-IL-15 either as individual treatments or in combination with the NKT cell immunotherapy and anti-PD-1 checkpoint blockades had to be sacrificed around day 50 due to increased incidences of hind limb paralysis, suggesting the possibility of virus induced neurotoxicity. However, these mice did not exhibit ascites buildup at sacrificed. These observations were surprising since VSV-IL-15 was engineered to express hIL-15 on a VSVΔM51 platform that is specifically designed to attenuate VSV induced host neuropathogenesis and required further investigation.

Although the combined VSV-GFP and NKT cell activation therapies improved overall survival than the standalone treatments, the addition of anti-PD-1 did not provide superior tumor protection (Figure 5B). Since only two mice received this triple combination therapy, additional experiments examining the therapeutic benefit of anti-PD-1 in combination therapies are needed.

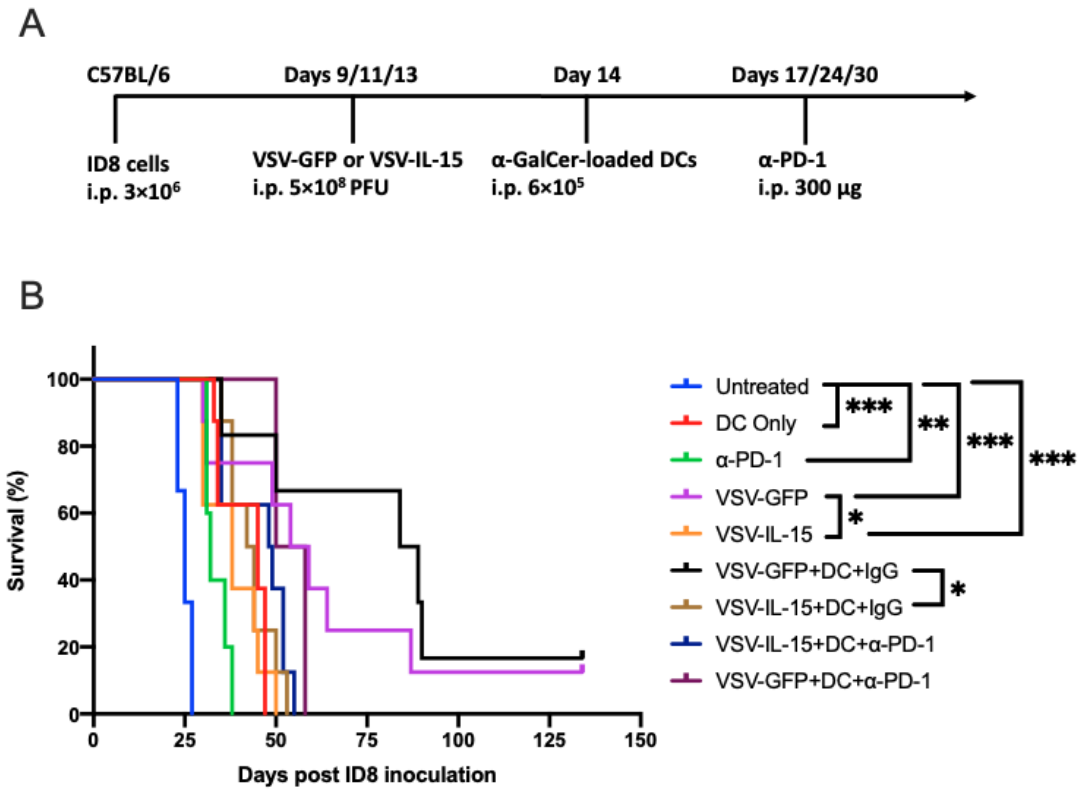

Figure 5 Targeting ovarian cancer with combined NKT cell activation therapy and VSV-IL-15 or VSV-GFP oncolytic virotherapy. (A) Schematic of treatments delivered in ID8 ovarian cancer mice model. Mice were intraperitoneally (i.p.) inoculated with 3 x10^6 ID8 ovarian carcinoma cells. Mice received i.p. injection of either VSVMΔ51-GFP or VSVMΔ51-hIL-15 (5x10^8 pfu) on days 9, 11 and 13. A single dose of α-GalCer loaded DC's (6x10^5 cells, i.p.) was delivered on day 14 for NKT cell-activation. Three doses of α-PD-1 treatments was given on days 17, 24 and 31 (100 µg, i.p. (B) Kaplan Meier curve was generated to assess survival curve using Log-rank (Mantel-Cox) test following treatments with α-GalCer-loaded DC's or α-PD-1 alone or in combination with VSVMΔ51-GFP or VSVMΔ51-hIL-15 (n = 7-10). ns = non-significant, *P<0.05, **P<0.01, ***P<0.001.

3.3 VSV-GFP and NKT cell activation increase *in-vitro* IFN-γ secretion in the re-challenged mice

To examine whether VSV-GFP treatment alone and in combination with NKT cells activation could induce durable anti-tumor immunity, 2 mice (1 per treatment group) that survived the first ID8 tumor inoculation from Figure 5B were re-challenged with ID8 cells (Figure 6A). Compared to the control, re-challenged mice did not develop

ascites and remained tumor-free, suggesting development of immune memory against the ID8 cells (Figure 6B).

Fifty days post re-challenge, mice were euthanized, and spleens were harvested (Figure 6A). Splenocytes were cocultured with CellTrace Violet-labelled ID8 cells at a 1:1 ratio for 18 hours to assess ID8-specific cytolytic activity. Apoptotic and dead ID8 cells were characterized by examining surface expression of Annexin V and 7-AAD uptake using flow cytometry (Figure 6C). Splenocytes obtained from the mouse that received VSV-GFP monotherapy prior to ID8 re-challenge increased 7AAD and Annexin V staining of ID8 cells compared to the naïve mouse - indicating presence of ID8-specific anti-tumor immunity. Furthermore, splenocytes obtained from the re-challenged survivor mouse that had received the VSV-GFP and NKT cell activation combination therapy exhibited superior killing of ID8 cells (Figure 6C). These findings indicate that both VSV-GFP and NKT cell activation therapy synergize to provide long-term anti-tumor immune memory.

The findings above were also found to agree with ID8-splenocytes co-cultures examining IFNγ and IL-4 production (Figure 6D). A significant increase in IFNγ production was observed in co-cultures containing VSV-GFP treated survivor mouse splenocytes compared to those from a naïve mouse. Splenocytes from the mouse that receive combination therapy elicited a further increase in IFNγ secretion in coculture. On the contrary, IL-4 levels were highest in naïve mouse 48 hours post incubation. The measured IFNγ and IL-4 levels were near the detection limits of the ELISA kits and therefore are subject to further validation.

Taken together, the *in-vitro* results obtained from our tumor re-challenge study has been met with limitations including small sample size (n=1/group) and low levels of detectable IFNγ and IL-4 providing only limited evidence to confirm VSV-GFP or NKT cell mediated development of ID8 immunity.

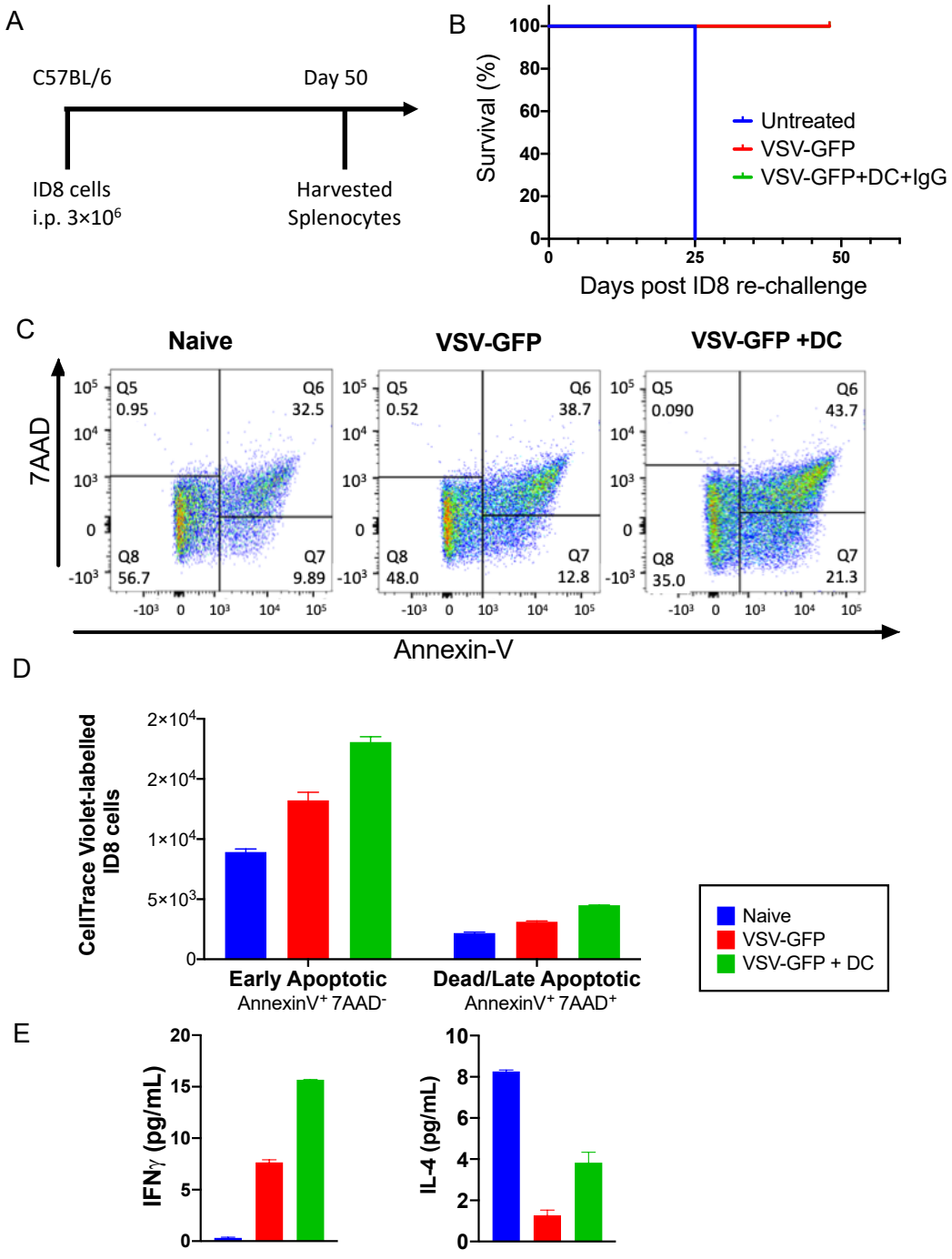

Figure 6 Combination therapy elicited increased IFNγ secretion in re-challenged mice. (A-B) Surviving mice from Figure 2 were re-challenged with 3 x10^6 ID8 cells (i.p.; n = 1 per group). Splenocytes were harvested 50 days post re-challenge and co-cultured in 1:1 ratio with CellTrace™ Violet labelled ID8 cells in duplicate for 18 hours. (C) and (D) Cytotoxicity was analyzed using flow cytometry immediately to assess annexin V/7-AAD staining. (E) IFN-γ and IL-4 levels were measured by ELISA. Data are representative of 2 internal replicates in (D) and (E).

3.4 Immune infiltration in ID8 ovarian cancer

I previously demonstrate that VSV-GFP oncolytic virotherapy when used alone and in combination with NKT cell activation therapy prolonged survival over the untreated control (Figure 4C); and while the therapeutic benefit of VSV-p14 as observed in a preliminary experiment, this could not replicated in successive experiment, I further sought to characterize the differential immune modulatory activities of VSV-GFP and VSV-p14 viral stocks previously used for survival studies, alone and in combination with NKT cell activation. Activation, expansion, and infiltration of $NK1.1^+$ NK cells, $CD1d\text{-}tet^+TCR\text{-}\beta^+$ NKT cells, $CD4^+$ and $CD8^+$ T-cells, $CD4^+CD25^+Foxp3^+$ Tregs, $CD11b^-CD11c^+MHC\text{-}II^+$ DCs, $Ly\text{-}6C^+$ monocytes and $Ly\text{-}6G^+$ granulocytes in ascites and spleen tissues were examined using flow cytometry.

3.4.1 NKT cell activation expands NKT cells in spleen and ascites

Our laboratory has previously demonstrated that NKT cell activation therapy significantly increased survival in 4T1 mammary and ID8 ovarian cancer mouse models [166]. To obtain insight into the immune response elicited by NKT cell activation in the ID8 model, the number and activation status of NKT cell populations were determined (Figure 7A, B). Mice that received α-GalCer-loaded DC monotherapy exhibited a significant increase in NKT cell counts in spleen and ascites compared to the untreated mice, whereas VSV-GFP and VSV-p14 individual treatments did not elicit NKT cell expansion. Interestingly, while the VSV-GFP and NKT cell activation combination therapy did not lead to NKT expansion, VSV-p14 and NKT cell combination treatments did exhibit NKT cell expansion response similar to levels observed for α-GalCer-loaded DC monotherapy.

NKT cells were further characterised based on surface expression of $CD4^+$ and $CD8^+$ (Figure 7 C). $CD4^+$ NKT cells secrete both Th1 and Th2 cytokines, whereas $CD4^-CD8^-$ NKT cells predominantly produce Th1-related anti-tumor cytokines [179,180]. While splenic NKT cells did exhibit an increase in $CD4^+$ NKT subpopulation in mice treated with GalCer-loaded DC, a corresponding reduction in DN subtype was not statistically significant. Thus, $CD4^+$ NKT cells constitute a significant proportion of expanded NKT cells in the spleen following NKT stimulation.

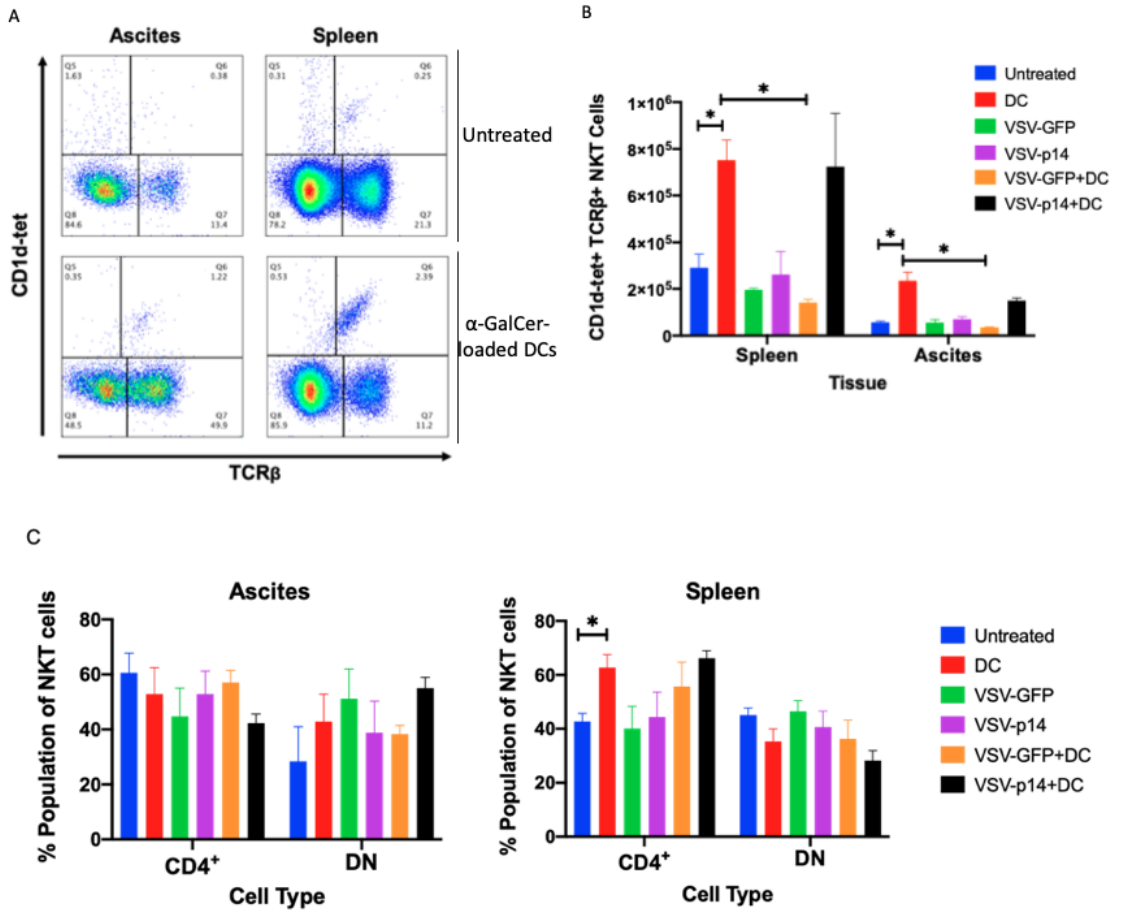

Figure 7 α-GalCer-loaded DCs induce NKT cell expansion in spleen and ascites. Mice received i.p. injection of either VSVMΔ51-GFP or VSVMΔ51-p14 (5 x 10^8 pfu) on days 9, 11 and 13 followed by a single dose of α-GalCer loaded DC's (6 x 10^5 cells, i.p.) on day 14 for NKT cell-activation. Spleen and ascites were harvested 7 days post treatment and (A) Total number of NKT cell counts (TCRβ$^+$CD1d tetramer$^+$) were examined in spleen and ascites using flow cytometry. (C) The frequency of CD4$^+$ and DN (CD4$^-$CD8$^-$) NKT subsets in spleen and ascites were also obtained. n = 2-5 per group, *P<0.05.

3.4.2 NKT Cell activation upregulates PD-1 expression in ascites

PD-1 deficient mice have been shown to resist development of NKT cell anergy in response to free α-GalCer [210]. To evaluate whether α-GalCer-loaded DCs elicited exhaustion of NKT cells, PD-1 cell surface expression was analyzed in ascites and spleen (Figure 8). Mice that received NKT cell activation as a monotherapy or in combination

with VSV-GFP exhibited upregulation of PD-1 on ascites NKT cells. Although VSV-p14 and NKT cell combination therapy also resulted into similar outcome, this did not reach statistical significance. In spleen, a modest increase in PD-1 expression was also observed in mice that received NKT cell activation monotherapy; the results, however, were not statistically significant when compared to untreated mice.

Our laboratory has previously reported that NKT cell activation achieved via α-GalCer-loaded DCs in tumor-free mice exhibit PD-1 expression levels similar to that of naïve mice in spleen and liver NKT cells [374]. These data implicate that α-GalCer-loaded DCs do not directly induce PD-1 upregulation, which is in line with other studies showing that α-GalCer loaded DCs prevent anergy induction [153]. The results from this study, however, show significant increase in PD-1 expression on NKT cells following α-GalCer-loaded DCs stimulation. It is possible that chronic antigen stimulation of NKT cells by endogenous ligands, for example, in the ascitic tumor microenvironment may have led to PD-1 upregulation.

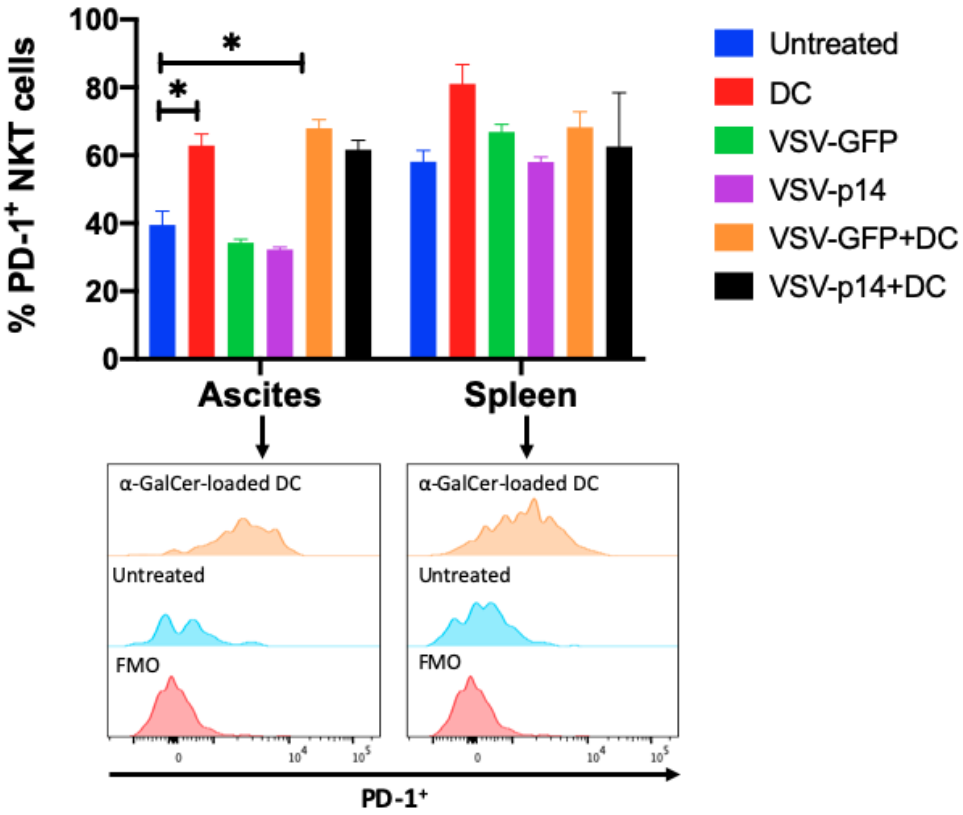

Figure 8 α-GalCer-loaded DCs induce PD-1 upregulation on NKT cells in ascites. (A) Frequency of PD-1$^+$ NKT cells (TCRβ+CD1d tetramer+) examined in ascites and spleen 7 days post stimulation with α-GalCer-loaded DCs (i.p. 6x10^5) using flow cytometry. Histograms depict upregulated surface expression of PD-1 compared to untreated mice and isotype control (FMO). n = 2-5 per group, *P<0.05.

3.4.3 NKT cell activation increases splenic dendritic cells

In order to evaluate the composition of major antigen presenting cells, total cell counts of CD11c$^+$MHC-II$^+$ dendritic cells were determined in spleen and ascites (Figure 9A, B). NKT cell activation led to significant expansion of the splenic DC population whereas this was not observed with the combined VSV-NKT cell therapies. A similar trend was also observed in ascites; except in mice that received combination therapy exhibited the least number of DCs in ascites. Activated DCs have a lifespan of a few days to weeks [375], thus, it is possible that some of the accumulated DCs detected in spleen and ascites are indeed α-GalCer-loaded DCs, used for activation of NKT cells.

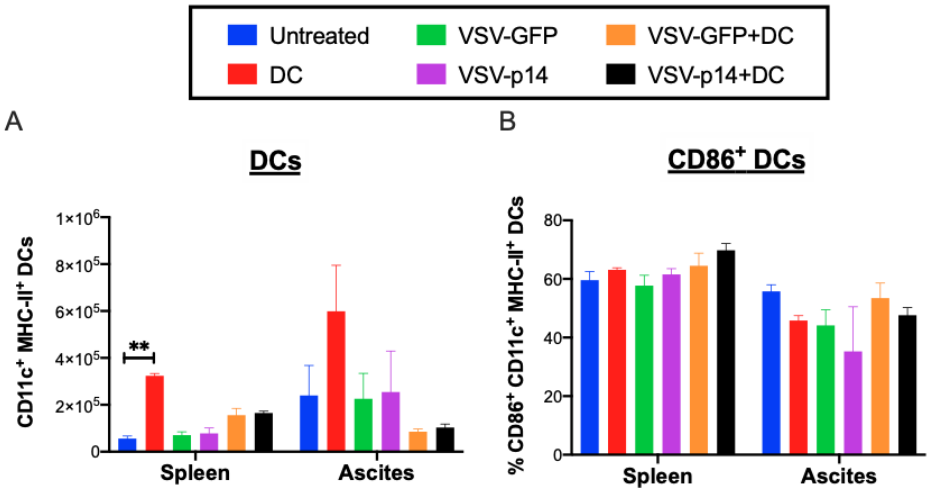

Figure 9 NKT cell activation induce DC expansion in spleen. Mice were treated as outlined in Figure 7. (A) Total cell counts of DCs ($CD11c^{+}MHC\text{-}II^{+}CD19^{-}CD11b^{-}$) in spleen and ascites was assessed. (B) Frequency of mature DC were characterized using CD86 activation marker. n = 2-5 per group, **P<0.01.

3.4.4 NKT cell activation expands splenic NK cells

To determine the extent of NK cell proliferation in response to NKT cell activation treatment alone or in combination with VSV-GFP or VSV-p14 virotherapy, NK cells from spleen and ascitic fluid were stained for $NK1.1^{+}$ surface marker. Following treatment with α-GalCer-loaded DCs, NK cells accumulated in spleen and ascites (Figure 10A). Interestingly, the ascitic NK cell counts in mice that received the combination therapy were lower than α-GalCer-loaded DC treatment alone. This suggests that the VSV treatments impeded NK expansion in ascites when used in conjunction with α-GalCer-loaded DCs.

In spleen, the combined VSV-GFP-NKT cell activation treatment also induced NK cell accumulation, but at levels similar to the NK cell counts obtained for mice treated with NKT cell activation alone. This demonstrates that the observed spike in NK cell count was likely due to α-GalCer-loaded DCs, and that the VSV treatments did not impact splenic NK cells count. Additionally, mice treated with only VSV-GFP or VSV-p14 viral treatments exhibited NK cell counts equivalent untreated tumor-bearing mice.

We next assessed NK cell exhaustion using PD-1 surface marker, but no significant trends were observed for either treatment type in spleen (Figure 10B). In ascites, the combined NKT cell therapy with VSV-GFP or VSV-p14 did result into lowest levels of exhausted NK cells, but the data did not reach significance.

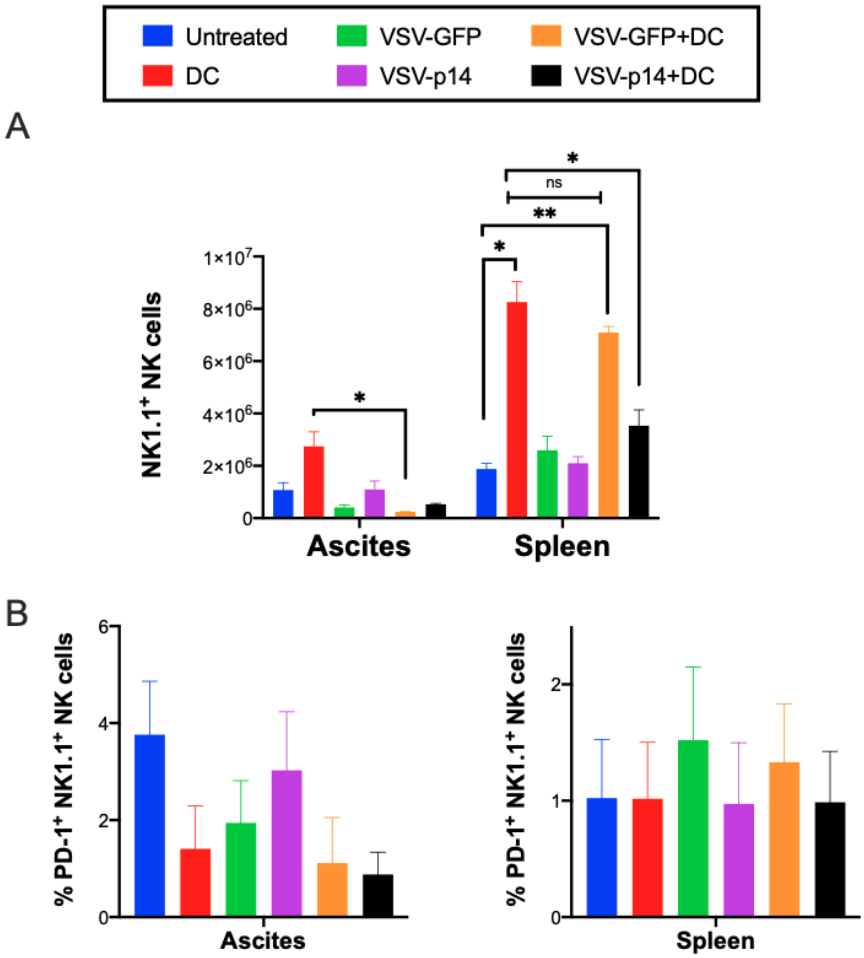

Figure 10 NKT cell activation induces NK cells expansion in spleen. Mice were treated as outlined in Figure 7. Total cell counts of (A) NK1.1$^+$ NK cells were determined in spleen and ascites and were gated to assess (B) surface expression of PD-1. n = 2-5 per group, ns = non-significant, *P<0.05, **P<0.01.

3.4.5 NKT activation induces T cells recruitment in ascites

To better understand the immune response elicited by T cells, we started by examining total TCR-β+ T cells in ascites and spleen (Figure 11A). Increased cell counts of total ascitic T cells were observed in mice treated with α-GalCer-loaded DC or VSV-

GFP monotherapies, compared to the untreated control. While VSV-p14 also induced a modest T-cell accumulation in ascites, albeit statistically insignificant, the accumulation was much lower than T-cell counts obtained for mice treated with VSV-GFP. The combined VSV-GFP and NKT-activation therapy resulted in maximal accumulation of T-cells. From the data obtained, it is difficult to ascertain whether the combined therapy elicited synergistic or additive effects on T-cell proliferation in ascites. No significant difference in splenic T-cell counts were observed across the treatment groups.

We next assessed the total number of $CD4^+$ and $CD8^+$ T lymphocytes in the spleen and ascites, and then determined the proportions of each type expressing CD44 memory and PD-1 activation/exhaustion markers (Figure 11 B-E). Compared to the control, all the treated mice, irrespective of the treatment type, exhibited similar levels of CD8+ T cell counts in ascites. However, only NKT cell activation and VSV-GFP therapy led to increase in CD4+ T cell counts in ascites. There were no significant differences in spleen.

We next determined the activation status of T-cell subtypes in spleen and ascites. Uniform frequencies of the CD44 memory marker were obtained for both CD4+ and CD8+ T cell subtypes across all the treated and untreated groups in spleen and ascites. The indicated levels are similar to those observed in untreated tumor-bearing mice, and thus CD44+ expression remained unmodulated regardless of the treatment type. In contrast to uniform CD44 expression across all T-cell subtypes or tissue origin, PD-1 expression was found to vary in ascitic T-cells. While elevated PD-1 expression levels were observed for CD8+ T cells in VSV-GFP treated mice, addition of NKT cell activation did not enhance nor limit PD-1 expression.

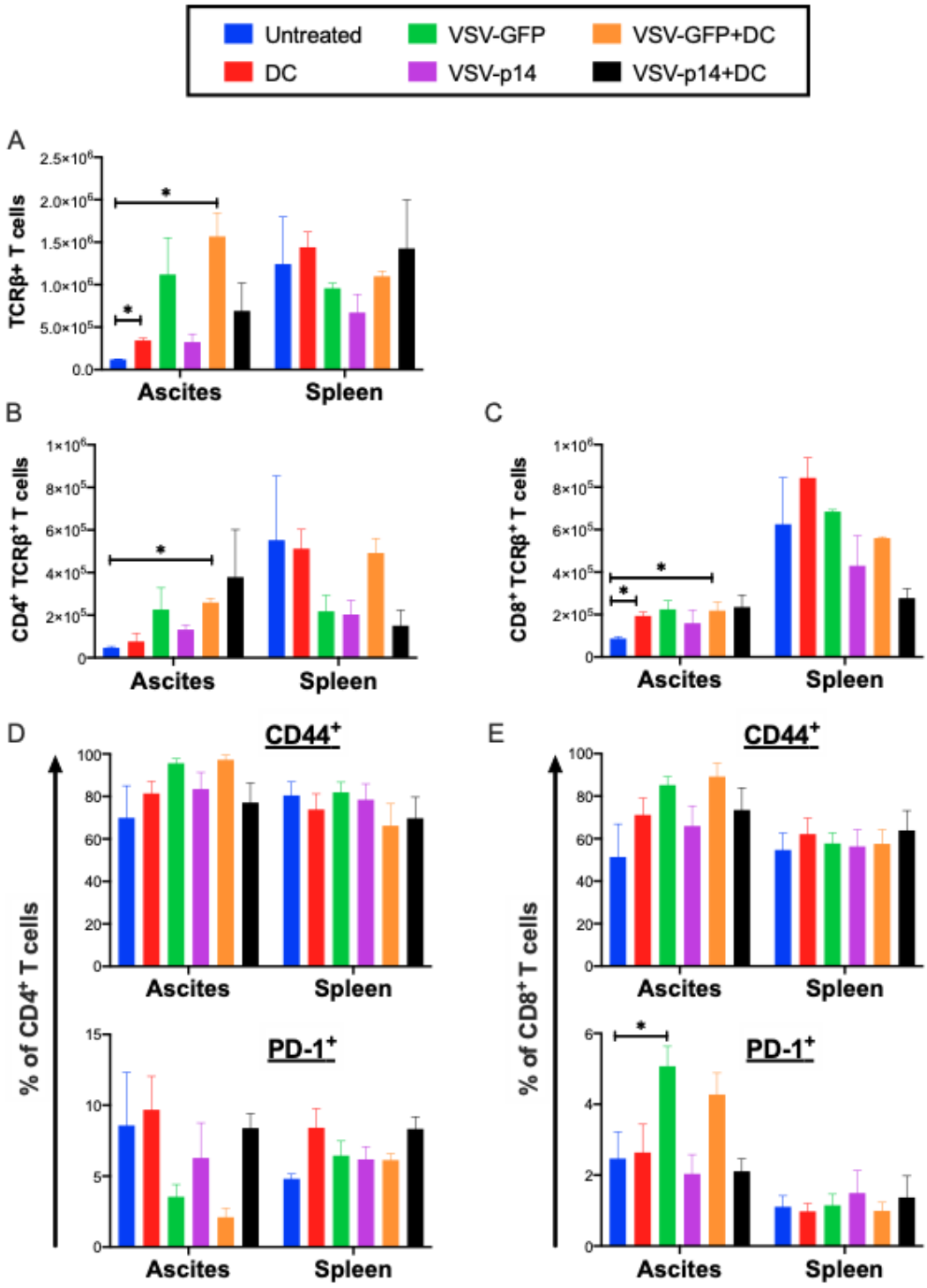

Figure 11 Characterization of TCRβ$^+$ T cells in ID8 ovarian cancer. Mice were treated as outlined in Figure 7. Total cell counts of (A) TCRβ$^+$ T cells were determined in spleen and ascites and TCRβ$^+$ T cells were gated to obtain (B) CD4$^+$ and (C) CD8$^+$ T cell counts. (D-E) Surface expression of CD44 and PD-1 on CD4+ and CD8+ T cells was also assessed. n = 2-5 per group, ns = non-significant, *P<0.05, **P<0.01.

3.4.6 Characterization of CD8+ T cells subsets

The CD8+ T cell population in spleen and ascites was further categorised into memory and naïve phenotypes based on the surface expression of CD44 and CD62L (Figure 12 A-B). Frequencies of $CD44^{-}CD62L^{+}$ naïve (T_N), $CD44^{+}CD62L^{+}$ central memory (T_{CM}), $CD44^{+}CD62L^{-}$ effector memory (T_{EM}) and $CD44^{-}CD62L^{-}$ double negative (T_{DN}) undifferentiated effector cells were obtained (Figure 12 A).

In ascites, the composition of T_N, T_{CM} and T_{EM} CD8+ T cell subsets in untreated mice were found to be uniformly distributed (≈20%), whereas T_{DN} cells constituted the dominating subset (≈35%). On the contrary, mice treated with VSV or α-GalCer-loaded DCs, either as monotherapy or in combination, exhibited a significant reduction in ascitic T_{DN} composition and elevated levels of the T_{CM} subtype. Most significant T_{CM} induction was observed in mice that received standalone NKT cell activation therapy. Standalone VSV-GFP treatments led to significant accumulation of T_{EM} cells in ascites whereas T_{EM} frequencies obtained in ascites of VSV-p14 treated mice were at par with the untreated control. Although VSV-GFP and NKT cell activation combination therapy exhibited maximal induction of the T_{EM} phenotype, no statistical significance was obtained when the combination therapy were compared to VSV-GFP monotherapy.

In spleen, maximal reduction in T_N cells was observed in mice treated with NKT cell activation therapy in comparison to all the treatment groups. These cells later acquired T_{EM} phenotype since the frequencies of T_{CM} and T_{DN} remained consistent in comparison to other treatment groups.

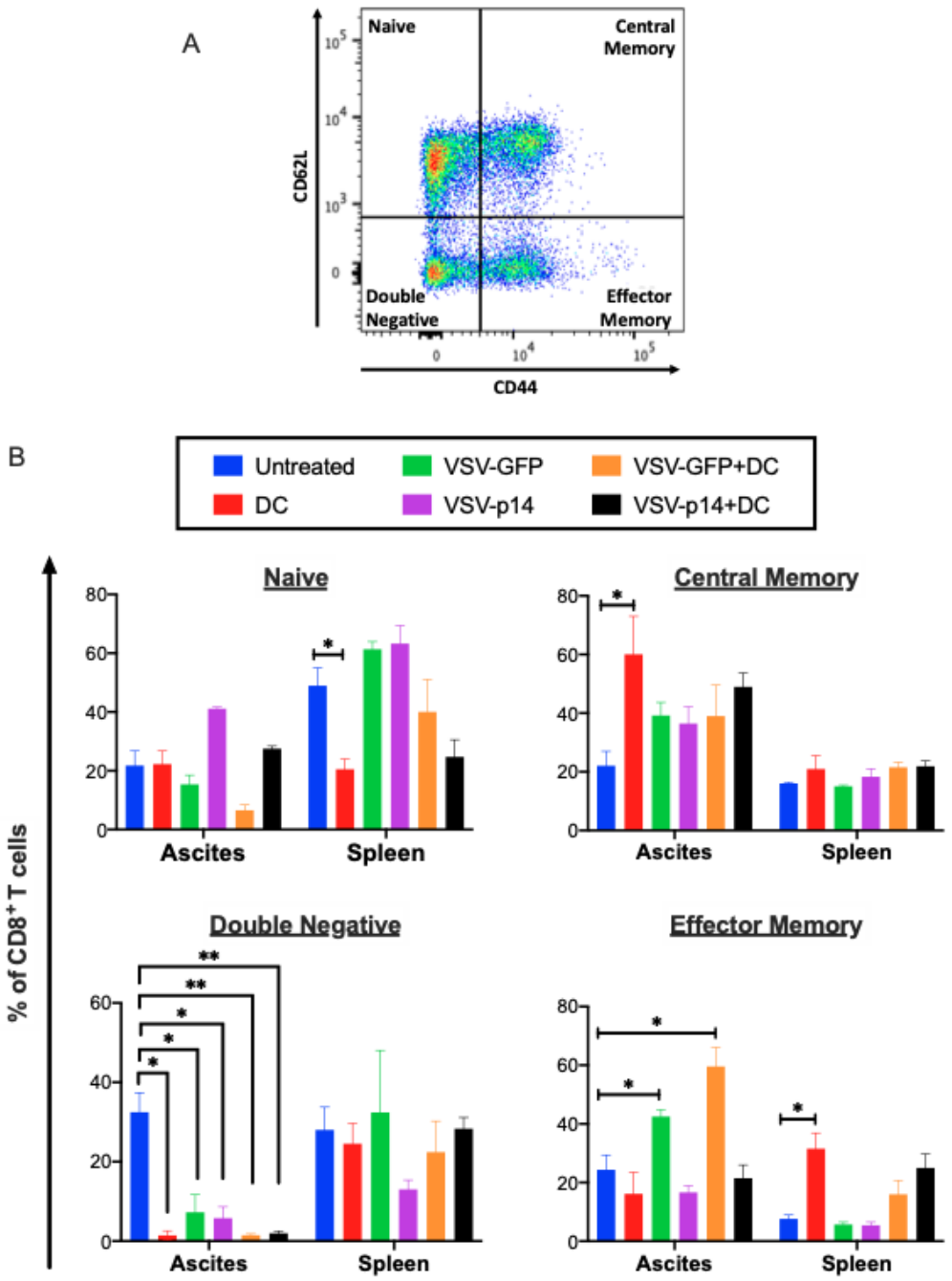

Figure 12 Characterization of CD8+ T cells based on surface expression of CD44 and CD62L. Frequencies of 4 distinct subsets of $CD8^+$ T cells from Figure 11 were gated: $CD44^-CD62L^+$ naïve, $CD44^+CD62L^+$ central memory, $CD44^+CD62L^-$ and $CD44^-CD62L^-$ double negative populations were assessed. n = 2-5 per group, *P<0.05, **P<0.01.

3.4.7 NKT cell activation decrease T-regs in ascites

To better understand immunosuppressive axis in the ID8 tumor model, we examined the cell counts of $Foxp3^+CD25^+CD4^+$ T-regulatory cells in ascites and spleen (Figure 13A, B). NKT cell activation led to a significant reduction of T-regs in ascites. Addition of VSV-GFP or VSV-p14, however, did not lead to a synergistic effect since cell counts obtained following NKT cell therapy monotherapy or in combination with VSV-GFP or VSV-p14 remained similar, suggesting that the Treg control was primarily mediated by ascitic NKT cells. Moreover, the VSV therapy did not impede NKT cell mediated Treg downregulation. In spleen, no significant difference was observed for T-regs amongst treatment groups, but untreated mice exhibited highest accumulation of Tregs.

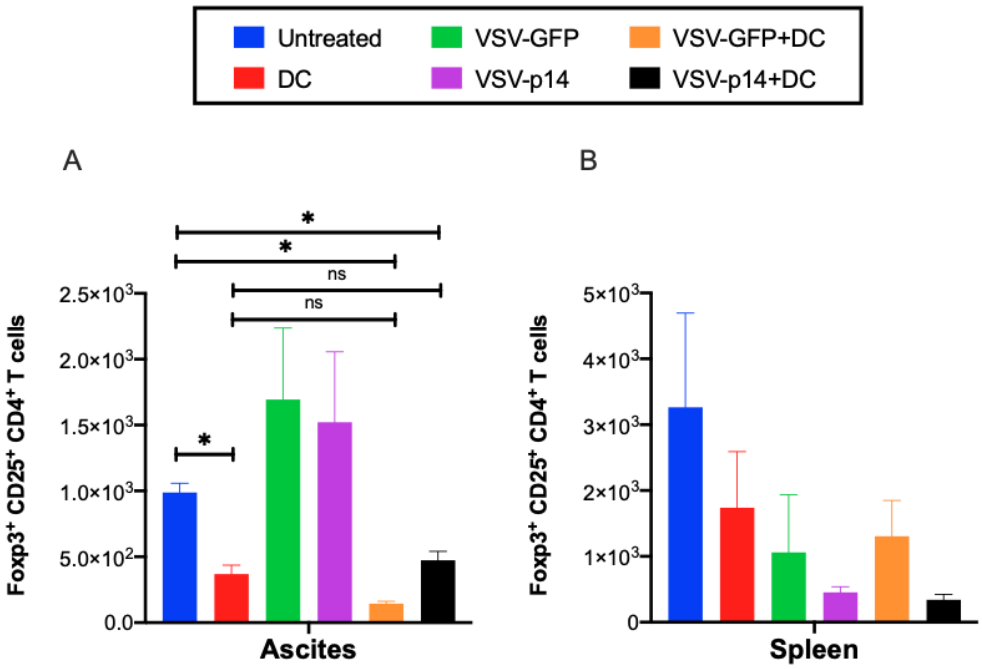

Figure 13 NKT cell activation reduce T-regs in the ID8 model. Total cell counts of $Foxp3^+CD25^+CD4^+TCR\beta^+$ regulatory T cells in (A) ascites and (B) spleen were obtained upon gating $CD4^+TCR\beta^+$ T cell population from Figure 11 and assessed. n = 2-5 per group, *P<0.05.

3.4.8 VSV-GFP increases granulocytic myeloid cells in spleen and ascites

VSV infections have previously been shown to recruit granulocytic neutrophils and MDSCs to the tumor bed [376]. While neutrophil infiltration has been associated with shutdown of tumor vascular and indirect killing of cancer cells, accumulation of MDSCs could negatively restrict VSV mediated anti-tumor mechanisms [377]. To better characterize whether VSV-GFP or VSV-p14 could induced infiltration of granulocytic cells in ID8 tumor model, $CD19^{-}CD11b^{+}Ly\text{-}6G^{+}$ granulocytic cells were examined in spleen and ascites (Figure 14A).

VSV-GFP treatments led to significant expansion of granulocytic cells in spleen and ascites. On the contrary, VSV-p14 treated mice had granulocytic cell counts relatively similar to the untreated tumor-bearing mice. In spleen, NKT cell activation also led to modest granulocyte infiltration, but the data did not reach significance. While the combined VSV-GFP and NKT cell therapy did lead to further accumulation of granulocytes over individual treatments, the data remained statistically insignificant. Nevertheless, it is likely that the combined treatments may synergize towards facilitating granulocyte infiltration. To determine whether the VSV-GFP induced expansion of granulocytic cells aids or hinders tumor control requires further examination of the $CD11b^{+}Ly\text{-}6G^{+}$ cell population using functional suppression assays.

We next assessed frequencies of monocytic $CD11b^{+}Ly\text{-}6G^{-}Ly\text{-}6C^{+}$ cells in ascites and spleen (Figure 14B). In the context of virus infection and tumor burden, $CD11b^{+}Ly\text{-}6G^{-}Ly\text{-}6C^{+}$ monocytes in some instances have been shown to prevent systemic spread of the virus and readily acquire immune stimulatory or regulatory functions and hence exhibit functional plasticity [378]. Similar to our previous observation with granulocytic myeloid cells, NKT cell therapy led to elevated $CD11b^{+}Ly\text{-}6G^{-}Ly\text{-}6C^{+}$ cells in spleen compared to untreated control, but remained statistically insignificant. In ascites, no statistically significant trend across treatment groups was observed.

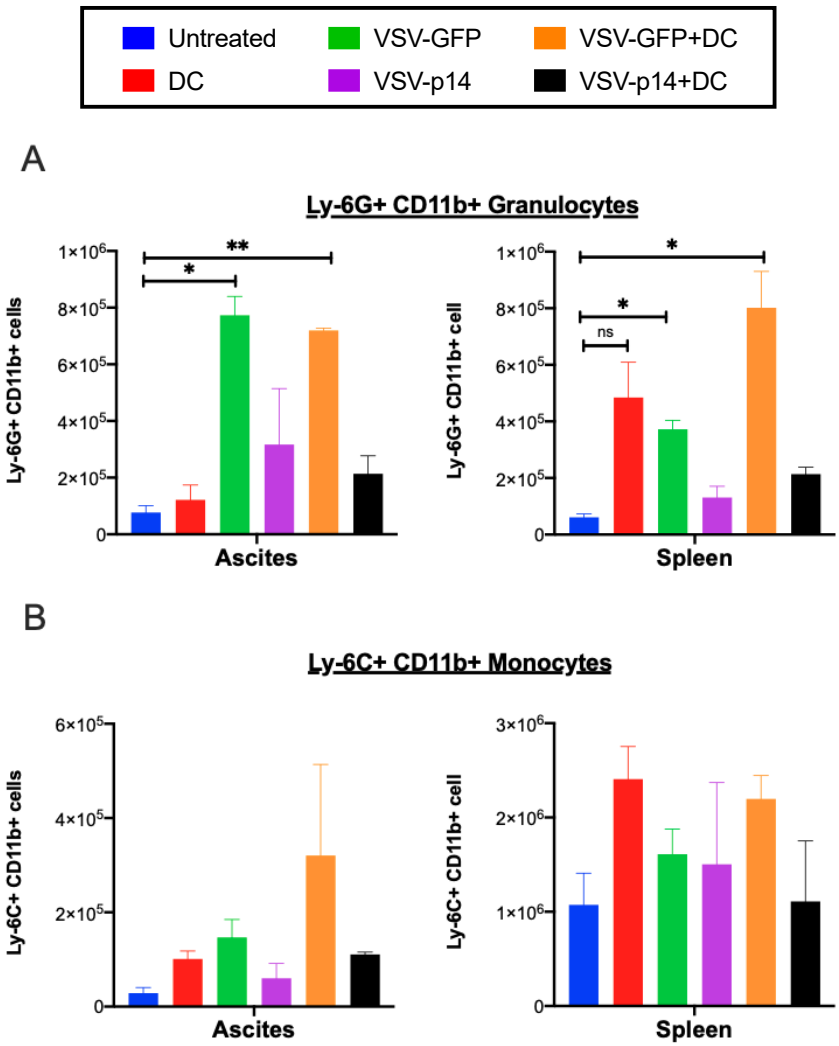

Figure 14 VSV-GFP increase granulocytic myeloid cells in spleen and ascites. Mice were treated as outline in Figure 7 and CD11b+ myeloid cells were gated to distinguish between cell counts of (A) Ly-6G+ granulocytic and (B) LY-6C+ monocytic subsets in spleen and ascites. n = 2-5 per group, *P<0.05, **P<0.01.

3.5 *In-vitro* characterization of cell viability by VSV-p14

One of the major objectives of this project was to test the oncolytic efficacies of VSV-p14 and VSV-IL-15 in the ID8 tumor model. *In-vivo* survival studies examining these recombinant viruses in this thesis demonstrated poor survival outcomes. While VSV-p14 failed to provide survival benefit, VSV-IL-15 treatments led to early development of hind limb paralysis and early termination of the study. Additionally, data from our immunophenotyping experiments examining VSV-p14 suggest suboptimal

induction of host tumor response in VSV-p14 treated mice compared to the responses elicited by VSV-GFP. Given that these viruses have been shown to provide superior survival benefits over VSV-GFP in other tumor models [314,379], we wanted to examine whether the observations in this project could be attributed to attenuation of oncolytic activity of the VSV-p14 or VSV-IL-15 viruses.

To characterize the oncolytic potency of VSV-GFP, VSV-p14 and VSV-IL-15, ID8 ovarian carcinoma and B16 melanoma cells were infected for 24 hours at varying multiplicities of infection (Figure 15). At an MOI of 1, VSV-IL-15 induced the greatest reduction in ID8 cell viability followed by VSV-GFP and VSV-p14, but the data did not reach statistical significance. Whether the reduced oncolytic potency of VSV-p14 is specific to ID8 cells or this observation could be attributed to the presence of defective interfering particles (DIPs) requires further investigation [380]. DIPs are viral mutants that fail to generate viable virus progenies, hinder propagation of replication competent viral particles, and usually accumulate over multiple viral passages [380]. All the examined viruses exhibited similar cytolytic activity in B16 melanoma cells.

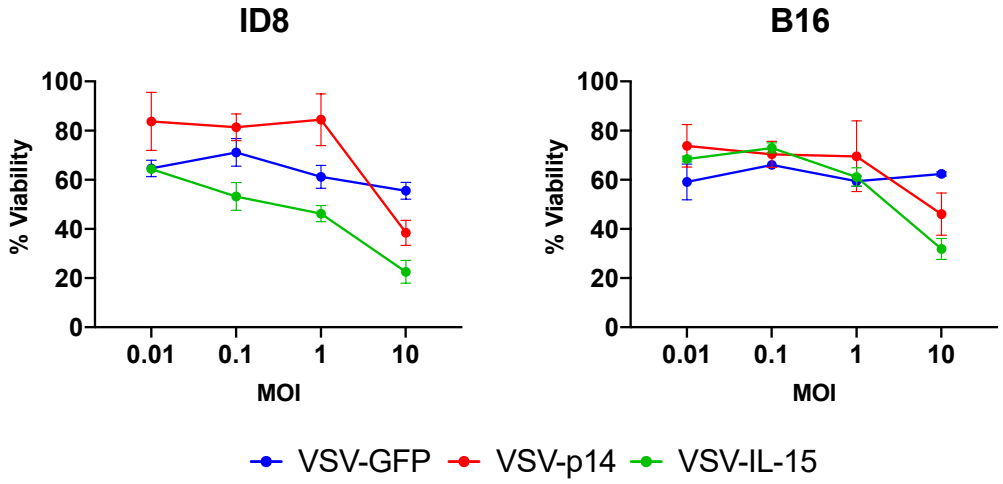

Figure 15 In-vitro viral cytotoxicity of recombinant VSV viruses. ID8 and B16 cell lines were infected with either VSV-GFP, VSV-p14 or VSV-IL-15 at various MOIs. Cell viability was assessed 24 hours pot infection using MTT viability assay and are expressed as the percentage of untreated control. Data representative as mean ± SEM. n = 2-4 per group.

3.6 Generation and *in-vitro* characterization of VSV encoding murine IL-12

An expression ready cassette containing an IRES sequence in frame with a single-chain murine IL-12 construct, composed of p35 and p40 subunits separated by an elastin linker, was incorporated into the pVSVΔM51-XN backbone generating the pVSVΔM51-XN-IRES-mIL-12 (VSV-IRES-mIL-12) oncolytic virus construct (Figure 16A).

To characterize the infectivity and cytotoxic potency of the recombinant VSV-IRES-mIL-12, five different tumor cell lines (ID8 ovarian carcinoma, B16 melanoma, 4T1 mammary carcinoma, Panc02 pancreatic carcinoma, LLC Lewis lung carcinoma), and Vero cells were infected at varying multiplicities of infection for 24 and 48 hours (Figure 16B, C). VSV-IRES-mIL-12 induced cytotoxicity in all the examined cell lines 24 hours post infection in a dose-dependent manner. Longer periods of infection, however, made differential sensitivity of tumor cells to the VSV-IRES-mIL-12 more apparent (Figure 13 B). Vero cells exhibited maximal viral oncolysis (48 hpi, MOI 0.01; Figure 13 C) which is likely attributed to the lack of interferon-dependent anti-viral mechanisms in Vero cells and hence increased susceptibility for VSV. In summary the *in-vitro* data demonstrates that the VSV-IRES-mIL-12 could infect and kill ID8 cells in addition to other cancer cell lines.

Insertion of the mIL-12 transgene did not impact replication kinetics of VSV-IRES-mIL-12 in either Vero or ID8 cells (Figure 16D, E). Single-step growth curves obtained for VSV-IRES-mIL-12 using either Vero or ID8 cells exhibited identical growth curves generated for the VSV-GFP and VSV-IRES-mIL-12 viruses.

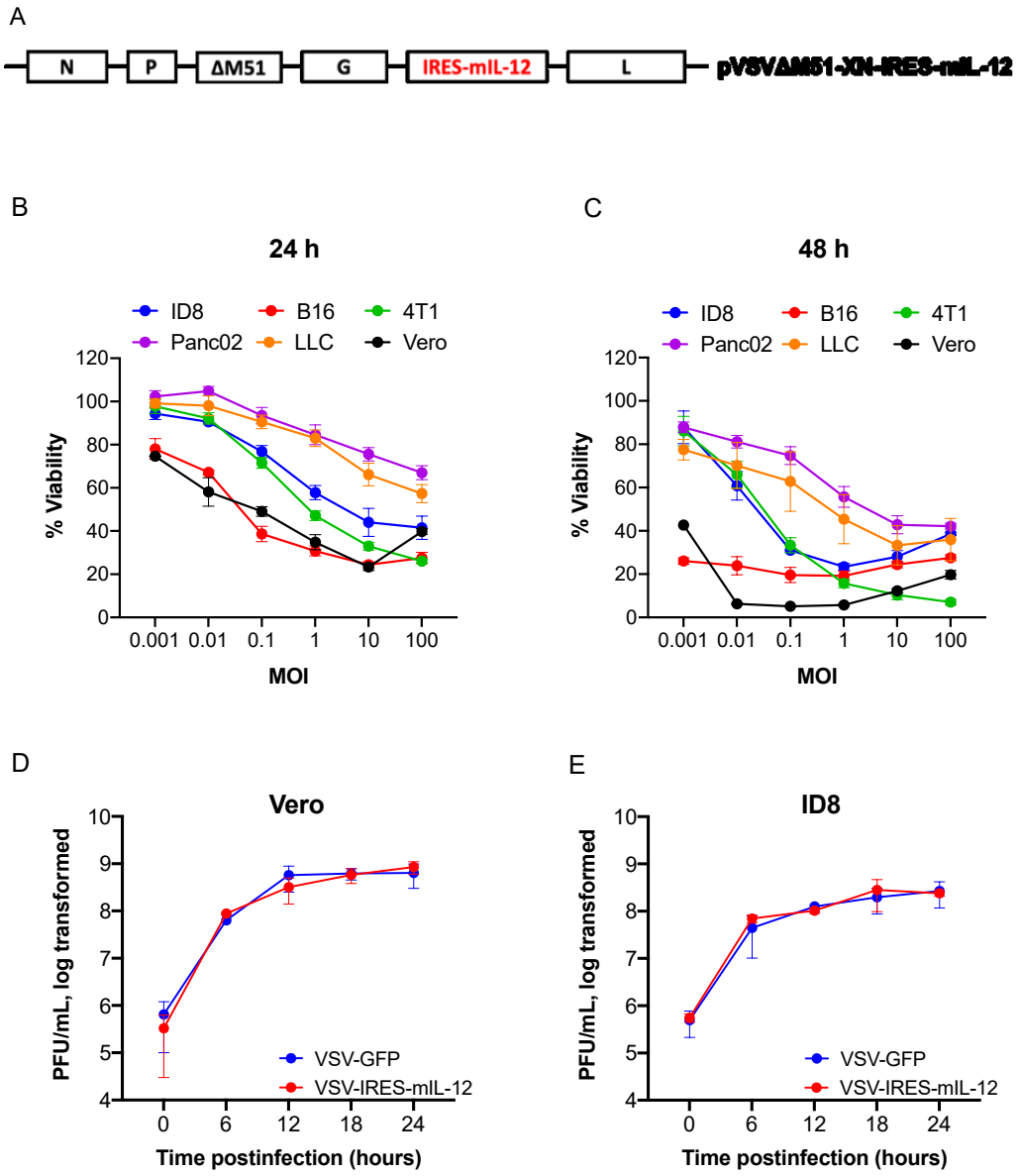

Figure 16 Construction of VSV-IRES-mIL-12. (A) Murine IL-12 was cloned into the VSVΔM51-XN backbone. (B-E) In-vitro viral cytotoxicity and replication kinetics of VSV-IRES-mIL-12. (B) ID8, B16, 4T1, Panc02, LLC and Vero cell lines were infected with VSV-IRES-mIL-12 for 24 and (C) 48 hours at various multiplicities of infection (MOI). Cell viabilities were analyzed using an MTT viability assay and are expressed as a percentage of the untreated control. Data in (B) and (C) is shown as ± standard error of the mean (SEM) and is representative of two independent experiments (n=2-4 per group). (D) Confluent monolayers of Vero and (E) ID8 cells were infected in duplicate with either VSV-GFP or VSV-IRES-mIL-12 at a MOI of 10 for 2 hours in serum-free medium. Supernatants were collected at indicated timepoints post infection, and virus titers were determined in duplicate by plaque assay on Vero cells. The mean ± SEM of log-transformed titers are shown.

To confirm transgene expression, culture supernatants obtained from Vero cells infected with VSV-GFP or VSV-IRES-mIL-12 at a MOI of 0.1 were harvested 12 hours post infection and analysed using ELISA (Figure 17 A). Supernatants obtained from VSV-IRES-mIL-12 infected Vero cells exhibited high levels of mIL12 secretion, compared to undetectable levels when infected with VSV-GFP. To ensure that murine IL-12 expression was also expressed and secreted by ID8 cells, confluent monolayers of Vero and ID8 cells were infected with VSV-IRES-mIL-12 at varying MOIs followed by supernatant harvest at indicated timepoints to determine IL-12 concentration by ELISA. The mIL-12 produced at any given MOI plateaued at 6,000 pg/ml 24 hours post infection in both Vero and ID8 cells (Figure 17 B and C).

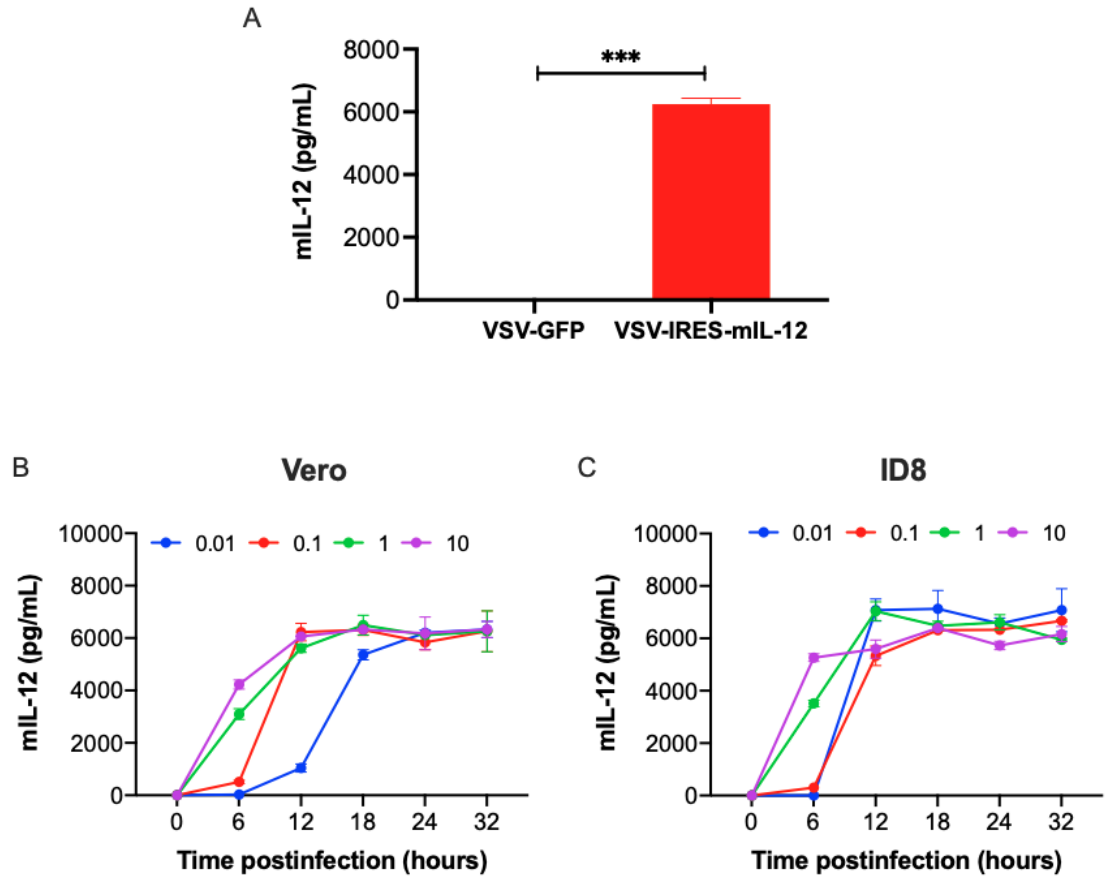

Figure 17 VSV-IRES-mIL-12 secretes mIL-12. (A) Supernatants from Vero cells infected with VSV-GFP or VSV-IRES-mIL-12 at a MOI of 0.1 for 12 hours were analysed using enzyme-linked immunosorbent assay (ELISA) to determine mIL-12 secretion and its concentration. Data represent values obtained from duplicate infections and is shown as ± standard error of the mean (SEM). ***P < 0.001 (B) Confluent monolayers of Vero and (C) ID8 cells were infected with VSV-IRES-mIL-12 at varying MOIs for 2 hours followed by supernatant harvest at indicated timepoints to determine IL-12 concentrations by ELISA.

3.7 VSV-IL-12 treated mice exhibited hind-limb impediments

Intratumoral delivery of mIL-12 via oncolytic virus is associated with improved survival in several pre-clinical tumor models [347–349,351]. This thesis utilized the VSV-ΔM51 oncolytic platform for targeted mIL-12 delivery to probe two research objectives: 1) to examine whether addition of IL-12 improved therapeutic efficacy of VSV and 2) whether local VSV-mIL-12 produced mIL-12 enhanced NKT cell activation, when combined with α-GalCer loaded DCs, leading to improved overall survival in ID8 tumor

model. While treatments with VSV-GFP increased survival compared to untreated control mice, addition of mIL-12 did not lead to superior survival benefit over VSV-GFP. The combined VSV-IL-12 and NKT cell therapy resulted in maximal survival outcome, however, no significant differences were noted compared to VSV-GFP-NKT cell combination therapy. Similar to VSV-IL-15, ~70% of mice treated with VSV-IL-12, either as monotherapy or in combination with α-GalCer loaded DCs, also presented with early end-points resulting from hind-limb impediments. Whether these observations are ID8 tumor specific or dose-dependent are subject to additional studies with increased sample size.

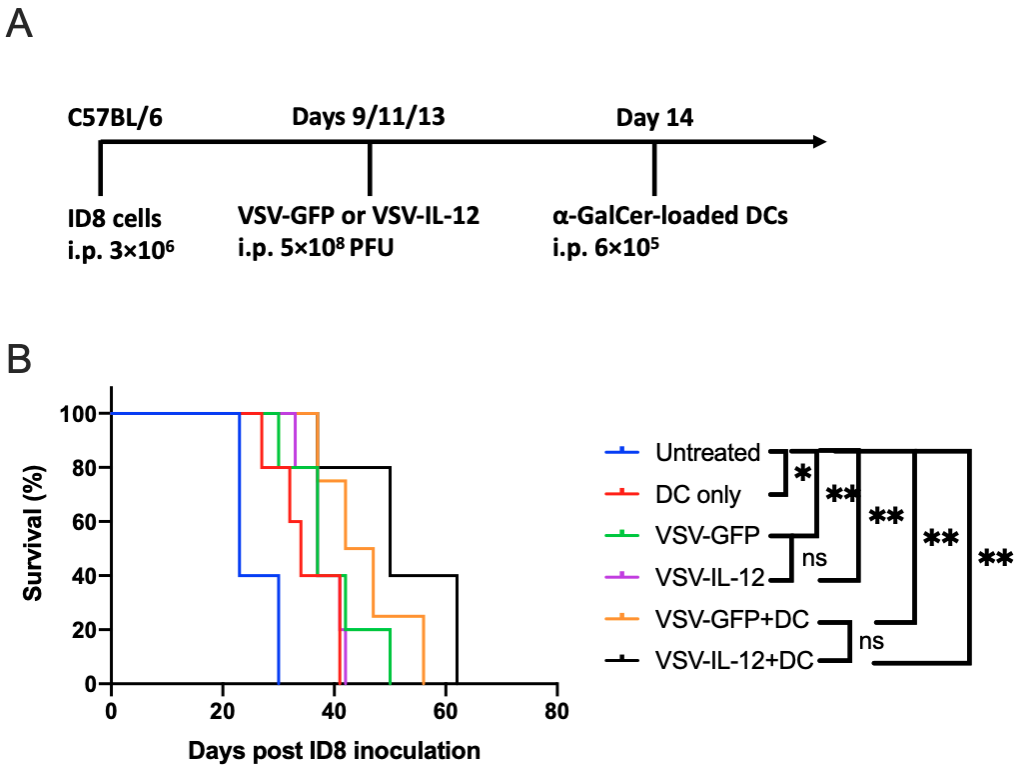

Figure 18 Targeting ovarian cancer with combined NKT cell activation therapy and VSV-IL-12 or VSV-GFP oncolytic virotherapy. (A) Schematic of treatments delivered in ID8 ovarian cancer mice model. Mice were intraperitoneally (i.p.) inoculated with 3 x 106 ID8 ovarian carcinoma cells. Mice received i.p. injection of either VSVMΔ51-GFP or VSVMΔ51-IRES-miL-12 (5 x 108 pfu) on days 9, 11 and 13. A single dose of α-GalCer loaded DC's (6 x 105 cells, i.p.) was delivered on day 14 for NKT cell-activation. (B) Kaplan Meier curves were generated to assess survival curve using Log-rank (Mantel-Cox) test following treatments with α-GalCer-loaded DC's alone or in combination with VSVMΔ51-GFP or VSVMΔ51-IRES-mIL-12 (n = 5). ns = non-significant, *P<0.05, **P<0.01.

CHAPTER 4: DISCUSSION

4.1 Overview

Infiltration of NKT cells into the tumor microenvironment has been associated with enhanced tumor control in several cancers [195]. Our lab has previously shown that therapeutic enhancement of NKT cell infiltration using α-GalCer loaded DCs prolongs survival in post-surgical 4T1 breast cancer and ID8 ovarian cancer mouse models [166]. Furthermore, the combination of NKT cell activation with VSV oncolytic therapy synergistically augmented survival over the single treatments [166]. Upon examining whether the order of VSV treatments either before or after NKT cell activation had an impact on survival outcomes, it was found that VSV treatments prior to NKT cell therapy lead to superior survival outcomes [166]. Treatments with oncolytic VSV-GFP have been shown to induce upregulation of antigen presenting molecules such as MHC and CD1d molecules on ID8 cells, making tumor cells more sensitive to immune cells for killing [166]. VSV infected ID8 cells have previously been shown to upregulate markers of immunogenic cell death (ICD), enhancing presentation of tumor antigens to the immune system, which is supported by NKT cell activation and cytokine production [166]. Additionally, NKT cell activation and VSV virotherapy are not dependent upon specific tumor epitopes and are able to target heterogenous tumors directly as well as indirectly by promoting immune presentation and activation [153,288]. While NKT cells can target both $CD1d^+$ and $CD1d^-$ tumor subtypes [153], VSV receptors are ubiquitously expressed on several cancer lines [288]. Thus, VSV treatments synergize with NKT cell therapy, leading to improved survival outcomes in multiple tumor models [166,379].

In order to further harness potential of oncolytic VSV, various viral constructs expressing immune stimulatory molecules including IL-15, IL-23, IFN-β, IFN-γ, IFN-λ, CXCL9 and p14 have been made by various groups and evaluated for their anti-tumor efficacy [313,314,381–383]. Each of these recombinant viruses differentially modulate tumor microenvironment and provide varying therapeutic outcomes. When coupled with the standalone oncolytic capability of VSV, IL-15 mediates *indirect* tumor control by promoting survival and downstream activation of NK, NKT and CD8+ T-cells; whereas p14 FAST protein-induced syncytia formation in tumor cells leads to enhanced viral

dissemination and *direct* tumor cell-death [313,314]. VSV-p14-mediated tumor control is not limited to its ability to directly induce tumor cell death, since FAST proteins can also induce indirect tumor control through ICD [314].

FAST proteins disrupt calcium homeostasis and induce translocation of calreticulin (CRT) from the lumen of the endoplasmic reticulum to the outer surface of the plasma membrane [314,368]. The role of CRT in ICD is well-established, such that it stimulates phagocytosis of tumor cells by antigen presenting cells (APCs) [384]. In process, uptake of tumor antigens by APCs is also enhanced thereby leading to increased priming of T-cell-mediated adaptive immunity downstream of ICD [384]. While VSV can induce ICD, p14 expressing constructs enhanced tumor immunogenicity and elicited downstream expansion of NK and T cells in a mouse model of 4T1 breast cancer [314]. Our lab has previously demonstrated that VSV-treated ID8 cells show increased levels of ICD biomarkers, including CRT mobilization and ATP and HMGB1 secretions [166]. Therapeutic translation of these findings to ID8 model of ovarian cancer, in principle, should lead to an enhanced anti-tumor immune response post VSV-p14 treatments.

In contrast to p14, which plays a role in both direct and indirect tumor control, IL-15 instead facilitates development of conditions including activation and proliferation of NK and CD8+ T cells that prolong VSV-induced indirect tumor control [313]. In summary, both IL-15 and p14 expressing VSV constructs are interesting candidates since the immunomodulatory properties of p14 and IL-15 differ greatly and target different components of the anti-tumor axis. We hypothesized that VSV-p14 and VSV-IL-15 oncolytic viruses when used in combination with NKT cell immunotherapy and anti-PD-1 checkpoint blockade would enhance oncolysis, immune recognition and survival in an ovarian cancer mouse model.

IL-12 is another potent cytokine that preferentially induces NKT cells to produce IFN-γ [150]. In turn, IFN-γ enhances IL-12 production by DCs in a positive feedback loop and together these cytokines synergize to facilitate downstream development of Th1 immunity [150]. We hypothesized that intratumoral delivery of IL-12 using the oncolytic VSV-ΔM51 platform would further augment local NKT cell activation when coupled with α-GalCer loaded DCs and lead to superior survival benefits in an ID8 ovarian cancer mouse model.

4.2 Therapeutic efficacy of VSV-p14 in ID8 model remains elusive

With the knowledge that VSV-p14 prolongs survival in 4T1 breast cancer and CT26 metastatic colon cancer models [314], we first examined the therapeutic efficacy of VSV-p14 in the ID8 model. Two independent survival experiments were conducted to this end, however, each presented with technical challenges that made interpretation of these results difficult. In our preliminary study, while VSV-p14 exhibited improved survival outcomes over VSV-GFP, mice treated with the latter exhibited significantly reduced therapeutic efficacy than our previously reported findings and warranted further investigation (Figure 4B) [166]. Upon re-examining the viral stocks used for this experiment, titer loss for both VSV-GFP and VSV-p14 was observed with long-term virus storage, and dosages were later determined to be suboptimal at 1.1×10^5 PFU and 3×10^5 PFU, respectively. Therefore, the results obtained in our preliminary study are consequent of sub-optimal VSV dosages. Interestingly, even at suboptimal doses VSV-p14 yielded slightly better protection over VSV-GFP treatments, whereas the combined VSV-p14 and NKT cell activation immunotherapy significantly enhanced survival (Figure 4B). In contrast to VSV-GFP, recombinant VSV-p14 has been shown to replicate more efficiently and produce 10-20-fold increased virus titer in 4T1 and MCF-7 spheroid cultures [314]. Therefore, unlike VSV-GFP, the increased replication kinetics associated with VSV-p14 may have potentially compensated for deleterious effects that would normally follow from low virus dose.

Given the challenges associated with our preliminary study examining VSV-p14, particularly concerning reduced VSV titers, a similar survival experiment was conducted using new viral stocks (Figure 4C). While survival outcomes obtained for NKT cell activation and anti-PD-1 treatments were found to be consistent with our preliminary study, VSV-p14 treatment failed to prolong survival irrespective of the treatment combinations. Additionally, VSV-GFP treated mice elicited superior tumor protection than VSV-p14. Subsequent in-vitro cell-viability assay revealed diminished oncolytic potency of VSV-p14 against ID8 cells, as compared to VSV-GFP (Figure 15).

We previously suspected that the VSV-p14 virus stock used for this experiment may have significant presence of viral mutants, also termed as defective interfering particles (DIPs), that are unable to generate viable progenies on their own and compete

with standard infectious particles to complete their replication cycles [380]. Multiple viral passages may have led to accumulation of DIPs, thereby reducing the oncolytic activity of VSV-p14 against ID8 tumors. However, plaque titrations of the virus batch revealed generation of high-titer virus stock – suggesting that the rationale for DIP infiltration might require further validation.

RNA viruses, such as rhabdoviruses, are prone to rapid mutations due to lack of proofreading functions in virus-encoded RdRp RNA polymerase [385]. Furthermore, this property of spontaneous mutations has been previously exploited to generate and select VSV serotypes, through repeated rounds of mutations and selections, that exhibit increased efficacy towards wild-type VSV-resistant cancer cell lines [386]. For instance, infection of human pancreatic cancer cells with two different VSV serotypes resulted in generation of two mutants with identical mutations, acquired independently over parallel viral passages, and enhancing replication kinetics over parental strains [387]. While this study may indicate that acquisition of mutations may be cancer cell dependent, it is unclear whether similar mutations would also follow from successive passages when examined in non-malignant cells such as Vero cells [387]. In this study, VSV-p14 was exclusively propagated using Vero cells and it is possible that mutants generated over repeated passages in Vero cells might have led to generation of VSV mutants with reduced oncolytic potency against ID8 cells.

Additional studies examining the VSV-p14 induced syncytia formation in ID8 cells and/or spheroid tissues may provide qualitative insight into virus's oncolytic efficiency, prior to *in-vivo* examinations. Nonetheless, the oncolytic potential of VSV-p14 in ID8 survival model remains elusive.

4.3 Anti-PD-1 monotherapy yields limited therapeutic efficacy in ID8 model

In line with other groups examining anti-PD-1 checkpoint blockade in ID8 mouse model we did not observe any robust tumor protection with PD-1 monotherapy (Figure 4B, C) [388,389]. However, when combined with VSV-p14 and NKT cell activation therapy, anti-PD-1 treatments yielded maximal survival advantage up to 120 days post tumor inoculation in 60% of the treated mice (Figure 4B). PD-L1 expression is not innate to ID8 cells and therefore, the anti-PD-1 monotherapy could only improve survival by a limited

margin [388,390]. However, PD-L1 expression on several tumor cells, including ID8 cells, could be induced by IFN-γ and both NKT-cell activation and oncolytic viruses have shown to be potent inducers of IFN-γ [390,391]. Thus, VSV-p14 treated mice could have elicited sustained IFN-γ production post virus injections, leading to early induction of PD-L1 expression on tumor cells and enabling anti-PD-1 blockade therapy to synergize with VSV-p14 treatments.

In addition, anti-PD-1 treatments are also shown to synergize with NKT cell activation in murine models of colon and liver cancer and prevent anergy induction that follows from free α-GalCer administration [153,392,393]. Here, we show that α-GalCer-loaded DCs could also upregulate PD-1 expression on ascitic NKT cells. Thus, it is likely that anti-PD-1 treatments post NKT cell activation in ID8 model prolonged NKT-cell-induced anti-tumor response - leading to enhanced survival.

4.4 NKT cell activation induced Th1 immune response

We further sought to compare and contrast the underlying immune landscape that followed from VSV-GFP or VSV-p14 treatments, either as monotherapies or in combination with α-GalCer loaded DCs. In line with existing literature, NKT cell activation induced expansion of both innate and adaptive components of Th1 immune cells including ascitic NKT, NK and T cells and DC cells in spleen, while inhibiting expansion of immunosuppressive Tregs in spleen (Figure 7B, 9A, 10A, 11A, 13A) [153].

It is well established that α-GalCer loaded DC-induced NKT cell stimulation leads to significant upregulation of IFN-γ and IL-12, that in turn, facilitates activation and proliferation of DCs [153]. Here we report that DC expansion post-NKT cell therapy may have led to increased frequency of primed CD8+ T cell responses. The upregulated NKT cell activation axis also led to an increased number of T_{CM} CD8+ cells in ascites and reduced frequencies of naïve CD8+ T cells, suggesting generation of adaptive immunity (Figure 12B).

4.5 Effect of VSV-GFP treatments on DCs

Despite an increase in T cells following VSV-GFP treatment, DC populations in the spleen and ascites remained similar to those observed in control mice (Figure 11A,

9A). Interestingly, the combined VSV-GFP and NKT cell activation therapy led to reduced number of ascitic DCs when compared to standalone NKT cell activation (Figure 9A). The data, however, did not reach statistical significance and further investigation with increased sample size is warranted. Nonetheless, it is unclear from this study whether VSV infections directly altered DC viability in spleen and ascites, or whether the lower DC counts are due to the VSV infections in DC precursor cells. Additionally, it is possible that VSV-GFP directly infects and kills DCs, which is also corroborated by another study in which VSV infections in B16 tumor model has been shown to directly infect DCs, reduce cell viability, and impede DC mediated tumor antigen presentation [394]. These observations are in contrast with our recent findings in which the VSV-GFP and NKT cell activation combination therapy increased DC infiltration over monotherapies in an orthotopic model of pancreatic cancer [379]. In another report, VSV infection of DCs led to DC maturation, and the subsequent administration VSV-infected DCs in tumor-bearing mice led to a significant tumor regression [395]. However, it is important to note that these VSV-immunized DCs were cultured *ex-vivo* and have been reported to be marginally permissible for VSV-replication for first 24 hours. Whether the VSV induced DC abrogation is consistent across various tumor types or whether this observation is ID8 specific requires further investigation. Alternatively, DCs may have migrated to lymph nodes. Future studies examining immune infiltration in lymph nodes may provide further insight.

4.6 Combination of VSV-GFP and NKT cell activation elicit ID8 specific immunity in re-challenged mice

When splenocytes obtained from a mouse that cleared ID8 following VSV-GFP treatment were stimulated in vitro with ID8 cells, increased cytolytic activity against ID8 cells and elevated IFN-γ levels were observed, indicating presence of some long-term immunity (Figure 6). In contrast, the combined VSV-GFP and NKT cell activation yielded better ID8 specific tumor immunity and may have synergized over individual treatments. These observations are similar to our previous findings in which 4T1 re-challenged mice that had previously received NKT cell therapy exhibited delayed tumor growth whereas few VSV-GFP treated surviving mice exhibited delayed tumor growth

[166]. While it is possible that mice treated with NKT cells may have developed a higher immune threshold against ID8s, further study with increased sample size is needed to investigate the development of ID8 specific immunity.

4.7 VSV-GFP induces accumulation of CD11b$^+$ Ly-6G$^+$ myeloid cells

In our previous report, we show that VSV-GFP infected 4T1 breast cancer cells increased pro-inflammatory chemokine expression including CCL3, CCL4, CXCL2 *in-vitro* [166]. These serve as chemoattractants that act on myeloid cells among other immune cell targets [166]. Here we show that VSV-GFP treatments in ID8 ovarian cancer mouse model led to increased levels of Ly-6G+ granulocytic myeloid cells in spleen and ascites. This observation is in line with our recent study demonstrating intratumoral infiltration of Ly-6G+ granulocytic cells following VSV-GFP and VSV-IL-15 treatments in subcutaneous and orthotopic Panc02 tumor models [379]. In the Panc02 model, this increase was not shown to enhance MDSC mediated immunosuppression [379]. In the context of ID8 tumor model, further assays are required to determine whether the accumulated myeloid cells following VSV treatments exhibit inflammatory or suppressive phenotypes.

Differentiation of myeloid cells in TME is stimuli dependent and exhibits functional plasticity [396]. For instance, macrophages acquire a pro-inflammatory M1 phenotype in response to stimuli such as IFN-γ and GM-CSF, whereas immunosuppressive M2 macrophages, also termed as tumor associated macrophages (TAMs), produce anti-inflammatory cytokines such as IL-4 and IL-10 [396]. In a recent study, in-vitro VSV infection enabled reprogramming of the pro-tumorigenic M2 macrophages to acquire the anti-tumor M1 phenotype [397]. In another study, M1 like macrophages exhibited increased susceptibility to reovirus infection in contrast to M2 like macrophages that readily induced antiviral innate immune responses [398]. Thus, additional studies examining myeloid plasticity are needed to further elucidate mechanisms that are unique to VSV based OV therapy.

Similar to the macrophage paradigm, neutrophils could be categorized into N1 and N2 subpopulations based on their anti or pro tumor properties, respectively [399,400]. Several oncolytic viruses have been shown to induce N2 to N1 polarization [400], however, there is a literature gap specifically examining the effects of VSV on neutrophil

polarization. In the context of VSV therapy, neutrophil infiltration is associated with tumor vascular shutdown, causing indirect killing of cancer cells; and in some instances, this innate response has been shown to be more effective than adaptive response [376,394,400]. In a B16-ova tumor model, a non-replicating VSV mutant was as effective as replication competent VSV in providing tumor protection [401].

In addition to above reports suggesting the ability of VSV to skew the myeloid population toward anti-tumor response, NKT cells have been also shown to reduce MDSC mediated immune suppression in 4T1 and Panc02 tumor models [379]. When combined with VSV, NKT cells maintained reversal of MDSC suppression [379]. Similar observations have also been cited in context of Influenza A infection [402].

4.8 Rationale for hind-limb impediments post VSV-IL-15 or VSV-IL-12 treatments

Approximately 70% of the mice treated with either VSV-IL-15 or VSV-IL-12 developed hind limb impediments around day 50 post-ID8 inoculation. While several studies have associated hind-limb paralysis in tumor bearing mice to VSV-specific neurotoxicity [289], it would be difficult to suggest a similar rationale in this study for the following reasons. First, both IL-12 and IL-15 transgenes are incorporated into the same VSVΔM51 backbone previously used to generate VSV-p14, which did not exhibit signs of hind limb impediment, and is also cited for its attenuated neurotropism [312,314]. Second, given that VSV-p14 replicates and disseminates much faster than IL-15 or IL-12 expressing VSV constructs [314], mice treated with the former should theoretically present with a higher incidence of hind limb impediment if it were to be VSV-specific. Third, peritoneal dissections of mice presenting with hind limb impediments revealed the presence of tumor mass around the ovarian bursa and an inflamed hind limb. However, a subset of these mice also developed ascites with metastasized tumor nodules at the time of sacrifice, indicating that the tumor cells were indeed placed correctly. It is likely that the local delivery of IL-15 or IL-12 cytokines could have led to excessive induction of Th1 immune response leading to hind limb inflammation.

Our lab has previously examined VSV-IL-15 in orthotopic and subcutaneous models of pancreatic cancer, in which the viral treatments were administered

intravenously and intratumorally, respectively [379]. While the standalone VSV-IL-15 therapy did induce tumor regression, treatments did not lead to hind-limb impairments [379]. However, it is important to note that VSV-IL-15 treatments on their own did not enhance tumor control over VSV-GFP in these pancreatic tumor models, and that the observed tumor control was largely due to the oncolytic activity of VSV [379]. In contrast, VSV-IL-15 enhanced the efficacy of NKT cell activation therapy over combinations with VSV-GFP, indicating that the Il-15 synergized with NKT cell activation. In a previous study, IL-15 production from VSV-IL-15 enhanced survival and antitumor immune responses in CT26 tumors without additional therapies [313]. Accordingly, the ability of VSV-IL-15 to enhance tumor control varies between two tumor models and is cancer-specific. In the context of ID8 tumor model, additional studies examining immune infiltration post VSV-IL-15 or VSV-IL-12 treatments are needed to confirm whether these treatments enhance intratumoral IL-15 or IL-12 activity, respectively. Additionally, these studies will also help establish whether the observed hind-limb impairments result from enhanced IL-15 or IL-12 production following viral treatments.

Previous studies that examined IL-12 expressed in oncolytic Sindbis and herpes simplex viruses in the mouse models of ovarian cancers did not report IL-12 induced hind limb impediments [403,404]. For instance, intraperitoneal treatments with herpes simplex virus expressing IL-12 prolonged survival in MISIIR-TAg syngeneic mouse model of epithelial ovarian carcinoma [403]. In another report, treatments with IL-12 expressing Sindbis virus (i.p.) led to tumor regression and improved survival in SCID mice bearing ES-2 human ovarian carcinoma cell line [404]. Thus, the underlying mechanisms inducing hind limb impediments post VSV-IL-15 or VSV-IL-12 treatments and whether this behavior is ID8 specific is currently unclear.

In conclusion, hind limb impediments observed in VSV-IL-15 or VSV-IL-12 treated mice are more likely to stem from progressive and localized tumor growth in the hind limb region disrupting pelvic movement, rather than VSV-specific neurotropism. Further studies examining virus spread in CNS in addition to histopathological analysis of inflamed hind limb are required to harness oncolytic potential of VSV-IL-15 and VSV-IL-12 in the ID8 model.

4.9 VSV-IL-12 in ID8 Ovarian Cancer

This study also aimed to further optimize VSV-NKT cell activation combination therapy using intratumoral delivery of IL-12 via VSV. While it was hypothesized that IL-12 would further augment local NKT cell activation, we did not observe a statistically significant difference between VSV-GFP and VSV-IL-12 when used in combination with α-GalCer-loaded DCs. However, it is too early to conclude ineffectiveness of VSV-IL-12 in ID8 model, given our small sample size and episodes of hind-limb impediments. Further studies with increased sample sizes are needed to establish therapeutic efficacy of VSV-IL-12 in ID8 model.

4.10 Troubleshooting

Objective 1: ***To generate a recombinant VSV construct expressing IL-12.***

Problem: A bioactive mouse IL-12, as a tandem dimer construct of the p40 and p35 subunits linked by a glycine-serine linker (Addgene: Plasmid #108665), was used as an insert for cloning between the G and L regions of the VSV plasmid. The open reading frame of the donor plasmid, however, had a *NheI* cut site between the p40 and p35 subunits rendering *NheI* incompatible for cloning into the vector pVSV-ΔM51-XN2. Therefore, an alternate cloning strategy independent of the *NheI* cut site was required. This was challenging at first since the *XhoI* and *NheI* dependent cloning system is tried and tested for generating various recombinant viruses on the pVSV-ΔM51-XN2 platform [312,314,405–407]; and improvising on this existing method required additional sequence information about the vector plasmid.

Approach 1: Given that the sequence information between the *XhoI* and *NheI* cut sites was the only sequencing information available for the 15 kb plasmid, there was a risk of untargeted restriction digestion when using enzymes other than *NheI*. Attempts were made to identify two cut sites compatible with both IL-12 donor and VSV vector plasmid. With the limited sequence availability, 7 potential restriction cut sites between *XhoI* and *NheI* were found to be non-cutters and compatible with the donor plasmid. However, some of these sites were also present in the unsequenced regions of VSV

backbone when checked with multiple restrictions digestions on a gel. The technique was deemed to be too time and resource consuming and warranted an alternative approach.

Approach 2: To eliminate the internal *NheI* cut site in the donor IL-12 encoding donor plasmid (Addgene: Plasmid #108665), I designed an in-silico gene construct encoding the IL-12 sequence as pORF-p40p35 (Addgene plasmid # 108665) flanking *XhoI* and *NheI* cut sites. The plasmid was synthesized and cloned into the pUC57 plasmid by Bio Basic Inc. I subsequently isolated and cloned the pORF-p40-$(G_4S)_3$-p35 gene fragment from this externally sourced plasmid into the pVSV-ΔM51-XN2 backbone (referred as V1; Figure 3). Although the resulting sequence was validated both by PCR and Sanger sequencing, attempts to rescue a functional VSV encoding ELISA-detectable mIL-12 remained unsuccessful. At this point, we questioned the quality of mIL-12 sequence since the only literature citing bioactivity of the mIL-12 construct was from the plasmid depositor (RRID: Addgene 108665). Additionally, it was also unknown at this point whether the glycine-serine linker connecting p40 and p35 subunits impeded proper protein folding as no publications have been generated using this construct.

Approach 3: In order to exclude any likelihood of sequence-specific limitations impacting mIL-12 expression and protein folding, a different plasmid (pUNO1-p40-$(VPGVG)_2$-p35 from InvivoGen) encoding an expression-ready mIL-12 clone with an elastin linker was used; bearing the sequence previously used for generating mIL-12 expressing Maraba virus [408]. Additionally, mIL-12 bioactivity derived from this plasmid is also established in other literature as well [409]. The mIL-12 sequence was then cloned into pVSV-ΔM51-XN2 backbone and validated by PCR and Sanger sequencing (referred as V2; Figure 3). While the recombinant virus did elicit cytopathic effects on Vero cells upon rescue, supernatant analysis did not reveal any detectable mIL-12 production by ELISA. This phenomenon was peculiar and raised a possibility of inefficient translation of the recombinant VSV template in host cells. We first attributed these effects to premature cell death upon virus infection, before the host machinery could translate mIL-12 template. To test that, confluent monolayers of Vero and ID8 cells were infected with the rescued VSV at varying MOIs (5, 1, 0.1 and 0.01) for 2 hours, followed by

supernatant harvest at 6, 12, 18, 24, 36, 48 and 72 hours. However, no detectable amounts of mIL-12 could be traced in either combination of examined conditions; nullifying our speculation concerning VSV induced early cell death and thereby limiting mIL-12 production.

Approach 4: The VSV template is transcribed in sequential and polar order; meaning that gene adjacent to 3′ promoter is transcribed first followed by transcription of successive gene with a relative decrease in abundance by 30%, and thus establishing a gradient in production of viral protein as follows: N>P>M>G>L. We thus attempted to optimize host translation efficiency by introducing a translation enhancing IRES sequence preceding p40-$(VPGVG)_2$-p35 gene construct. For that an in-silico gene construct was designed encoding IRES sequence in frame with the 1.6-kb single-chain mIL-12 expression ready cassette (pORF-p40-$(VPGVG)_2$-p35 (InvivoGen)) that flanked *XhoI* and *NheI* cut sites at 5' and 3' ends, respectively. The synthetic sequence was generated by Bio Basic Inc. Next, the IRES-mIL-12 gene construct was sub-cloned into the pVSV-ΔM51-XN2 backbone and verified by PCR and Sanger sequencing (referred as V3, VSV-IRES-mIL-12 or simply VSV-IL-12; Figure 3). While the first attempt to rescue mIL-12 producing recombinant virus failed, examination under confocal microscope revealed emission of green fluorescence in infected cells- suggesting contamination with VSV-GFP. The source of contamination was later detected in the MVA-p3 virus stock, previously used to drive T7 expression in QM5 cells during the rescue of recombinant VSV experiment (see materials and methods). It is likely that all the previously rescued VSVs (in approach 2 and 3) had also been contaminated with VSV-GFP since this reagent was common to all rescue experiments.

Approach 5 and Solution: A new MVA-p3 stock was generated and used to simultaneously rescue all of the previously generated recombinant VSV plasmid constructs (in approach 2, 3 and 4). Of the 3 constructs, only the IRES sequence bearing plasmid construct could be successfully rescued as a functional mIL-12 producing VSV virus. The remaining constructs did not exhibit any signs of cytopathic effect during the rescue process (see materials and methods), and hence could not be rescued. It is possible

that the IRES sequence preceding the mIL-12 gene may have enhanced recruitment of ribosome subunits- leading to better translation efficiency given the size of large construct size post mIL-12 gene introduction. However, multiple rescue experiments using VSV-IL-12 plasmid constructs lacking IRES sequence (made in approach 2 and 3) are needed to validate the necessity of IRES element, especially while considering large transgenes similar to the mIL-12 gene.

In summary, three distinct VSV plasmid constructs were designed (V1, V2 and V3) with each encoding a different sequence of mIL-12. The V1 construct encoded for a mIL-12 sequence linking p40 and p35 IL-12 subunits by glycine-serine linker. The construct, however, could not rescued into a functional mIL-12 expressing VSV. Here we questioned whether the linker impeded appropriate protein mIL-12 folding, rendering its detection by ELISA. The V2 construct also encoded for a similar mIL-12 sequence, except its subunits were linked by an elastin linker. In addition, this mIL-12 expression ready cassette used for the V2 construct had previously been used to generate IL-12 expressing Maraba virus [408], suggesting that the elastin linker does not impede protein folding. This construct could also not be rescued. We then attempted to increase host translation efficiency by adding a translation enhancing IRES sequence preceding mIL-12 gene construct (V3). While initial attempts to rescue V3 construct remained futile, it was later revealed under a confocal microscope that the MVA-p3 used for driving T7 expression during VSV rescue had been contaminated with VSV-GFP, and therefore the rescue attempts for V1, V2 and V3 indeed resulted in VSV-GFP propagation. Therefore, a new MVA-p3 stock was used to simultaneously rescue V1, V2 and V3 constructs, Only the V3 construct bearing the IRES sequence could be successfully rescued as a functional mIL-12 producing VSV virus. It is possible that V1 and V2 constructs lacking IRES sequence may also be rescuable to generate functional mIL-12 expressing viruses; this study, however, did not make additional attempts to optimize the rescue process associated with these constructs.

Objective 2: ***Eliminating technical challenges during early in-vivo survival experiments.***

Problem: Episodes of tumor ulceration post ID8 inoculation. My first survival experiment was aimed at replicating a previously established experiment design examining whether the order of treatments involving NKT cell activation and oncolytic VSV, when used in combination, impacted survival in ID8 inoculated mice. Our lab has previously demonstrated that in contrast to individual therapies, both the combined approaches lead to increased survival and that the treatment with oncolytic VSV before NKT cell activation results into superior survival. However, similar findings could not be replicated during my first *in-vivo* experiment, primarily due to some mice presenting with tumor ulcerations around day 60 post ID8 inoculation. It was suspected that the tumor cells might have been accidentally placed subcutaneously rather than in the peritoneal cavity.

Approach and Solution: Optimization of the intraperitoneal (ip) injection technique: After depressing the plunger until the suspension was fully administered during ID8 tumor inoculation, I left the needle inside the peritoneum for additional 15 seconds before removing the needle. This technique allowed the ID8 suspension to settle while minimizing the risk of subcutaneous tumor implantation.

Objective 3: ***To examine the effects of VSV-p14 in ID8 tumor model.***

Problem: VSV-p14 was found to have an increased anti-tumor efficacy in our preliminary study when compared to VSV-GFP, either alone or in combination with NKT cell therapy and anti-PD-1 treatments. However, this finding could not be replicated in subsequent survival experiment. Furthermore, findings from immune phenotype experiments, using the same VSV-p14 batch previously examined in survival studies, indicate that VSV-p14 elicited a weaker anti-tumor immune response than VSV-GFP. Here we suspected that repeated passages during virus production may have led to accumulation of DIPs, resulting in a reduced oncolytic potency of VSV-p14.

Approach: To characterize the ID8 specific oncolytic potency of VSV-p14, an MTT assay was performed (Figure 15). In contrast to VSV-GFP, VSV-p14 mediated

cytotoxicity was found to be slightly reduced at MOI of 1. The data, however, did not reach statistical significance and warrants additional studies to conclude whether these observations are ID8 specific or due to DIP infiltration. Nonetheless, therapeutic efficacy of VSV-p14 in ID8 model could not be successfully established. In order to maintain the oncolytic potency of the virus or to prevent the accumulation of DIPs, subsequent virus productions were conducted with infections at low MOI, by tracking passage counts and ensuring periodic plaque purifications.

4.11 Future Directions

4.11.1 Examining the effects of VSV-p14 on ID8 spheroids and optimizing OV therapy

Unlike DNA based oncolytic viruses, RNA viruses such as VSV exhibit faster replication kinetics, and while this may allow faster eradication of tumor cells, highly lytic viruses could also trigger undesired hyperactivation of innate immune response [400]. For instance, persistent activation of anti-viral responses could lead to significant upregulation of myeloid cells causing rapid virus clearance - even before OV could prime an adequate adaptive response. This has been shown to negatively affect recruitment and development of polyfunctional T cells, including memory T cells, thereby limiting generation of durable anti-tumor immunity [400,410]. In particular, this may apply to syncytia forming fusogenic oncolytic viruses that display significantly enhanced lytic potential.

A recent study demonstrated that a fusogenic Myxoma virus used in a murine LLC tumor model did not enhance OV efficacy compared to a non-fusogenic control [411]. While fusogenic Myxoma constructs did exhibit higher spread *in-vitro*, rapid titer loss was observed *in-vivo* and has been correlated to rapid cell lysis – preventing viral spread [411]. Moreover, this observation was consistent in both immune-competent and immune-deficient settings suggesting that virus clearance was not immune-mediated [411]. In another report, p14 expressing adenovirus infection in 4T1 breast cancer cells induced apoptosis; even before the completion of the viral replication cycle [412]. A similar rapid apoptotic response was also observed in multiple myeloma cells post Myxoma virus infection [411]. Thus, highly lytic viruses may inadvertently hinder development of desired anti-tumor immune responses, even while showing promising oncolytic potential *in-vitro*;

and that persistent infection might be crucial for inducing OV mediated immunotherapy [400].

While this thesis could not establish the therapeutic efficacy of VSV-p14 in the murine ID8 model, a follow-up *in-vitro* study examining whether VSV-p14 could induce syncytia in ID8 cells or spheroid cultures is needed to further elucidate ID8-VSV-p14 interactions. It would also be interesting to determine whether the dominant mechanism for virus clearance following VSV-p14 treatment in ID8 inoculated mice is immune-mediated or caused by the rapid activation of apoptotic pathways that prevent the virus spread. A recent study in our lab demonstrates that fusogenic VSV constructs expressing p14 and p15 could increase apoptosis and necrosis markers in 4T1 breast cancer cells (unpublished data). However, it is possible that these findings may not translate into the ID8 tumor model given that OV response may be dependent on tumor type. For instance, while the lack of immune infiltration in solid tumors may benefit from high lytic potential of OV, other tumor types including ovarian cancers and melanoma may benefit from further optimization of OV-induced ICD [413].

4.11.2 Strategies to overcome episodes of hind paralysis post VSV-IL-12 or VSV-IL-15 treatments

In this study, the VSV treatment regimen entailed 3 doses of 5 x 10^8 PFU on days 9, 11 and 13 post-ID8 inoculation. While VSV-GFP and VSV-p14 treated mice did not exhibit hind limb impediments, such manifestations were common in VSV-IL-15 and VSV-IL-12 treated mice. As explained previously, both VSV-IL-15 and VSV-IL-12 viruses deliver potent pro-inflammatory cytokines that lead to downstream induction of IFN-γ, a molecule central in inducing anti-viral mechanism. Examining activation and infiltration of immune cells, particularly myeloid populations, is needed to probe the extent of innate activation and toxicity observed in VSV-IL-15 or VSV-IL-12 treated mice in ID8 tumor model. Furthermore, it would also be interesting to revise the VSV treatment regimen such that either the duration between two successive treatments are effectively spaced out, or the virus doses are reduced.

4.11.3 Examining VSV-IL-12 in other cancers

Our *in-vitro* tests indicate that in addition to ID8 cells, VSV-IL-12 is also cytotoxic against other cancer cell lines including B16 melanoma, 4T1 mammary carcinoma, Panc02 pancreatic carcinoma and LLC lung cancer, suggesting that many cancer types could be receptive to VSV therapy (Figure 16B, C). Amongst these cell lines, B16 cells were more prone to VSV-IL-12 killing even at reduced titers, suggesting that VSV-IL-12 may be a promising candidate for treating melanoma. While this study did not examine surface expression of IL-12 receptors on ID8 cells, B16 melanoma cells express IL-12 receptor and have been reported to induce apoptosis and reduced tumor proliferation upon IL-12 stimulation [414]. This effect when coupled with NKT cell activation may further improve VSV efficacy in B16 melanoma models. This thesis also aimed to characterize immune responses after VSV-GFP treatments, and while the OV therapy did lead to expansion of myeloid and T cells, VSV-IL-12 induced immune response in ID8 tumor remains to be examined. Additionally, intratumoral IL-12 delivery using oncolytic platforms such as adenovirus and Semliki Forest virus have been shown to prolong survival in murine models of 4T1 breast cancer [415,416]. Thus, IL-12 delivery using VSV-IL-12 in 4T1 models would be expected to enhance treatment outcome in contrast to VSV-GFP.

4.11.4 Examining NKT cell therapy in combination with recombinant VSV-IL-2

In line with maximizing NKT cell activation, we show that NKT cells in ascites significantly upregulated PD-1 expression. This observation was surprising since several reports have suggested that, in contrast to free α-GalCer injections, α-GalCer-loaded DCs preserved NKT cell activation and prevented anergy induction [153,194]. However, reports specific to ID8 tumor model in the context of PD-1 expression upon NKT stimulation were absent. This may partially explain the reduced survival efficacy when compared to VSV treatments. Nonetheless, a previous report by Parekh *et. al*. demonstrates that anergic NKT cells could be re-stimulated to proliferate when treated with IL-2 [210]. In addition to NKT cells, IL-2 signaling is extensively cited for inducing anergy reversal in exhausted T-cells, but therapeutic translation of systemic IL-2 based cytokine therapy is

burdened with toxic side effects [417]. In addition, IL-2 is also implicated in development and proliferation of immunosuppressive Tregs. To overcome this limitation, some studies have engineered IL-2 variants that preferentially binds to IL-2 receptors on effector NK and CD8+ T cells over Tregs to stimulate anti-tumor immunity [418,419]. Recently, treatments using an adenovirus construct encoding an IL-2 variant led to complete tumor regression in >60% of hamsters bearing pancreatic tumors [418]. With the knowledge that combined VSV and NKT cell activation therapies synergize over individual treatments, an engineered VSV vector designed to express an IL-2 variant that preferentially stimulates effector immune cells is hypothesized to further prolong NKT cell activation, whilst simultaneously preventing T-cell exhaustion.

4.11.5 ID8 proteome analysis to optimize anti-PD-1 therapy

While our preliminary data examining VSV-p14 in combination with NKT cell activation therapy and anti-PD-1 blockade did provide additional tumor protection over other treatments, technical challenges associated with the use of DIP infiltrated VSV-p14 stock in the subsequent study prevented validation of these results and are subject to further evaluation (Figure 4B, C). Nonetheless, the standalone anti-PD-1 therapy provided limited survival benefit, consistent with reports showing that ≥ 80% of ovarian cancer patients do not respond to anti-PD-1 therapy [260,420,421].

In recent years, several studies that incorporated PD-1 blockade in combination with chemotherapy, oncolytic viruses, and other checkpoint blockade therapies reported an improved antitumor response over standalone anti-PD-1 treatments [422]. Chemotherapeutic agents and oncolytic viruses are potent ICD inducers and play a crucial role in initial priming of anti-tumor response, but often lead to upregulation of PD-1/PD-L1 ligands in the TME [422]. Here we show that VSV-GFP treatments in ID8 tumor bearing mice also led to increased PD-1 expression on CD8+ T cells in ascites (Figure 11E). This observation is consistent with our recent report, in which we further demonstrate that anti-PD-1 treatment improves the therapeutic efficacy of combined VSV-IL-15 and NKT cell activation in a Panc02 tumor model and enabled increased infiltration and activation of NKT, NK, and CD8+ T cells [379]. Similarly, IL-15 expressing vaccinia virus has also been shown to elicit PD-1 expression on MC38 colon

adenocarcinoma tumor cells and when targeted with PD-1 blockade resulted into complete tumor regression [423]. In the context of ID8 tumors, combined use of adenovirus and anti-PD-1 blockade therapy resulted in delayed tumor development, suggesting a synergistic effect between these two therapies [424]. While this thesis was unable to establish the potential of anti-PD-1 therapy in combination with VSV and NKT cell therapy, the above reports prompt re-evaluation of this triple combination therapy in the ID8 tumor model.

Histological and genomic characterization of predictive response markers rely on parameters such as expression of checkpoint proteins, mutational load and immune gene signatures, but largely overlap between responders and non-responders, and are therefore deemed of low predictive value [425,426]. Bioinformatic analysis of transcriptomic signatures and proteomic analysis in anti-PD-1 treatment responders in the context of ovarian cancer yet remains unexamined [427,428]. Proteomic analysis reflects the cellular metabolic status and proteome much more accurately, and there are major functional differences between proteomic and transcriptomic layers that could impact cancer classification and biomarker identification [429]. Therefore, an untargeted mass-spectrometry based proteomic analysis would reveal differentially expressed proteins of therapeutic value, following anti-PD-1 treatments.

4.12 Concluding remarks

NKT cells play a crucial role in cancer immune surveillance and are potent stimulators of anti-tumor immunity. Therapeutic activation of NKT cells using α-GalCer loaded DCs lead to significant improvement in survival outcomes in pre-clinical models. This study sought to improve the therapeutic benefits of NKT cell activation in ID8 ovarian cancer by combining the therapy with recombinant VSV-ΔM51 constructs expressing p14 FAST protein or IL-15. Additionally, an IL-12 expressing VSV-ΔM51 construct was also engineered to augment local NKT cell activation. NKT cell therapy significantly prolonged survival and increased NKT, NK, and T cell accumulation in ascites and inhibited Treg expansion in the spleen. Combination therapy with VSV-GFP exhibited prolonged survival and increased IFNγ secretion following ID8 re-challenge and suggest potential development of anti-tumor immunity. Therapeutic efficacy and

immune response associated with VSV-p14 treatments in the ID8 tumor model could not be established due to technical challenges associated with a reduction in virus potency and titer loss over long-term storage. In addition, mice treated with recombinant VSV-IL-15 and VSV-IL-12 developed hind limb impediments, preventing the determination of the therapeutic benefit of these recombinant viruses. Nonetheless, it is too early to conclude ineffectiveness of these recombinant viruses in ID8 tumor and require future studies examining dose-limiting toxicities and histopathological analysis of the inflamed hind-limbs.

REFERENCES

1. Reid, F., Chakrabarti, D. M., Gardiner, D. & Maxwell, R. WORLD OVARIAN CANCER COALITION ATLAS 2020. 42.
2. Bhatla, N. & Denny, L. FIGO Cancer Report 2018. *Int. J. Gynecol. Obstet.* **143**, 2–3 (2018).
3. Lengyel, E. Ovarian Cancer Development and Metastasis. *Am. J. Pathol.* **177**, 1053–1064 (2010).
4. Torre, L. A. *et al.* Ovarian cancer statistics, 2018. *CA. Cancer J. Clin.* **68**, 284–296 (2018).
5. Coburn, S. B., Bray, F., Sherman, M. E. & Trabert, B. International patterns and trends in ovarian cancer incidence, overall and by histologic subtype. *Int. J. Cancer* **140**, 2451–2460 (2017).
6. Kaufman, H. L., Kohlhapp, F. J. & Zloza, A. Oncolytic viruses: a new class of immunotherapy drugs. *Nat. Rev. Drug Discov.* **14**, 642–662 (2015).
7. Nair, S. & Dhodapkar, M. V. Natural killer T cells in cancer immunotherapy. *Front. Immunol.* **8**, 1178 (2017).
8. Nicholas P Restifo, Mark E Dudley, & Steven A Rosenberg. Adoptive immunotherapy for cancer: harnessing the T cell response. *Nat. Rev. Immunol.* **12**, 269–281 (2012).
9. Yamasaki, K., Shigetoshi|Kurosaki, Motoyoshi|Kunii, Naoki|Nagato, Kaoru|Hanaoka, Hideki|Shimizu, Naomi|Ueno, Naoyuki|Yamamoto, Seiji|Taniguchi, Masaru|Motohashi, Shinichiro|Nakayama, Toshinori|Okamoto, Yoshitaka. Induction of NKT cell-specific immune responses in cancer tissues after NKT cell-targeted adoptive immunotherapy. *Clin. Immunol.* **138**, 255–265 (2010).
10. Kim, J. *et al.* Cell Origins of High-Grade Serous Ovarian Cancer. *Cancers* **10**, 433 (2018).
11. Karst, A. M. & Drapkin, R. Ovarian Cancer Pathogenesis: A Model in Evolution. *J. Oncol.* **2010**, 1–13 (2010).
12. Budiana, I. N. G., Angelina, M. & Pemayun, T. G. A. Ovarian cancer: Pathogenesis and current recommendations for prophylactic surgery. *J. Turk. Ger. Gynecol. Assoc.* **20**, 47–54 (2019).

13. Murdoch, W. J. & Martinchick, J. F. Oxidative damage to DNA of ovarian surface epithelial cells affected by ovulation: carcinogenic implication and chemoprevention. *Exp. Biol. Med. Maywood NJ* **229**, 546–552 (2004).
14. Masoodi, T. *et al.* Genetic heterogeneity and evolutionary history of high-grade ovarian carcinoma and matched distant metastases. *Br. J. Cancer* **122**, 1219–1230 (2020).
15. Kossaï, M., Leary, A., Scoazec, J.-Y. & Genestie, C. Ovarian Cancer: A Heterogeneous Disease. *Pathobiology* **85**, 41–49 (2018).
16. Cho, K. R. & Shih, I.-M. Ovarian Cancer. *Annu. Rev. Pathol. Mech. Dis.* **4**, 287–313 (2009).
17. Roberts, C. M., Cardenas, C. & Tedja, R. The Role of Intra-Tumoral Heterogeneity and Its Clinical Relevance in Epithelial Ovarian Cancer Recurrence and Metastasis. *Cancers* **11**, 1083 (2019).
18. Zhang, X.-Y. & Zhang, P.-Y. Recent perspectives of epithelial ovarian carcinoma. *Oncol. Lett.* **12**, 3055–3058 (2016).
19. Rosen, D. G. *et al.* Ovarian cancer: pathology, biology, and disease models. *Front. Biosci. J. Virtual Libr.* **14**, 2089–2102 (2009).
20. Bell, D. A. Origins and molecular pathology of ovarian cancer. *Mod. Pathol.* **18**, S19–S32 (2005).
21. Shih, I.-M. & Kurman, R. J. Ovarian tumorigenesis: a proposed model based on morphological and molecular genetic analysis. *Am. J. Pathol.* **164**, 1511–1518 (2004).
22. RJ, K., ML, C., CS, H. & RH, Y. *WHO Classification of Tumours of Female Reproductive Organs*.
23. Crum, C. P. *et al.* Lessons from BRCA: The Tubal Fimbria Emerges as an Origin for Pelvic Serous Cancer. *Clin. Med. Res.* **5**, 35–44 (2007).
24. Crum, C. P. *et al.* Through the glass darkly: intraepithelial neoplasia, top-down differentiation and the road to pelvic serous cancer. *J. Pathol.* **231**, 402–412 (2013).
25. George, S. H. L. & Shaw, P. BRCA and Early Events in the Development of Serous Ovarian Cancer. *Front. Oncol.* **4**, 5 (2014).

26. Kindelberger, D. W. *et al.* Intraepithelial carcinoma of the fimbria and pelvic serous carcinoma: Evidence for a causal relationship. *Am. J. Surg. Pathol.* **31**, 161–169 (2007).
27. Lee, Y. *et al.* A candidate precursor to serous carcinoma that originates in the distal fallopian tube. *J. Pathol.* **211**, 26–35 (2007).
28. Medeiros, F. *et al.* The tubal fimbria is a preferred site for early adenocarcinoma in women with familial ovarian cancer syndrome. *Am. J. Surg. Pathol.* **30**, 230–236 (2006).
29. Piek, J. M. *et al.* Dysplastic changes in prophylactically removed Fallopian tubes of women predisposed to developing ovarian cancer. *J. Pathol.* **195**, 451–456 (2001).
30. Stasenko, M., Fillipova, O. & Tew, W. P. Fallopian Tube Carcinoma. *J. Oncol. Pract.* **15**, 375–382 (2019).
31. Nieman, K. M. *et al.* Adipocytes promote ovarian cancer metastasis and provide energy for rapid tumor growth. *Nat. Med.* **17**, 1498–1503 (2011).
32. Petruzzelli, M. *et al.* A switch from white to brown fat increases energy expenditure in cancer-associated cachexia. *Cell Metab.* **20**, 433–447 (2014).
33. Kim, S. *et al.* Tumor evolution and chemoresistance in ovarian cancer. *Npj Precis. Oncol.* **2**, 1–9 (2018).
34. Chang, S.-J. & Bristow, R. E. Evolution of surgical treatment paradigms for advanced-stage ovarian cancer: redefining 'optimal' residual disease. *Gynecol. Oncol.* **125**, 483–492 (2012).
35. Chandra, A. *et al.* Ovarian cancer: Current status and strategies for improving therapeutic outcomes. *Cancer Med.* **8**, 7018–7031 (2019).
36. Vergote, I. *et al.* Neoadjuvant chemotherapy or primary surgery in stage IIIC or IV ovarian cancer. *N. Engl. J. Med.* **363**, 943–953 (2010).
37. Pignata, S. *et al.* Carboplatin-based doublet plus bevacizumab beyond progression versus carboplatin-based doublet alone in patients with platinum-sensitive ovarian cancer: a randomised, phase 3 trial. *Lancet Oncol.* **22**, 267–276 (2021).
38. Moore, K. *et al.* Maintenance Olaparib in Patients with Newly Diagnosed Advanced Ovarian Cancer. *N. Engl. J. Med.* **379**, 2495–2505 (2018).

39. Kurnit, K. C., Fleming, G. F. & Lengyel, E. Updates and New Options in Advanced Epithelial Ovarian Cancer Treatment. *Obstet. Gynecol.* **137**, 108–121 (2021).
40. Arora, T., Mullangi, S. & Lekkala, M. R. Ovarian Cancer. in *StatPearls* (StatPearls Publishing, 2021).
41. Morice, P.-M. *et al.* Myelodysplastic syndrome and acute myeloid leukaemia in patients treated with PARP inhibitors: a safety meta-analysis of randomised controlled trials and a retrospective study of the WHO pharmacovigilance database. *Lancet Haematol.* **8**, e122–e134 (2021).
42. Yang, C. *et al.* Immunotherapy for Ovarian Cancer: Adjuvant, Combination, and Neoadjuvant. *Front. Immunol.* **11**, 2595 (2020).
43. Davidson, B., Trope, C. G. & Reich, R. The Role of the Tumor Stroma in Ovarian Cancer. *Front. Oncol.* **4**, 104 (2014).
44. Valkenburg, K. C., de Groot, A. E. & Pienta, K. J. Targeting the tumour stroma to improve cancer therapy. *Nat. Rev. Clin. Oncol.* **15**, 366–381 (2018).
45. Nersesian, S., Glazebrook, H., Toulany, J., Grantham, S. R. & Boudreau, J. E. Naturally Killing the Silent Killer: NK Cell-Based Immunotherapy for Ovarian Cancer. *Front. Immunol.* **10**, (2019).
46. Mantia-Smaldone, G. M., Corr, B. & Chu, C. S. Immunotherapy in ovarian cancer. *Hum. Vaccines Immunother.* **8**, 1179–1191 (2012).
47. Rodriguez, G. M., Galpin, K. J. C., McCloskey, C. W. & Vanderhyden, B. C. The Tumor Microenvironment of Epithelial Ovarian Cancer and Its Influence on Response to Immunotherapy. *Cancers* **10**, 242 (2018).
48. Dunn, G. P., Old, L. J. & Schreiber, R. D. The Immunobiology of Cancer Immunosurveillance and Immunoediting. *Immunity* **21**, 137–148 (2004).
49. Dunn, G. P., Bruce, A. T., Ikeda, H., Old, L. J. & Schreiber, R. D. Cancer immunoediting: from immunosurveillance to tumor escape. *Nat. Immunol.* **3**, 991–998 (2002).
50. Shankaran, V. *et al.* IFNgamma and lymphocytes prevent primary tumour development and shape tumour immunogenicity. *Nature* **410**, 1107–1111 (2001).
51. Dunn, G. P. *et al.* A critical function for type I interferons in cancer immunoediting. *Nat. Immunol.* **6**, 722–729 (2005).

52. Roos, W. P., Thomas, A. D. & Kaina, B. DNA damage and the balance between survival and death in cancer biology. *Nat. Rev. Cancer* **16**, 20–33 (2016).
53. Lowe, S. W. & Lin, A. W. Apoptosis in cancer. *Carcinogenesis* **21**, 485–495 (2000).
54. Norbury, C. J. & Zhivotovsky, B. DNA damage-induced apoptosis. *Oncogene* **23**, 2797–2808 (2004).
55. Chen, D. S. & Mellman, I. Oncology meets immunology: the cancer-immunity cycle. *Immunity* **39**, 1–10 (2013).
56. Nausch, N. & Cerwenka, A. NKG2D ligands in tumor immunity. *Oncogene* **27**, 5944–5958 (2008).
57. Kuylenstierna, C. *et al.* NKG2D performs two functions in invariant NKT cells: Direct TCR-independent activation of NK-like cytolysis, and co-stimulation of activation by CD1d. *Eur. J. Immunol.* **41**, 1913–1923 (2011).
58. Chao, M. P. *et al.* Calreticulin is the dominant pro-phagocytic signal on multiple human cancers and is counterbalanced by CD47. *Sci. Transl. Med.* **2**, 63ra94 (2010).
59. Durgeau, A., Virk, Y., Corgnac, S. & Mami-Chouaib, F. Recent Advances in Targeting CD8 T-Cell Immunity for More Effective Cancer Immunotherapy. *Front. Immunol.* **9**, (2018).
60. Vivier, E., Tomasello, E., Baratin, M., Walzer, T. & Ugolini, S. Functions of natural killer cells. *Nat. Immunol.* **9**, 503–510 (2008).
61. Becknell, B. & Caligiuri, M. A. Natural killer cells in innate immunity and cancer. *J. Immunother. Hagerstown Md 1997* **31**, 685–692 (2008).
62. Caligiuri, M. A. Human natural killer cells. *Blood* **112**, 461–469 (2008).
63. Hayakawa, Y., Huntington, N. D., Nutt, S. L. & Smyth, M. J. Functional subsets of mouse natural killer cells. *Immunol. Rev.* **214**, 47–55 (2006).
64. Cheent, K. & Khakoo, S. I. Natural killer cells: integrating diversity with function. *Immunology* **126**, 449–457 (2009).
65. Kannan, G. S., Aquino-Lopez, A. & Lee, D. A. Natural killer cells in malignant hematology: A primer for the non-immunologist. *Blood Rev.* **31**, 1–10 (2017).
66. Hu, W., Wang, G., Huang, D., Sui, M. & Xu, Y. Cancer Immunotherapy Based on Natural Killer Cells: Current Progress and New Opportunities. *Front. Immunol.* **10**, 1205 (2019).

67. Wu, S.-Y., Fu, T., Jiang, Y.-Z. & Shao, Z.-M. Natural killer cells in cancer biology and therapy. *Mol. Cancer* **19**, 120 (2020).
68. Shimasaki, N., Jain, A. & Campana, D. NK cells for cancer immunotherapy. *Nat. Rev. Drug Discov.* **19**, 200–218 (2020).
69. Schmiedel, D. & Mandelboim, O. NKG2D Ligands–Critical Targets for Cancer Immune Escape and Therapy. *Front. Immunol.* **9**, (2018).
70. Ardolino, M. *et al.* Cytokine therapy reverses NK cell anergy in MHC-deficient tumors. *J. Clin. Invest.* **124**, 4781–4794 (2014).
71. Albertsson, P. A. *et al.* NK cells and the tumour microenvironment: implications for NK-cell function and anti-tumour activity. *Trends Immunol.* **24**, 603–609 (2003).
72. Wu, J. & Lanier, L. L. Natural killer cells and cancer. *Adv. Cancer Res.* **90**, 127–156 (2003).
73. Bubeník, J. Tumour MHC class I downregulation and immunotherapy (Review). *Oncol. Rep.* **10**, 2005–2008 (2003).
74. Cornel, A. M., Mimpen, I. L. & Nierkens, S. MHC Class I Downregulation in Cancer: Underlying Mechanisms and Potential Targets for Cancer Immunotherapy. *Cancers* **12**, 1760 (2020).
75. Cooper, M. A., Fehniger, T. A. & Caligiuri, M. A. The biology of human natural killer-cell subsets. *Trends Immunol.* **22**, 633–640 (2001).
76. Sun, Y. *et al.* Natural killer cells inhibit metastasis of ovarian carcinoma cells and show therapeutic effects in a murine model of ovarian cancer. *Exp. Ther. Med.* **16**, 1071–1078 (2018).
77. Poznanski, S. M. *et al.* Expanded CD56superbrightCD16+ NK Cells from Ovarian Cancer Patients Are Cytotoxic against Autologous Tumor in a Patient-Derived Xenograft Murine Model. *Cancer Immunol. Res.* **6**, 1174–1185 (2018).
78. Mandal, R. *et al.* The head and neck cancer immune landscape and its immunotherapeutic implications. *JCI Insight* **1**, e89829 (2016).
79. Sato, E. *et al.* Intraepithelial CD8+ tumor-infiltrating lymphocytes and a high CD8+/regulatory T cell ratio are associated with favorable prognosis in ovarian cancer. *Proc. Natl. Acad. Sci.* **102**, 18538–18543 (2005).

80. Zhang, L. *et al.* Intratumoral T Cells, Recurrence, and Survival in Epithelial Ovarian Cancer. *N. Engl. J. Med.* **348**, 203–213 (2003).
81. Lai, P. *et al.* Alterations in expression and function of signal-transducing proteins in tumor-associated T and natural killer cells in patients with ovarian carcinoma. *Clin. Cancer Res. Off. J. Am. Assoc. Cancer Res.* **2**, 161–173 (1996).
82. Yung, M. M.-H. *et al.* GRO-α and IL-8 enhance ovarian cancer metastatic potential via the CXCR2-mediated TAK1/NFκB signaling cascade. *Theranostics* **8**, 1270–1285 (2018).
83. Toker, A. *et al.* Regulatory T Cells in Ovarian Cancer Are Characterized by a Highly Activated Phenotype Distinct from that in Melanoma. *Clin. Cancer Res. Off. J. Am. Assoc. Cancer Res.* **24**, 5685–5696 (2018).
84. Barnett, B., Kryczek, I., Cheng, P., Zou, W. & Curiel, T. J. Regulatory T cells in ovarian cancer: biology and therapeutic potential. *Am. J. Reprod. Immunol. N. Y. N 1989* **54**, 369–377 (2005).
85. Bruno, A., Mortara, L., Baci, D., Noonan, D. M. & Albini, A. Myeloid Derived Suppressor Cells Interactions With Natural Killer Cells and Pro-angiogenic Activities: Roles in Tumor Progression. *Front. Immunol.* **10**, 771 (2019).
86. Baert, T. *et al.* Myeloid Derived Suppressor Cells: Key Drivers of Immunosuppression in Ovarian Cancer. *Front. Immunol.* **10**, 1273 (2019).
87. Patankar, M. S. *et al.* Potent suppression of natural killer cell response mediated by the ovarian tumor marker CA125. *Gynecol. Oncol.* **99**, 704–713 (2005).
88. Krockenberger, M. *et al.* Macrophage Migration Inhibitory Factor (MIF) Contributes to the Immune Escape of Ovarian Cancer by Downregulating NKG2D. *J. Immunol. Baltim. Md 1950* **180**, 7338–7348 (2008).
89. Reina-Campos, M., Scharping, N. E. & Goldrath, A. W. CD8+ T cell metabolism in infection and cancer. *Nat. Rev. Immunol.* 1–21 (2021) doi:10.1038/s41577-021-00537-8.
90. Mempel, T. R., Henrickson, S. E. & von Andrian, U. H. T-cell priming by dendritic cells in lymph nodes occurs in three distinct phases. *Nature* **427**, 154–159 (2004).
91. Zehn, D., Lee, S. Y. & Bevan, M. J. Complete but curtailed T-cell response to very low-affinity antigen. *Nature* **458**, 211–214 (2009).

92. Blair, D. A. & Dustin, M. L. T cell priming goes through a new phase. *Nat. Immunol.* **14**, 311–312 (2013).
93. Tay, N. Q. *et al.* CD40L Expression Allows CD8+ T Cells to Promote Their Own Expansion and Differentiation through Dendritic Cells. *Front. Immunol.* **8**, (2017).
94. Watts, T. H. TNF/TNFR family members in costimulation of T cell responses. *Annu. Rev. Immunol.* **23**, 23–68 (2005).
95. Blattman, J. N. *et al.* Estimating the precursor frequency of naive antigen-specific CD8 T cells. *J. Exp. Med.* **195**, 657–664 (2002).
96. Trinité, B. *et al.* Suppression of Foxo1 Activity and Down-Modulation of CD62L (L-Selectin) in HIV-1 Infected Resting CD4 T Cells. *PLOS ONE* **9**, e110719 (2014).
97. Voskoboinik, I., Smyth, M. J. & Trapani, J. A. Perforin-mediated target-cell death and immune homeostasis. *Nat. Rev. Immunol.* **6**, 940–952 (2006).
98. Gordy, C. & He, Y.-W. Endocytosis by target cells: an essential means for perforin- and granzyme-mediated killing. *Cell. Mol. Immunol.* **9**, 5–6 (2012).
99. Hoves, S., Trapani, J. A. & Voskoboinik, I. The battlefield of perforin/granzyme cell death pathways. *J. Leukoc. Biol.* **87**, 237–243 (2010).
100. Fu, Q. *et al.* Structural Basis and Functional Role of Intramembrane Trimerization of the Fas/CD95 Death Receptor. *Mol. Cell* **61**, 602–613 (2016).
101. Rao, R. R., Li, Q., Gubbels Bupp, M. R. & Shrikant, P. A. Transcription factor Foxo1 represses T-bet-mediated effector functions and promotes memory CD8(+) T cell differentiation. *Immunity* **36**, 374–387 (2012).
102. Mueller, S. N., Gebhardt, T., Carbone, F. R. & Heath, W. R. Memory T cell subsets, migration patterns, and tissue residence. *Annu. Rev. Immunol.* **31**, 137–161 (2013).
103. Lighvani, A. A. *et al.* T-bet is rapidly induced by interferon-γ in lymphoid and myeloid cells. *Proc. Natl. Acad. Sci.* **98**, 15137–15142 (2001).
104. Siddiqui, I. *et al.* Intratumoral Tcf1+PD-1+CD8+ T Cells with Stem-like Properties Promote Tumor Control in Response to Vaccination and Checkpoint Blockade Immunotherapy. *Immunity* **50**, 195-211.e10 (2019).
105. Zhang, Y., Joe, G., Hexner, E., Zhu, J. & Emerson, S. G. Host-reactive CD8+ memory stem cells in graft-versus-host disease. *Nat. Med.* **11**, 1299–1305 (2005).

106. Gattinoni, L., Speiser, D. E., Lichterfeld, M. & Bonini, C. T memory stem cells in health and disease. *Nat. Med.* **23**, 18–27 (2017).
107. Galon, J. *et al.* Type, density, and location of immune cells within human colorectal tumors predict clinical outcome. *Science* **313**, 1960–1964 (2006).
108. Fridman, W. H., Pagès, F., Sautès-Fridman, C. & Galon, J. The immune contexture in human tumours: impact on clinical outcome. *Nat. Rev. Cancer* **12**, 298–306 (2012).
109. Fridman, W. H., Zitvogel, L., Sautès-Fridman, C. & Kroemer, G. The immune contexture in cancer prognosis and treatment. *Nat. Rev. Clin. Oncol.* **14**, 717–734 (2017).
110. Hu, Z., Gu, X., Zhong, R. & Zhong, H. Tumor-infiltrating CD45RO+ memory cells correlate with favorable prognosis in patients with lung adenocarcinoma. *J. Thorac. Dis.* **10**, 2089–2099 (2018).
111. Remark, R. *et al.* Characteristics and clinical impacts of the immune environments in colorectal and renal cell carcinoma lung metastases: influence of tumor origin. *Clin. Cancer Res. Off. J. Am. Assoc. Cancer Res.* **19**, 4079–4091 (2013).
112. Petitprez, F. *et al.* PD-L1 Expression and CD8+ T-cell Infiltrate are Associated with Clinical Progression in Patients with Node-positive Prostate Cancer. *Eur. Urol. Focus* **5**, 192–196 (2019).
113. Bruni, D., Angell, H. K. & Galon, J. The immune contexture and Immunoscore in cancer prognosis and therapeutic efficacy. *Nat. Rev. Cancer* **20**, 662–680 (2020).
114. Liu, Y.-T. & Sun, Z.-J. Turning cold tumors into hot tumors by improving T-cell infiltration. *Theranostics* **11**, 5365–5386 (2021).
115. Spranger, S., Bao, R. & Gajewski, T. F. Melanoma-intrinsic β-catenin signalling prevents anti-tumour immunity. *Nature* **523**, 231–235 (2015).
116. Apte, R. S., Chen, D. S. & Ferrara, N. VEGF in Signaling and Disease: Beyond Discovery and Development. *Cell* **176**, 1248–1264 (2019).
117. Mariathasan, S. *et al.* TGFβ attenuates tumour response to PD-L1 blockade by contributing to exclusion of T cells. *Nature* **554**, 544–548 (2018).
118. Tauriello, D. V. F. *et al.* TGFβ drives immune evasion in genetically reconstituted colon cancer metastasis. *Nature* **554**, 538–543 (2018).

119. Holmgaard, R. B. *et al.* Tumor-Expressed IDO Recruits and Activates MDSCs in a Treg-Dependent Manner. *Cell Rep.* **13**, 412–424 (2015).
120. Liu, Z. *et al.* Tumor Vasculatures: A New Target for Cancer Immunotherapy. *Trends Pharmacol. Sci.* **40**, 613–623 (2019).
121. Hamarsheh, S., Groß, O., Brummer, T. & Zeiser, R. Immune modulatory effects of oncogenic KRAS in cancer. *Nat. Commun.* **11**, 5439 (2020).
122. Huang, Y. *et al.* Improving immune–vascular crosstalk for cancer immunotherapy. *Nat. Rev. Immunol.* **18**, 195–203 (2018).
123. Semenza, G. L. Hypoxia-inducible factors in physiology and medicine. *Cell* **148**, 399–408 (2012).
124. Damgaci, S. *et al.* Hypoxia and acidosis: immune suppressors and therapeutic targets. *Immunology* **154**, 354–362 (2018).
125. Jing, X. *et al.* Role of hypoxia in cancer therapy by regulating the tumor microenvironment. *Mol. Cancer* **18**, 157 (2019).
126. Salmon, H. *et al.* Matrix architecture defines the preferential localization and migration of T cells into the stroma of human lung tumors. *J. Clin. Invest.* **122**, 899–910 (2012).
127. Sahai, E. *et al.* A framework for advancing our understanding of cancer-associated fibroblasts. *Nat. Rev. Cancer* **20**, 174–186 (2020).
128. Liu, T., Zhou, L., Li, D., Andl, T. & Zhang, Y. Cancer-Associated Fibroblasts Build and Secure the Tumor Microenvironment. *Front. Cell Dev. Biol.* **7**, 60 (2019).
129. Binnewies, M. *et al.* Understanding the tumor immune microenvironment (TIME) for effective therapy. *Nat. Med.* **24**, 541–550 (2018).
130. Ademmer, K. *et al.* Effector T lymphocyte subsets in human pancreatic cancer: detection of CD8+CD18+ cells and CD8+CD103+ cells by multi-epitope imaging. *Clin. Exp. Immunol.* **112**, 21–26 (1998).
131. Herbst, R. S. *et al.* Predictive correlates of response to the anti-PD-L1 antibody MPDL3280A in cancer patients. *Nature* **515**, 563–567 (2014).
132. Mlecnik, B. *et al.* Integrative Analyses of Colorectal Cancer Show Immunoscore Is a Stronger Predictor of Patient Survival Than Microsatellite Instability. *Immunity* **44**, 698–711 (2016).

133. Wherry, E. J. & Kurachi, M. Molecular and cellular insights into T cell exhaustion. *Nat. Rev. Immunol.* **15**, 486–499 (2015).
134. Huang, R.-Y. *et al.* LAG3 and PD1 co-inhibitory molecules collaborate to limit CD8+ T cell signaling and dampen antitumor immunity in a murine ovarian cancer model. *Oncotarget* **6**, 27359–27377 (2015).
135. Pitt, J. M. *et al.* Resistance Mechanisms to Immune-Checkpoint Blockade in Cancer: Tumor-Intrinsic and -Extrinsic Factors. *Immunity* **44**, 1255–1269 (2016).
136. Lee, J., Ahn, E., Kissick, H. T. & Ahmed, R. Reinvigorating Exhausted T Cells by Blockade of the PD-1 Pathway. *Forum Immunopathol. Dis. Ther.* **6**, 7–17 (2015).
137. Tabana, Y., Moon, T. C., Siraki, A., Elahi, S. & Barakat, K. Reversing T-cell exhaustion in immunotherapy: a review on current approaches and limitations. *Expert Opin. Ther. Targets* **25**, 347–363 (2021).
138. Qin, Y. *et al.* Invariant NKT cells facilitate cytotoxic T-cell activation via direct recognition of CD1d on T cells. *Exp. Mol. Med.* **51**, 1–9 (2019).
139. Rossjohn, J., Pellicci, D. G., Patel, O., Gapin, L. & Godfrey, D. I. Recognition of CD1d-restricted antigens by natural killer T cells. *Nat. Rev. Immunol.* **12**, 845–857 (2012).
140. Brennan, P. J., Brigl, M. & Brenner, M. B. Invariant natural killer T cells: an innate activation scheme linked to diverse effector functions. *Nat. Rev. Immunol.* **13**, 101–117 (2013).
141. Van Kaer, L., Parekh, V. V. & Wu, L. Invariant natural killer T cells: bridging innate and adaptive immunity. *Cell Tissue Res.* **343**, 43–55 (2011).
142. Matsuda, J. L. *et al.* Tracking the Response of Natural Killer T Cells to a Glycolipid Antigen Using Cd1d Tetramers. *J. Exp. Med.* **192**, 741–754 (2000).
143. Girardi, E. *et al.* Type II natural killer T cells use features of both innate-like and conventional T cells to recognize sulfatide self antigens. *Nat. Immunol.* **13**, 851–856 (2012).
144. Patel, O. *et al.* Recognition of CD1d-sulfatide mediated by a type II natural killer T cell antigen receptor. *Nat. Immunol.* **13**, 857–863 (2012).

145. Arrenberg, P., Halder, R., Dai, Y., Maricic, I. & Kumar, V. Oligoclonality and innate-like features in the TCR repertoire of type II NKT cells reactive to a beta-linked self-glycolipid. *Proc. Natl. Acad. Sci. U. S. A.* **107**, 10984–10989 (2010).
146. Ambrosino, E. *et al.* Cross-Regulation between Type I and Type II NKT Cells in Regulating Tumor Immunity: A New Immunoregulatory Axis. *J. Immunol.* **179**, 5126–5136 (2007).
147. Dhodapkar, M. V. & Kumar, V. Type II Natural Killer T (NKT) Cells And Their Emerging Role In Health And Disease. *J. Immunol. Baltim. Md 1950* **198**, 1015–1021 (2017).
148. Webb, T. J., Yuan, W., Meyer, E. & Dellabona, P. Editorial: NKT Cells in Cancer Immunotherapy. *Front. Immunol.* **11**, 1314 (2020).
149. Hogquist, K. & Georgiev, H. Recent advances in iNKT cell development. *F1000Research* **9**, F1000 Faculty Rev-127 (2020).
150. Wolf, B. J., Exley, M. A., Exley, M. A. & Exley, M. A. Novel Approaches to Exploiting Invariant NKT Cells in Cancer Immunotherapy. *Front. Immunol.* (2018) doi:10.3389/fimmu.2018.00384.
151. Hogquist, K. & Georgiev, H. Recent advances in iNKT cell development. *F1000Research* **9**, F1000 Faculty Rev-127 (2020).
152. Wu, D. Y., Segal, N. H., Sidobre, S., Kronenberg, M. & Chapman, P. B. Cross-presentation of Disialoganglioside GD3 to Natural Killer T Cells. *J. Exp. Med.* **198**, 173–181 (2003).
153. Nelson, A., Lukacs, J. D. & Johnston, B. The Current Landscape of NKT Cell Immunotherapy and the Hills Ahead. *Cancers* **13**, 5174 (2021).
154. Eberl, G. & MacDonald, H. R. Selective induction of NK cell proliferation and cytotoxicity by activated NKT cells. *Eur. J. Immunol.* **30**, 985–992 (2000).
155. Sag, D., Özkan, M., Kronenberg, M. & Wingender, G. Improved Detection of Cytokines Produced by Invariant NKT Cells. *Sci. Rep.* **7**, 16607 (2017).
156. Coquet, J. M. *et al.* Diverse cytokine production by NKT cell subsets and identification of an IL-17–producing CD4−NK1.1− NKT cell population. *Proc. Natl. Acad. Sci.* **105**, 11287–11292 (2008).

157. Ligocki, A. J. & Niederkorn, J. Y. Natural Killer T Cells Contribute to Neutrophil Recruitment and Ocular Tissue Damage in a Model of Intraocular Tumor Rejection. *Invest. Ophthalmol. Vis. Sci.* **57**, 813–823 (2016).
158. Michel, M.-L. *et al.* Identification of an IL-17–producing NK1.1neg iNKT cell population involved in airway neutrophilia. *J. Exp. Med.* **204**, 995–1001 (2007).
159. Huang, E. *et al.* NKT cells mediate the recruitment of neutrophils by stimulating epithelial chemokine secretion during colitis. *Biochem. Biophys. Res. Commun.* **474**, 252–258 (2016).
160. Kim, J. H. & Chung, D. H. CD1d-restricted IFN-γ-secreting NKT cells promote immune complex-induced acute lung injury by regulating macrophage-inflammatory protein-1α production and activation of macrophages and dendritic cells. *J. Immunol. Baltim. Md 1950* **186**, 1432–1441 (2011).
161. Paul, S., Chhatar, S., Mishra, A. & Lal, G. Natural killer T cell activation increases iNOS+CD206- M1 macrophage and controls the growth of solid tumor. *J. Immunother. Cancer* **7**, 208 (2019).
162. Lynch, L. *et al.* Regulatory iNKT cells lack PLZF expression and control Treg cell and macrophage homeostasis in adipose tissue. *Nat. Immunol.* **16**, 85–95 (2015).
163. Ji, Y. *et al.* Activation of Natural Killer T Cells Promotes M2 Macrophage Polarization in Adipose Tissue and Improves Systemic Glucose Tolerance via Interleukin-4 (IL-4)/STAT6 Protein Signaling Axis in Obesity*. *J. Biol. Chem.* **287**, 13561–13571 (2012).
164. Matsuda, J. L., Mallevaey, T., Scott-Browne, J. & Gapin, L. CD1d-restricted iNKT cells, the “Swiss-Army knife” of the immune system. *Curr. Opin. Immunol.* **20**, 358–368 (2008).
165. Gebremeskel, S. *et al.* Natural Killer T-cell Immunotherapy in Combination with Chemotherapy-Induced Immunogenic Cell Death Targets Metastatic Breast Cancer. *Cancer Immunol. Res.* **5**, 1086–1097 (2017).
166. Gebremeskel, S. *et al.* Natural killer T cell immunotherapy combined with oncolytic vesicular stomatitis virus or reovirus treatments differentially increases survival in mouse models of ovarian and breast cancer metastasis. *J. Immunother. Cancer* **9**, e002096 (2021).

167. Gebremeskel, S., Slauenwhite, D. & Johnston, B. Reconstitution models to evaluate natural killer T cell function in tumor control. *Immunol. Cell Biol.* **94**, 90–100 (2016).
168. Fujii, S.-I., Shimizu, K., Smith, C., Bonifaz, L. & Steinman, R. M. Activation of natural killer T cells by alpha-galactosylceramide rapidly induces the full maturation of dendritic cells in vivo and thereby acts as an adjuvant for combined CD4 and CD8 T cell immunity to a coadministered protein. *J. Exp. Med.* **198**, 267–279 (2003).
169. Hermans, I. F. *et al.* NKT Cells Enhance CD4+ and CD8+ T Cell Responses to Soluble Antigen In Vivo through Direct Interaction with Dendritic Cells. *J. Immunol.* **171**, 5140–5147 (2003).
170. Tonti, E. *et al.* NKT-cell help to B lymphocytes can occur independently of cognate interaction. *Blood* **113**, 370–376 (2009).
171. Leadbetter, E. A. & Karlsson, M. C. I. Invariant natural killer T cells balance B cell immunity. *Immunol. Rev.* **299**, 93–107 (2021).
172. Cui, J. *et al.* Requirement for Valpha14 NKT cells in IL-12-mediated rejection of tumors. *Science* **278**, 1623–1626 (1997).
173. Metelitsa, L. S. Anti-tumor potential of type-I NKT cells against CD1d-positive and CD1d-negative tumors in humans. *Clin. Immunol. Orlando Fla* **140**, 119–129 (2011).
174. Godfrey, D. I., Stankovic, S. & Baxter, A. G. Raising the NKT cell family. *Nat. Immunol.* **11**, 197–206 (2010).
175. Georgiev, H., Ravens, I., Benarafa, C., Förster, R. & Bernhardt, G. Distinct gene expression patterns correlate with developmental and functional traits of iNKT subsets. *Nat. Commun.* **7**, 13116 (2016).
176. Kronenberg, M. & Gapin, L. The unconventional lifestyle of NKT cells. *Nat. Rev. Immunol.* **2**, 557–568 (2002).
177. Bendelac, A., Savage, P. B. & Teyton, L. The biology of NKT cells. *Annu. Rev. Immunol.* **25**, 297–336 (2007).
178. Tuttle, K. D. *et al.* TCR signal strength controls thymic differentiation of iNKT cell subsets. *Nat. Commun.* **9**, 2650 (2018).

179. Crowe, N. Y. *et al.* Differential antitumor immunity mediated by NKT cell subsets in vivo. *J. Exp. Med.* **202**, 1279–1288 (2005).
180. Lee, P. T., Benlagha, K., Teyton, L. & Bendelac, A. Distinct functional lineages of human V(alpha)24 natural killer T cells. *J. Exp. Med.* **195**, 637–641 (2002).
181. Gumperz, J. E., Miyake, S., Yamamura, T. & Brenner, M. B. Functionally distinct subsets of CD1d-restricted natural killer T cells revealed by CD1d tetramer staining. *J. Exp. Med.* **195**, 625–636 (2002).
182. Slauenwhite, D. & Johnston, B. Regulation of NKT Cell Localization in Homeostasis and Infection. *Front. Immunol.* **6**, 255 (2015).
183. Wingender, G. *et al.* Intestinal microbes affect phenotypes and functions of invariant natural killer T cells in mice. *Gastroenterology* **143**, 418–428 (2012).
184. Laloux, V., Beaudoin, L., Ronet, C. & Lehuen, A. Phenotypic and functional differences between NKT cells colonizing splanchnic and peripheral lymph nodes. *J. Immunol. Baltim. Md 1950* **168**, 3251–3258 (2002).
185. Mattner, J. *et al.* Exogenous and endogenous glycolipid antigens activate NKT cells during microbial infections. *Nature* **434**, 525–529 (2005).
186. Natori, T., Koezuka, Y. & Higa, T. Agelasphins, novel α-galactosylceramides from the marine sponge Agelas mauritianus. *Tetrahedron Lett.* **34**, 5591–5592 (1993).
187. Kawano, T. *et al.* Natural killer-like nonspecific tumor cell lysis mediated by specific ligand-activated Vα14 NKT cells. *Proc. Natl. Acad. Sci.* **95**, 5690–5693 (1998).
188. Nakagawa, R. *et al.* Treatment of hepatic metastasis of the Colon26 adenocarcinoma with an α-Galactosylceramide, KRN7000. *Cancer Res.* **58**, 1202–1207 (1998).
189. Giaccone, G. *et al.* A Phase I Study of the Natural Killer T-Cell Ligand α-Galactosylceramide (KRN7000) in Patients with Solid Tumors. *Clin. Cancer Res.* **8**, 3702–3709 (2002).
190. Hayakawa, Y., Rovero, S., Forni, G. & Smyth, M. J. α-Galactosylceramide (KRN7000) suppression of chemical- and oncogene-dependent carcinogenesis. *Proc. Natl. Acad. Sci.* **100**, 9464–9469 (2003).

191. Spada, F. M., Koezuka, Y. & Porcelli, S. A. CD1d-restricted Recognition of Synthetic Glycolipid Antigens by Human Natural Killer T Cells. *J. Exp. Med.* **188**, 1529–1534 (1998).
192. Fernandez, C. S., Cameron, G., Godfrey, D. I. & Kent, S. J. Ex-vivo α-galactosylceramide activation of NKT cells in humans and macaques. *J. Immunol. Methods* (2012) doi:10.1016/j.jim.2012.05.019.
193. Ishikawa, A. *et al.* A phase I study of alpha-galactosylceramide (KRN7000)-pulsed dendritic cells in patients with advanced and recurrent non-small cell lung cancer. *Clin. Cancer Res. Off. J. Am. Assoc. Cancer Res.* **11**, 1910–1917 (2005).
194. Zhang, Y. *et al.* α-GalCer and iNKT Cell-Based Cancer Immunotherapy: Realizing the Therapeutic Potentials. *Front. Immunol.* **10**, 1126 (2019).
195. Bae, E.-A., Seo, H., Kim, I.-K., Jeon, I. & Kang, C.-Y. Roles of NKT cells in cancer immunotherapy. *Arch. Pharm. Res.* **42**, 543–548 (2019).
196. Cullen, R., Germanov, E., Shimaoka, T. & Johnston, B. Enhanced tumor metastasis in response to blockade of the chemokine receptor CXCR6 is overcome by NKT cell activation. *J. Immunol. Baltim. Md 1950* **183**, 5807–5815 (2009).
197. Godfrey, D. I. & Kronenberg, M. Going both ways: Immune regulation via CD1d-dependent NKT cells. *J. Clin. Invest.* **114**, 1379–1388 (2004).
198. McCarthy, C. *et al.* The length of lipids bound to human CD1d molecules modulates the affinity of NKT cell TCR and the threshold of NKT cell activation. *J. Exp. Med.* **204**, 1131–1144 (2007).
199. Schmieg, J., Yang, G., Franck, R. W. & Tsuji, M. Superior protection against malaria and melanoma metastases by a C-glycoside analogue of the natural killer T cell ligand alpha-Galactosylceramide. *J. Exp. Med.* **198**, 1631–1641 (2003).
200. Oki, S., Chiba, A., Yamamura, T. & Miyake, S. The clinical implication and molecular mechanism of preferential IL-4 production by modified glycolipid-stimulated NKT cells. *J. Clin. Invest.* **113**, 1631–1640 (2004).
201. Ly, D. *et al.* An alpha-galactosylceramide C20:2 N-acyl variant enhances anti-inflammatory and regulatory T cell-independent responses that prevent type 1 diabetes. *Clin. Exp. Immunol.* **160**, 185–198 (2010).

202. Blumenfeld, H. J. *et al.* Structure-guided design of an invariant natural killer T cell agonist for optimum protection from type 1 diabetes in non-obese diabetic mice. *Clin. Exp. Immunol.* **166**, 121–133 (2011).
203. Zhou, D. *et al.* Lysosomal Glycosphingolipid Recognition by NKT Cells. *Science* **306**, 1786–1789 (2004).
204. Brennan, P. J. *et al.* Invariant natural killer T cells recognize lipid self antigen induced by microbial danger signals. *Nat. Immunol.* **12**, 1202–1211 (2011).
205. Darmoise, A. *et al.* Lysosomal α-Galactosidase Controls the Generation of Self Lipid Antigens for Natural Killer T Cells. *Immunity* **33**, 216–228 (2010).
206. Facciotti, F. *et al.* Peroxisome-derived lipids are self antigens that stimulate invariant natural killer T cells in the thymus. *Nat. Immunol.* **13**, 474–480 (2012).
207. Hung, J.-T., Huang, J.-R. & Yu, A. L. Tailored design of NKT-stimulatory glycolipids for polarization of immune responses. *J. Biomed. Sci.* **24**, 22 (2017).
208. Im, J. S. *et al.* Kinetics and Cellular Site of Glycolipid Loading Control the Outcome of Natural Killer T Cell Activation. *Immunity* **30**, 888–898 (2009).
209. Sullivan, B. A. & Kronenberg, M. Activation or anergy: NKT cells are stunned by alpha-galactosylceramide. *J. Clin. Invest.* **115**, 2328–2329 (2005).
210. Parekh, V. V. *et al.* Glycolipid antigen induces long-term natural killer T cell anergy in mice. *J. Clin. Invest.* **115**, 2572–2583 (2005).
211. Kim, Y.-J. *et al.* alpha-Galactosylceramide-loaded, antigen-expressing B cells prime a wide spectrum of antitumor immunity. *Int. J. Cancer* **122**, 2774–2783 (2008).
212. Chang, D. H. *et al.* Sustained expansion of NKT cells and antigen-specific T cells after injection of alpha-galactosyl-ceramide loaded mature dendritic cells in cancer patients. *J. Exp. Med.* **201**, 1503–1517 (2005).
213. Chung, Y. *et al.* CD1d-restricted T cells license B cells to generate long-lasting cytotoxic antitumor immunity in vivo. *Cancer Res.* **66**, 6843–6850 (2006).
214. Fujii, S., Shimizu, K., Kronenberg, M. & Steinman, R. M. Prolonged IFN-γ–producing NKT response induced with α-galactosylceramide–loaded DCs. *Nat. Immunol.* **3**, 867–874 (2002).
215. Steinman, R. M. & Hemmi, H. Dendritic cells: translating innate to adaptive immunity. *Curr. Top. Microbiol. Immunol.* **311**, 17–58 (2006).

216. Sallusto, F. & Lanzavecchia, A. Efficient presentation of soluble antigen by cultured human dendritic cells is maintained by granulocyte/macrophage colony-stimulating factor plus interleukin 4 and downregulated by tumor necrosis factor alpha. *J. Exp. Med.* **179**, 1109–1118 (1994).
217. Cella, M., Sallusto, F. & Lanzavecchia, A. Origin, maturation and antigen presenting function of dendritic cells. *Curr. Opin. Immunol.* **9**, 10–16 (1997).
218. Sabado, R. L., Balan, S. & Bhardwaj, N. Dendritic cell-based immunotherapy. *Cell Res.* **27**, 74–95 (2017).
219. Dalod, M., Chelbi, R., Malissen, B. & Lawrence, T. Dendritic cell maturation: functional specialization through signaling specificity and transcriptional programming. *EMBO J.* **33**, 1104–1116 (2014).
220. Sallusto, F. & Lanzavecchia, A. The instructive role of dendritic cells on T-cell responses. *Arthritis Res. Ther.* **4**, S127 (2002).
221. Obermajer, N., Muthuswamy, R., Odunsi, K., Edwards, R. P. & Kalinski, P. PGE(2)-induced CXCL12 production and CXCR4 expression controls the accumulation of human MDSCs in ovarian cancer environment. *Cancer Res.* **71**, 7463–7470 (2011).
222. Komura, N. *et al.* The role of myeloid-derived suppressor cells in increasing cancer stem-like cells and promoting PD-L1 expression in epithelial ovarian cancer. *Cancer Immunol. Immunother. CII* **69**, 2477–2499 (2020).
223. Lee, J.-M. *et al.* Patients with BRCA mutated ovarian cancer may have fewer circulating MDSC and more peripheral CD8+ T cells compared with women with BRCA wild-type disease during the early disease course. *Oncol. Lett.* **18**, 3914–3924 (2019).
224. Cui, T. X. *et al.* Myeloid-derived suppressor cells enhance stemness of cancer cells by inducing microRNA101 and suppressing the corepressor CtBP2. *Immunity* **39**, 611–621 (2013).
225. Taki, M. *et al.* Snail promotes ovarian cancer progression by recruiting myeloid-derived suppressor cells via CXCR2 ligand upregulation. *Nat. Commun.* **9**, 1685 (2018).

226. Okła, K. *et al.* Clinical Relevance and Immunosuppressive Pattern of Circulating and Infiltrating Subsets of Myeloid-Derived Suppressor Cells (MDSCs) in Epithelial Ovarian Cancer. *Front. Immunol.* **10**, 691 (2019).
227. Bronte, V. *et al.* Recommendations for myeloid-derived suppressor cell nomenclature and characterization standards. *Nat. Commun.* **7**, 12150 (2016).
228. Gabrilovich, D. I. *et al.* The terminology issue for myeloid-derived suppressor cells. *Cancer Res.* **67**, 425; author reply 426 (2007).
229. Santegoets, S. J. a. M. *et al.* The blood mMDSC to DC ratio is a sensitive and easy to assess independent predictive factor for epithelial ovarian cancer survival. *Oncoimmunology* **7**, e1465166 (2018).
230. Wu, L. *et al.* Ascites-derived IL-6 and IL-10 synergistically expand CD14+HLA-DR-/low myeloid-derived suppressor cells in ovarian cancer patients. *Oncotarget* **8**, 76843–76856 (2017).
231. Mabuchi, S., Sasano, T. & Komura, N. Targeting Myeloid-Derived Suppressor Cells in Ovarian Cancer. *Cells* **10**, 329 (2021).
232. Baniyash, M. TCR zeta-chain downregulation: curtailing an excessive inflammatory immune response. *Nat. Rev. Immunol.* **4**, 675–687 (2004).
233. Mundy-Bosse, B. L. *et al.* Myeloid-derived suppressor cell inhibition of the IFN response in tumor-bearing mice. *Cancer Res.* **71**, 5101–5110 (2011).
234. Stiff, A. *et al.* Nitric Oxide Production by Myeloid-Derived Suppressor Cells Plays a Role in Impairing Fc Receptor-Mediated Natural Killer Cell Function. *Clin. Cancer Res. Off. J. Am. Assoc. Cancer Res.* **24**, 1891–1904 (2018).
235. Wang, Z. *et al.* A myeloid cell population induced by Freund adjuvant suppresses T-cell-mediated antitumor immunity. *J. Immunother. Hagerstown Md 1997* **33**, 167–177 (2010).
236. Kusmartsev, S., Nefedova, Y., Yoder, D. & Gabrilovich, D. I. Antigen-specific inhibition of CD8+ T cell response by immature myeloid cells in cancer is mediated by reactive oxygen species. *J. Immunol. Baltim. Md 1950* **172**, 989–999 (2004).
237. Tartour, E. *et al.* Angiogenesis and immunity: a bidirectional link potentially relevant for the monitoring of antiangiogenic therapy and the development of novel

therapeutic combination with immunotherapy. *Cancer Metastasis Rev.* **30**, 83–95 (2011).

238. Horikawa, N. *et al.* Expression of Vascular Endothelial Growth Factor in Ovarian Cancer Inhibits Tumor Immunity through the Accumulation of Myeloid-Derived Suppressor Cells. *Clin. Cancer Res. Off. J. Am. Assoc. Cancer Res.* **23**, 587–599 (2017).
239. Yang, S., Liu, F., Wang, Q. J., Rosenberg, S. A. & Morgan, R. A. The shedding of CD62L (L-selectin) regulates the acquisition of lytic activity in human tumor reactive T lymphocytes. *PloS One* **6**, e22560 (2011).
240. Couzin-Frankel, J. Breakthrough of the year 2013. Cancer immunotherapy. *Science* **342**, 1432–1433 (2013).
241. Hodi, F. S. *et al.* Improved survival with ipilimumab in patients with metastatic melanoma. *N. Engl. J. Med.* **363**, 711–723 (2010).
242. Borghaei, H. *et al.* Nivolumab versus Docetaxel in Advanced Nonsquamous Non-Small-Cell Lung Cancer. *N. Engl. J. Med.* **373**, 1627–1639 (2015).
243. Brahmer, J. *et al.* Nivolumab versus Docetaxel in Advanced Squamous-Cell Non-Small-Cell Lung Cancer. *N. Engl. J. Med.* **373**, 123–135 (2015).
244. Robert, C. *et al.* Nivolumab in Previously Untreated Melanoma without BRAF Mutation. *N. Engl. J. Med.* **372**, 320–330 (2015).
245. Wei, S. C., Duffy, C. R. & Allison, J. P. Fundamental Mechanisms of Immune Checkpoint Blockade Therapy. *Cancer Discov.* **8**, 1069–1086 (2018).
246. Goodman, A., Patel, S. P. & Kurzrock, R. PD-1-PD-L1 immune-checkpoint blockade in B-cell lymphomas. *Nat. Rev. Clin. Oncol.* **14**, 203–220 (2017).
247. Zhang, Z. *et al.* T Cell Dysfunction and Exhaustion in Cancer. *Front. Cell Dev. Biol.* **8**, 17 (2020).
248. Dyck, L. & Mills, K. H. G. Immune checkpoints and their inhibition in cancer and infectious diseases. *Eur. J. Immunol.* **47**, 765–779 (2017).
249. Schadendorf, D. *et al.* Pooled Analysis of Long-Term Survival Data From Phase II and Phase III Trials of Ipilimumab in Unresectable or Metastatic Melanoma. *J. Clin. Oncol. Off. J. Am. Soc. Clin. Oncol.* **33**, 1889–1894 (2015).

250. Weber, J. *et al.* Adjuvant Nivolumab versus Ipilimumab in Resected Stage III or IV Melanoma. *N. Engl. J. Med.* **377**, 1824–1835 (2017).
251. Borella, F. *et al.* Immune Checkpoint Inhibitors in Epithelial Ovarian Cancer: An Overview on Efficacy and Future Perspectives. *Diagnostics* **10**, 146 (2020).
252. Zamarin, D. *et al.* Randomized Phase II Trial of Nivolumab Versus Nivolumab and Ipilimumab for Recurrent or Persistent Ovarian Cancer: An NRG Oncology Study. *J. Clin. Oncol. Off. J. Am. Soc. Clin. Oncol.* **38**, 1814–1823 (2020).
253. Verma, V. *et al.* PD-1 blockade in subprimed CD8 cells induces dysfunctional PD-1+CD38hi cells and anti-PD-1 resistance. *Nat. Immunol.* **20**, 1231–1243 (2019).
254. Sun, C., Mezzadra, R. & Schumacher, T. N. Regulation and Function of the PD-L1 Checkpoint. *Immunity* **48**, 434–452 (2018).
255. Hegde, P. S., Karanikas, V. & Evers, S. The Where, the When, and the How of Immune Monitoring for Cancer Immunotherapies in the Era of Checkpoint Inhibition. *Clin. Cancer Res. Off. J. Am. Assoc. Cancer Res.* **22**, 1865–1874 (2016).
256. Galon, J. & Bruni, D. Approaches to treat immune hot, altered and cold tumours with combination immunotherapies. *Nat. Rev. Drug Discov.* **18**, 197–218 (2019).
257. Hamanishi, J., Mandai, M. & Konishi, I. Immune checkpoint inhibition in ovarian cancer. *Int. Immunol.* **28**, 339–348 (2016).
258. Hamanishi, J. *et al.* Safety and Antitumor Activity of Anti-PD-1 Antibody, Nivolumab, in Patients With Platinum-Resistant Ovarian Cancer. *J. Clin. Oncol. Off. J. Am. Soc. Clin. Oncol.* **33**, 4015–4022 (2015).
259. Yahata, T. *et al.* Programmed cell death ligand 1 disruption by clustered regularly interspaced short palindromic repeats/Cas9-genome editing promotes antitumor immunity and suppresses ovarian cancer progression. *Cancer Sci.* **110**, 1279–1292 (2019).
260. Ghisoni, E., Imbimbo, M., Zimmermann, S. & Valabrega, G. Ovarian Cancer Immunotherapy: Turning up the Heat. *Int. J. Mol. Sci.* **20**, 2927 (2019).
261. Kelly, E. & Russell, S. J. History of Oncolytic Viruses: Genesis to Genetic Engineering. *Mol. Ther.* **15**, 651–659 (2007).
262. Pelner, L., Fowler, G. A. & Nauts, H. C. Effects of concurrent infections and their toxins on the course of leukemia. *Acta Med. Scand. Suppl.* **338**, 1–47 (1958).

263. Cao, G. *et al.* The Oncolytic Virus in Cancer Diagnosis and Treatment. *Front. Oncol.* **10**, 1786 (2020).
264. Russell, S. J., Peng, K.-W. & Bell, J. C. ONCOLYTIC VIROTHERAPY. *Nat. Biotechnol.* **30**, 658–670 (2012).
265. Davola, M. E. & Mossman, K. L. Oncolytic viruses: how "lytic" must they be for therapeutic efficacy? *Oncoimmunology* **8**, e1581528 (2019).
266. Kwan, A., Winder, N. & Muthana, M. Oncolytic Virotherapy Treatment of Breast Cancer: Barriers and Recent Advances. *Viruses* **13**, 1128 (2021).
267. Puzanov, I. *et al.* Talimogene Laherparepvec in Combination With Ipilimumab in Previously Untreated, Unresectable Stage IIIB-IV Melanoma. *J. Clin. Oncol. Off. J. Am. Soc. Clin. Oncol.* **34**, 2619–2626 (2016).
268. Matveeva, O. V. & Chumakov, P. M. Defects in interferon pathways as potential biomarkers of sensitivity to oncolytic viruses. *Rev. Med. Virol.* **28**, e2008 (2018).
269. Komatsu, Y. *et al.* Oncogenic Ras inhibits IRF1 to promote viral oncolysis. *Oncogene* **34**, 3985–3993 (2015).
270. Stojdl, D. F. *et al.* Exploiting tumor-specific defects in the interferon pathway with a previously unknown oncolytic virus. *Nat. Med.* **6**, 821–825 (2000).
271. McAllister, C. S., Taghavi, N. & Samuel, C. E. Protein Kinase PKR Amplification of Interferon β Induction Occurs through Initiation Factor eIF-2α-mediated Translational Control. *J. Biol. Chem.* **287**, 36384–36392 (2012).
272. Krysko, D. V. *et al.* Immunogenic cell death and DAMPs in cancer therapy. *Nat. Rev. Cancer* **12**, 860–875 (2012).
273. Garg, A. D. *et al.* Molecular and Translational Classifications of DAMPs in Immunogenic Cell Death. *Front. Immunol.* **6**, 588 (2015).
274. Krysko, D. V., D'Herde, K. & Vandenabeele, P. Clearance of apoptotic and necrotic cells and its immunological consequences. *Apoptosis Int. J. Program. Cell Death* **11**, 1709–1726 (2006).
275. Heinrich, B. *et al.* Immunogenicity of oncolytic vaccinia viruses JX-GFP and TG6002 in a human melanoma in vitro model: studying immunogenic cell death, dendritic cell maturation and interaction with cytotoxic T lymphocytes. *OncoTargets Ther.* **10**, 2389–2401 (2017).

276. Kepp, O. *et al.* Consensus guidelines for the detection of immunogenic cell death. *Oncoimmunology* **3**, e955691 (2014).
277. Zhang, Y., Li, Y., Chen, K., Qian, L. & Wang, P. Oncolytic virotherapy reverses the immunosuppressive tumor microenvironment and its potential in combination with immunotherapy. *Cancer Cell Int.* **21**, 262 (2021).
278. Twumasi-Boateng, K., Pettigrew, J. L., Kwok, Y. Y. E., Bell, J. C. & Nelson, B. H. Oncolytic viruses as engineering platforms for combination immunotherapy. *Nat. Rev. Cancer* **18**, 419–432 (2018).
279. Duan, Z. & Luo, Y. Targeting macrophages in cancer immunotherapy. *Signal Transduct. Target. Ther.* **6**, 1–21 (2021).
280. Zamarin, D. *et al.* PD-L1 in tumor microenvironment mediates resistance to oncolytic immunotherapy. *J. Clin. Invest.* **128**, 1413–1428 (2018).
281. Wang, G. *et al.* An engineered oncolytic virus expressing PD-L1 inhibitors activates tumor neoantigen-specific T cell responses. *Nat. Commun.* **11**, 1395 (2020).
282. Ribas, A. *et al.* Oncolytic Virotherapy Promotes Intratumoral T Cell Infiltration and Improves Anti-PD-1 Immunotherapy. *Cell* **170**, 110-1119.e10 (2017).
283. Kaufman, H. L. *et al.* Phase Ib study of intratumoral oncolytic coxsackievirus A21 (CVA21) and pembrolizumab in subjects with advanced melanoma. *Ann. Oncol.* **27**, vi400 (2016).
284. Silk, A. W. *et al.* Abstract CT026: Phase 1b study of intratumoral Coxsackievirus A21 (CVA21) and systemic pembrolizumab in advanced melanoma patients: Interim results of the CAPRA clinical trial. *Cancer Res.* **77**, CT026–CT026 (2017).
285. Barber, G. N. Vesicular stomatitis virus as an oncolytic vector. *Viral Immunol.* **17**, 516–527 (2004).
286. Rodríguez, L. L. Emergence and re-emergence of vesicular stomatitis in the United States. *Virus Res.* **85**, 211–219 (2002).
287. Martinez, I. & Wertz, G. W. Biological Differences between Vesicular Stomatitis Virus Indiana and New Jersey Serotype Glycoproteins: Identification of Amino Acid Residues Modulating pH-Dependent Infectivity. *J. Virol.* **79**, 3578–3585 (2005).

288. Hastie, E. & Grdzelishvili, V. Z. Vesicular stomatitis virus as a flexible platform for oncolytic virotherapy against cancer. *J. Gen. Virol.* **93**, 2529–2545 (2012).
289. Felt, S. A. & Grdzelishvili, V. Z. Recent advances in vesicular stomatitis virus-based oncolytic virotherapy: a 5-year update. *J. Gen. Virol.* **98**, 2895–2911 (2017).
290. Black, B. L. & Lyles, D. S. Vesicular stomatitis virus matrix protein inhibits host cell-directed transcription of target genes in vivo. *J. Virol.* **66**, 4058–4064 (1992).
291. Lichty, B. D., Power, A. T., Stojdl, D. F. & Bell, J. C. Vesicular stomatitis virus: re-inventing the bullet. *Trends Mol. Med.* **10**, 210–216 (2004).
292. Morin, B., Rahmeh, A. A. & Whelan, S. P. Mechanism of RNA synthesis initiation by the vesicular stomatitis virus polymerase. *EMBO J.* **31**, 1320–1329 (2012).
293. Ahmed, M. *et al.* Ability of the Matrix Protein of Vesicular Stomatitis Virus To Suppress Beta Interferon Gene Expression Is Genetically Correlated with the Inhibition of Host RNA and Protein Synthesis. *J. Virol.* **77**, 4646–4657 (2003).
294. Sun, X., Roth, S. L., Bialecki, M. A. & Whittaker, G. R. Internalization and fusion mechanism of vesicular stomatitis virus and related rhabdoviruses. *Future Virol.* **5**, 85–96 (2010).
295. Florkiewicz, R. Z. & Rose, J. K. A cell line expressing vesicular stomatitis virus glycoprotein fuses at low pH. *Science* **225**, 721–724 (1984).
296. Iverson, L. E. & Rose, J. K. Sequential synthesis of 5'-proximal vesicular stomatitis virus mRNA sequences. *J. Virol.* **44**, 356–365 (1982).
297. Rose, J. K. Complete intergenic and flanking gene sequences from the genome of vesicular stomatitis virus. *Cell* **19**, 415–421 (1980).
298. Iverson, L. E. & Rose, J. K. Localized attenuation and discontinuous synthesis during vesicular stomatitis virus transcription. *Cell* **23**, 477–484 (1981).
299. Barr, J. N., Tang, X., Hinzman, E., Shen, R. & Wertz, G. W. The VSV polymerase can initiate at mRNA start sites located either up or downstream of a transcription termination signal but size of the intervening intergenic region affects efficiency of initiation. *Virology* **374**, 361–370 (2008).
300. Banerjee, A. K. & Barik, S. Gene expression of vesicular stomatitis virus genome RNA. *Virology* **188**, 417–428 (1992).

301. Kim, I. S. *et al.* Mechanism of membrane fusion induced by vesicular stomatitis virus G protein. *Proc. Natl. Acad. Sci.* **114**, E28–E36 (2017).
302. Balachandran, S. & Barber, G. N. Vesicular Stomatitis Virus (VSV) Therapy of Tumors. *IUBMB Life* **50**, 135–138 (2000).
303. Kramer, M. J. *et al.* Cell and virus sensitivity studies with recombinant human alpha interferons. *J. Interferon Res.* **3**, 425–435 (1983).
304. Rieder, M. & Conzelmann, K.-K. Rhabdovirus evasion of the interferon system. *J. Interferon Cytokine Res. Off. J. Int. Soc. Interferon Cytokine Res.* **29**, 499–509 (2009).
305. von Kobbe C, null *et al.* Vesicular stomatitis virus matrix protein inhibits host cell gene expression by targeting the nucleoporin Nup98. *Mol. Cell* **6**, 1243–1252 (2000).
306. Ahmed, M. & Lyles, D. S. Effect of Vesicular Stomatitis Virus Matrix Protein on Transcription Directed by Host RNA Polymerases I, II, and III. *J. Virol.* **72**, 8413–8419 (1998).
307. Weck, P. K. & Wagner, R. R. Vesicular stomatitis virus infection reduces the number of active DNA-dependent RNA polymerases in myeloma cells. *J. Biol. Chem.* **254**, 5430–5434 (1979).
308. Kopecky, S. A., Willingham, M. C. & Lyles, D. S. Matrix protein and another viral component contribute to induction of apoptosis in cells infected with vesicular stomatitis virus. *J. Virol.* **75**, 12169–12181 (2001).
309. Plakhov, I. V., Arlund, E. E., Aoki, C. & Reiss, C. S. The earliest events in vesicular stomatitis virus infection of the murine olfactory neuroepithelium and entry of the central nervous system. *Virology* **209**, 257–262 (1995).
310. Schellekens, H., Smiers-de Vreede, E., de Reus, A. & Dijkema, R. Antiviral activity of interferon in rats and the effect of immune suppression. *J. Gen. Virol.* **65 (Pt 2)**, 391–396 (1984).
311. Johnson, J. E. *et al.* Neurovirulence properties of recombinant vesicular stomatitis virus vectors in non-human primates. *Virology* **360**, 36–49 (2007).
312. Stojdl, D. F. *et al.* VSV strains with defects in their ability to shutdown innate immunity are potent systemic anti-cancer agents. *Cancer Cell* **4**, 263–275 (2003).

313. K B Stephenson, N G Barra, E Davies, A A Ashkar, & B D Lichty. Expressing human interleukin-15 from oncolytic vesicular stomatitis virus improves survival in a murine metastatic colon adenocarcinoma model through the enhancement of anti-tumor immunity. *Cancer Gene Ther.* **19**, 238–246 (2012).
314. Le Boeuf, F. *et al.* Reovirus FAST Protein Enhances Vesicular Stomatitis Virus Oncolytic Virotherapy in Primary and Metastatic Tumor Models. *Mol. Ther. - Oncolytics* **6**, 80–89 (2017).
315. Tugues, S. *et al.* New insights into IL-12-mediated tumor suppression. *Cell Death Differ.* **22**, 237–246 (2015).
316. Taniguchi, M., Seino, K. & Nakayama, T. The NKT cell system: bridging innate and acquired immunity. *Nat. Immunol.* **4**, 1164–1165 (2003).
317. Gubler, U. *et al.* Coexpression of two distinct genes is required to generate secreted bioactive cytotoxic lymphocyte maturation factor. *Proc. Natl. Acad. Sci. U. S. A.* **88**, 4143–4147 (1991).
318. Trinchieri, G. *et al.* Producer cells of interleukin 12. *Parasitol. Today Pers. Ed* **9**, 97 (1993).
319. Aste-Amezaga, M., D'Andrea, A., Kubin, M. & Trinchieri, G. Cooperation of natural killer cell stimulatory factor/interleukin-12 with other stimuli in the induction of cytokines and cytotoxic cell-associated molecules in human T and NK cells. *Cell. Immunol.* **156**, 480–492 (1994).
320. Bacon, C. M. *et al.* Interleukin 12 (IL-12) induces tyrosine phosphorylation of JAK2 and TYK2: differential use of Janus family tyrosine kinases by IL-2 and IL-12. *J. Exp. Med.* **181**, 399–404 (1995).
321. Bacon, C. M. *et al.* Interleukin 12 induces tyrosine phosphorylation and activation of STAT4 in human lymphocytes. *Proc. Natl. Acad. Sci. U. S. A.* **92**, 7307–7311 (1995).
322. Perussia, B. *et al.* Natural killer (NK) cell stimulatory factor or IL-12 has differential effects on the proliferation of TCR-alpha beta+, TCR-gamma delta+ T lymphocytes, and NK cells. *J. Immunol. Baltim. Md 1950* **149**, 3495–3502 (1992).

323. Manetti, R. *et al.* Natural killer cell stimulatory factor (interleukin 12 [IL-12]) induces T helper type 1 (Th1)-specific immune responses and inhibits the development of IL-4-producing Th cells. *J. Exp. Med.* **177**, 1199–1204 (1993).
324. Micallef, M. J. *et al.* Interferon-gamma-inducing factor enhances T helper 1 cytokine production by stimulated human T cells: synergism with interleukin-12 for interferon-gamma production. *Eur. J. Immunol.* **26**, 1647–1651 (1996).
325. Watkins, S. K., Egilmez, N. K., Suttles, J. & Stout, R. D. IL-12 rapidly alters the functional profile of tumor-associated and tumor-infiltrating macrophages in vitro and in vivo. *J. Immunol. Baltim. Md 1950* **178**, 1357–1362 (2007).
326. Steding, C. E. *et al.* The role of interleukin-12 on modulating myeloid-derived suppressor cells, increasing overall survival and reducing metastasis. *Immunology* **133**, 221–238 (2011).
327. Zhao, J., Zhao, J. & Perlman, S. Differential effects of IL-12 on Tregs and non-Treg T cells: roles of IFN-γ, IL-2 and IL-2R. *PloS One* **7**, e46241 (2012).
328. Voest, E. E. *et al.* Inhibition of angiogenesis in vivo by interleukin 12. *J. Natl. Cancer Inst.* **87**, 581–586 (1995).
329. Tannenbaum, C. S. *et al.* The CXC chemokines IP-10 and Mig are necessary for IL-12-mediated regression of the mouse RENCA tumor. *J. Immunol. Baltim. Md 1950* **161**, 927–932 (1998).
330. Mitola, S., Strasly, M., Prato, M., Ghia, P. & Bussolino, F. IL-12 Regulates an Endothelial Cell-Lymphocyte Network: Effect on Metalloproteinase-9 Production. *J. Immunol.* **171**, 3725–3733 (2003).
331. Berraondo, P., Etxeberria, I., Ponz-Sarvise, M. & Melero, I. Revisiting Interleukin-12 as a Cancer Immunotherapy Agent. *Clin. Cancer Res.* **24**, 2716–2718 (2018).
332. Boehm, U., Klamp, T., Groot, M. & Howard, J. C. Cellular responses to interferon-gamma. *Annu. Rev. Immunol.* **15**, 749–795 (1997).
333. Kanegane, C. *et al.* Contribution of the CXC chemokines IP-10 and Mig to the antitumor effects of IL-12. *J. Leukoc. Biol.* **64**, 384–392 (1998).
334. Dias, S., Boyd, R. & Balkwill, F. IL-12 regulates VEGF and MMPs in a murine breast cancer model. *Int. J. Cancer* **78**, 361–365 (1998).

335. Kim, C. G. *et al.* VEGF-A drives TOX-dependent T cell exhaustion in anti-PD-1-resistant microsatellite stable colorectal cancers. *Sci. Immunol.* **4**, eaay0555 (2019).
336. Lee, W. S., Yang, H., Chon, H. J. & Kim, C. Combination of anti-angiogenic therapy and immune checkpoint blockade normalizes vascular-immune crosstalk to potentiate cancer immunity. *Exp. Mol. Med.* **52**, 1475–1485 (2020).
337. Oyama, T. *et al.* Vascular endothelial growth factor affects dendritic cell maturation through the inhibition of nuclear factor-kappa B activation in hemopoietic progenitor cells. *J. Immunol. Baltim. Md 1950* **160**, 1224–1232 (1998).
338. Grohmann, U. *et al.* Positive regulatory role of IL-12 in macrophages and modulation by IFN-gamma. *J. Immunol. Baltim. Md 1950* **167**, 221–227 (2001).
339. Leonard, J. P. *et al.* Effects of single-dose interleukin-12 exposure on interleukin-12-associated toxicity and interferon-gamma production. *Blood* **90**, 2541–2548 (1997).
340. Lasek, W., Zagożdżon, R. & Jakobisiak, M. Interleukin 12: still a promising candidate for tumor immunotherapy? *Cancer Immunol. Immunother.* **63**, 419–435 (2014).
341. Atkins, M. B. *et al.* Phase I evaluation of intravenous recombinant human interleukin 12 in patients with advanced malignancies. *Clin. Cancer Res. Off. J. Am. Assoc. Cancer Res.* **3**, 409–417 (1997).
342. Nguyen, K. G. *et al.* Localized Interleukin-12 for Cancer Immunotherapy. *Front. Immunol.* **11**, 2510 (2020).
343. Portielje, J. E. A. *et al.* Repeated administrations of interleukin (IL)-12 are associated with persistently elevated plasma levels of IL-10 and declining IFN-gamma, tumor necrosis factor-alpha, IL-6, and IL-8 responses. *Clin. Cancer Res. Off. J. Am. Assoc. Cancer Res.* **9**, 76–83 (2003).
344. Ansell, S. M. *et al.* Phase 1 study of interleukin-12 in combination with rituximab in patients with B-cell non-Hodgkin lymphoma. *Blood* **99**, 67–74 (2002).
345. Mahvi, D. M. *et al.* Intratumoral injection of IL-12 plasmid DNA – results of a phase I/IB clinical trial. *Cancer Gene Ther.* **14**, 717–723 (2007).

346. Heinzerling, L. *et al.* Intratumoral injection of DNA encoding human interleukin 12 into patients with metastatic melanoma: clinical efficacy. *Hum. Gene Ther.* **16**, 35–48 (2005).
347. Zhang, L. *et al.* Tumor-infiltrating lymphocytes genetically engineered with an inducible gene encoding interleukin-12 for the immunotherapy of metastatic melanoma. *Clin. Cancer Res. Off. J. Am. Assoc. Cancer Res.* **21**, 2278–2288 (2015).
348. Nguyen, H.-M., Guz-Montgomery, K. & Saha, D. Oncolytic Virus Encoding a Master Pro-Inflammatory Cytokine Interleukin 12 in Cancer Immunotherapy. *Cells* **9**, E400 (2020).
349. Omar, N. B. *et al.* Safety and interim survival data after intracranial administration of M032, a genetically engineered oncolytic HSV-1 expressing IL-12, in pet dogs with sporadic gliomas. *Neurosurg. Focus* **50**, E5 (2021).
350. MD, J. M. *A Phase 1 Study of M032 (NSC 733972), a Genetically Engineered HSV-1 Expressing IL-12, in Patients With Recurrent/Progressive Glioblastoma Multiforme, Anaplastic Astrocytoma, or Gliosarcoma*. https://clinicaltrials.gov/ct2/show/NCT02062827 (2022).
351. Pengju Wang *et al.* Re-designing interleukin-12 to enhance its safety and potential as an anti-tumor immunotherapeutic agent. *Nat. Commun.* **8**, 1–15 (2017).
352. Choi, I.-K. *et al.* Oncolytic adenovirus co-expressing IL-12 and IL-18 improves tumor-specific immunity via differentiation of T cells expressing IL-12Rβ2 or IL-18Rα. *Gene Ther.* **18**, 898–909 (2011).
353. Sung, M. *Phase I Trial of Adenoviral Vector Delivery of the Human Interleukin-12 cDNA by Intratumoral Injection in Patents With Metastatic Breast Cancer*. https://clinicaltrials.gov/ct2/show/NCT00849459 (2017).
354. MD, D. K. *PHASE 1 TRIAL OF ONCOLYTIC ADENOVIRUS-MEDIATED CYTOTOXIC AND IL-12 GENE THERAPY IN COMBINATION WITH CHEMOTHERAPY FOR THE TREATMENT OF METASTATIC PANCREATIC CANCER*. https://clinicaltrials.gov/ct2/show/NCT03281382 (2022).
355. Steel, J. C., Waldmann, T. A. & Morris, J. C. Interleukin-15 biology and its therapeutic implications in cancer. *Trends Pharmacol. Sci.* **33**, 35–41 (2012).

356. Budagian, V., Bulanova, E., Paus, R. & Bulfone-Paus, S. IL-15/IL-15 receptor biology: A guided tour through an expanding universe. *Cytokine Growth Factor Rev.* **17**, 259–280 (2006).
357. Gordy, L. E. *et al.* IL-15 regulates homeostasis and terminal maturation of NKT cells. *J. Immunol. Baltim. Md 1950* **187**, 6335–6345 (2011).
358. Waldmann, T. A. & Tagaya, Y. The multifaceted regulation of interleukin-15 expression and the role of this cytokine in NK cell differentiation and host response to intracellular pathogens. *Annu. Rev. Immunol.* **17**, 19–49 (1999).
359. Armitage, R. J., Macduff, B. M., Eisenman, J., Paxton, R. & Grabstein, K. H. IL-15 has stimulatory activity for the induction of B cell proliferation and differentiation. *J. Immunol. Baltim. Md 1950* **154**, 483–490 (1995).
360. Kim, P. S. *et al.* IL-15 superagonist/IL-15RαSushi-Fc fusion complex (IL-15SA/IL-15RαSu-Fc; ALT-803) markedly enhances specific subpopulations of NK and memory CD8+ T cells, and mediates potent anti-tumor activity against murine breast and colon carcinomas. *Oncotarget* **7**, 16130–16145 (2016).
361. Zhang, X., Sun, S., Hwang, I., Tough, D. F. & Sprent, J. Potent and selective stimulation of memory-phenotype CD8+ T cells in vivo by IL-15. *Immunity* **8**, 591–599 (1998).
362. Waldmann, T. A. *et al.* Safety (toxicity), pharmacokinetics, immunogenicity, and impact on elements of the normal immune system of recombinant human IL-15 in rhesus macaques. *Blood* **117**, 4787–4795 (2011).
363. Robinson, T. O. & Schluns, K. S. The potential and promise of IL-15 in immuno-oncogenic therapies. *Immunol. Lett.* **190**, 159–168 (2017).
364. Waldmann, T. A. Interleukin-15 in the treatment of cancer. *Expert Rev. Clin. Immunol.* **10**, 1689–1701 (2014).
365. Isvoranu, G. *et al.* Therapeutic potential of interleukin-15 in cancer (Review). *Exp. Ther. Med.* **22**, 1–6 (2021).
366. Stephenson, K. B., Barra, N. G., Davies, E., Ashkar, A. A. & Lichty, B. D. Expressing human interleukin-15 from oncolytic vesicular stomatitis virus improves survival in a murine metastatic colon adenocarcinoma model through the enhancement of anti-tumor immunity. *Cancer Gene Ther.* **19**, 238–246 (2012).

367. Corcoran, J. A. & Duncan, R. Reptilian reovirus utilizes a small type III protein with an external myristylated amino terminus to mediate cell-cell fusion. *J. Virol.* **78**, 4342–4351 (2004).
368. Brown, C. W. *et al.* The p14 FAST Protein of Reptilian Reovirus Increases Vesicular Stomatitis Virus Neuropathogenesis. *J. Virol.* **83**, 552–561 (2009).
369. Krabbe, T. & Altomonte, J. Fusogenic Viruses in Oncolytic Immunotherapy. *Cancers* **10**, 216 (2018).
370. Ebert, O. *et al.* Syncytia induction enhances the oncolytic potential of vesicular stomatitis virus in virotherapy for cancer. *Cancer Res.* **64**, 3265–3270 (2004).
371. Shin, E. J. *et al.* Fusogenic vesicular stomatitis virus for the treatment of head and neck squamous carcinomas. *Otolaryngol.--Head Neck Surg. Off. J. Am. Acad. Otolaryngol.-Head Neck Surg.* **136**, 811–817 (2007).
372. Lawson, N. D., Stillman, E. A., Whitt, M. A. & Rose, J. K. Recombinant vesicular stomatitis viruses from DNA. *Proc. Natl. Acad. Sci. U. S. A.* **92**, 4477–4481 (1995).
373. Gosavi, R. A. *et al.* Optimization of Ex Vivo Murine Bone Marrow Derived Immature Dendritic Cells: A Comparative Analysis of Flask Culture Method and Mouse CD11c Positive Selection Kit Method. *Bone Marrow Res.* **2018**, 3495086 (2018).
374. Gebremeskel, S. DEVELOPING NATURAL KILLER T CELL BASED TOOLS AND STRATEGIES FOR TARGETING BREAST CANCER. 213.
375. Collin, M. & Bigley, V. Human dendritic cell subsets: an update. *Immunology* **154**, 3–20 (2018).
376. Breitbach, C. J. *et al.* Targeted Inflammation During Oncolytic Virus Therapy Severely Compromises Tumor Blood Flow. *Mol. Ther.* **15**, 1686–1693 (2007).
377. O'Connor, M. A., Rastad, J. L. & Green, W. R. The Role of Myeloid-Derived Suppressor Cells in Viral Infection. *Viral Immunol.* **30**, 82–97 (2017).
378. Fischer, M. A. *et al.* CD11b+, Ly6G+ Cells Produce Type I Interferon and Exhibit Tissue Protective Properties Following Peripheral Virus Infection. *PLOS Pathog.* **7**, e1002374 (2011).
379. Nelson, A., Gebremeskel, S., Lichty, B. D. & Johnston, B. Natural killer T cell immunotherapy combined with IL-15-expressing oncolytic virotherapy and PD-1

blockade mediates pancreatic tumor regression. *J. Immunother. Cancer* **10**, e003923 (2022).

380. Yang, Y. *et al.* The Antiviral and Antitumor Effects of Defective Interfering Particles/Genomes and Their Mechanisms. *Front. Microbiol.* **10**, (2019).
381. Willmon, C. L. *et al.* Expression of IFN-beta enhances both efficacy and safety of oncolytic vesicular stomatitis virus for therapy of mesothelioma. *Cancer Res.* **69**, 7713–7720 (2009).
382. Patel, M. R. *et al.* Vesicular stomatitis virus expressing interferon-β is oncolytic and promotes antitumor immune responses in a syngeneic murine model of non-small cell lung cancer. *Oncotarget* **6**, (2015).
383. Miller, J. M., Bidula, S. M., Jensen, T. M. & Reiss, C. S. Vesicular stomatitis virus modified with single chain IL-23 exhibits oncolytic activity against tumor cells in vitro and in vivo. *Int. J. Interferon Cytokine Mediat. Res.* **2010**, 63–72 (2010).
384. Kielbik, M., Szulc-Kielbik, I. & Klink, M. Calreticulin—Multifunctional Chaperone in Immunogenic Cell Death: Potential Significance as a Prognostic Biomarker in Ovarian Cancer Patients. *Cells* **10**, 130 (2021).
385. Steinhauer, D. A., Domingo, E. & Holland, J. J. Lack of evidence for proofreading mechanisms associated with an RNA virus polymerase. *Gene* **122**, 281–288 (1992).
386. Zainutdinov, S. S., Kochneva, G. V., Netesov, S. V., Chumakov, P. M. & Matveeva, O. V. Directed evolution as a tool for the selection of oncolytic RNA viruses with desired phenotypes. *Oncolytic Virotherapy* **8**, 9–26 (2019).
387. Seegers, S. L., Frasier, C., Greene, S., Nesmelova, I. V. & Grdzelishvili, V. Z. Experimental Evolution Generates Novel Oncolytic Vesicular Stomatitis Viruses with Improved Replication in Virus-Resistant Pancreatic Cancer Cells. *J. Virol.* **94**, e01643-19 (2020).
388. Lu, L. *et al.* Combined PD-1 blockade and GITR triggering induce a potent antitumor immunity in murine cancer models and synergizes with chemotherapeutic drugs. *J. Transl. Med.* **12**, 36 (2014).
389. Guo, Z. *et al.* PD-1 Blockade and OX40 Triggering Synergistically Protects against Tumor Growth in a Murine Model of Ovarian Cancer. *PLOS ONE* **9**, e89350 (2014).

390. Linch, S. N., McNamara, M. J. & Redmond, W. L. OX40 Agonists and Combination Immunotherapy: Putting the Pedal to the Metal. *Front. Oncol.* **5**, (2015).
391. Harrington, K., Freeman, D. J., Kelly, B., Harper, J. & Soria, J.-C. Optimizing oncolytic virotherapy in cancer treatment. *Nat. Rev. Drug Discov.* **18**, 689–706 (2019).
392. Ishii, K. *et al.* A combination of check-point blockade and α-galactosylceramide elicits long-lasting suppressive effects on murine hepatoma cell growth in vivo. *Immunobiology* **225**, 151860 (2020).
393. Wang, Y., Bhave, M. S., Yagita, H. & Cardell, S. L. Natural Killer T-Cell Agonist α-Galactosylceramide and PD-1 Blockade Synergize to Reduce Tumor Development in a Preclinical Model of Colon Cancer. *Front. Immunol.* **11**, (2020).
394. Leveille, S., Goulet, M.-L., Lichty, B. D. & Hiscott, J. Vesicular Stomatitis Virus Oncolytic Treatment Interferes with Tumor-Associated Dendritic Cell Functions and Abrogates Tumor Antigen Presentation ▿ . *J. Virol.* **85**, 12160–12169 (2011).
395. Boudreau, J. E. *et al.* Recombinant Vesicular Stomatitis Virus Transduction of Dendritic Cells Enhances Their Ability to Prime Innate and Adaptive Antitumor Immunity. *Mol. Ther. J. Am. Soc. Gene Ther.* **17**, 1465–1472 (2009).
396. Kumar, V., Giacomantonio, M. A. & Gujar, S. Role of Myeloid Cells in Oncolytic Reovirus-Based Cancer Therapy. *Viruses* **13**, 654 (2021).
397. Polzin, M. *et al.* Oncolytic vesicular stomatitis viruses selectively target M2 macrophages. *Virus Res.* **284**, 197991 (2020).
398. Giacomantonio, M. A. *et al.* Quantitative Proteome Responses to Oncolytic Reovirus in GM-CSF-and M-CSF-Differentiated Bone Marrow-Derived Cells. *J. Proteome Res.* **19**, 708–718 (2020).
399. Fridlender, Z. G. *et al.* Polarization of Tumor-Associated Neutrophil (TAN) Phenotype by TGF-β: "N1" versus "N2" TAN. *Cancer Cell* **16**, 183–194 (2009).
400. Mealiea, D. & McCart, J. A. Cutting both ways: the innate immune response to oncolytic virotherapy. *Cancer Gene Ther.* 1–18 (2021) doi:10.1038/s41417-021-00351-3.

401. Galivo, F. *et al.* Single-cycle viral gene expression, rather than progressive replication and oncolysis, is required for VSV therapy of B16 melanoma. *Gene Ther.* **17**, 158–170 (2010).
402. De Santo, C. *et al.* Invariant NKT cells reduce the immunosuppressive activity of influenza A virus-induced myeloid-derived suppressor cells in mice and humans. *J. Clin. Invest.* **118**, 4036–4048 (2008).
403. Thomas, E. D. *et al.* IL-12 Expressing oncolytic herpes simplex virus promotes anti-tumor activity and immunologic control of metastatic ovarian cancer in mice. *J. Ovarian Res.* **9**, 70 (2016).
404. Tseng, J.-C. *et al.* Systemic tumor targeting and killing by Sindbis viral vectors. *Nat. Biotechnol.* **22**, 70–77 (2004).
405. Buonocore, L., Blight, K. J., Rice, C. M. & Rose, J. K. Characterization of Vesicular Stomatitis Virus Recombinants That Express and Incorporate High Levels of Hepatitis C Virus Glycoproteins. *J. Virol.* **76**, 6865–6872 (2002).
406. Bourgeois-Daigneault, M.-C. *et al.* Oncolytic vesicular stomatitis virus expressing interferon-γ has enhanced therapeutic activity. *Mol. Ther. Oncolytics* **3**, 16001 (2016).
407. Kottke, T. *et al.* Oncolytic virotherapy induced CSDE1 neo-antigenesis restricts VSV replication but can be targeted by immunotherapy. *Nat. Commun.* **12**, 1930 (2021).
408. Alkayyal, A. A. *et al.* NK-Cell Recruitment Is Necessary for Eradication of Peritoneal Carcinomatosis with an IL12-Expressing Maraba Virus Cellular Vaccine. *Cancer Immunol. Res.* **5**, 211–221 (2017).
409. Lieschke, G. J., Rao, P. K., Gately, M. K. & Mulligan, R. C. Bioactive murine and human interleukin-12 fusion proteins which retain antitumor activity in vivo. *Nat. Biotechnol.* **15**, 35–40 (1997).
410. Marelli, G., Howells, A., Lemoine, N. R. & Wang, Y. Oncolytic Viral Therapy and the Immune System: A Double-Edged Sword Against Cancer. *Front. Immunol.* **9**, 866 (2018).
411. Burton, C., Bartee, M. Y. & Bartee, E. Impact of Induced Syncytia Formation on the Oncolytic Potential of Myxoma Virus. *Oncolytic Virotherapy* **8**, 57–69 (2019).

412. Wong, C. M. *et al.* Expression of the fusogenic p14 FAST protein from a replication-defective adenovirus vector does not provide a therapeutic benefit in an immunocompetent mouse model of cancer. *Cancer Gene Ther.* **23**, 355–364 (2016).
413. Jin, K.-T. *et al.* Oncolytic Virotherapy in Solid Tumors: The Challenges and Achievements. *Cancers* **13**, 588 (2021).
414. Byrne-Hoffman, C. N. *et al.* Interleukin-12 elicits a non-canonical response in B16 melanoma cells to enhance survival. *Cell Commun. Signal. CCS* **18**, 78 (2020).
415. Oh, E., Choi, I.-K., Hong, J. & Yun, C.-O. Oncolytic adenovirus coexpressing interleukin-12 and decorin overcomes Treg-mediated immunosuppression inducing potent antitumor effects in a weakly immunogenic tumor model. *Oncotarget* **8**, 4730–4746 (2016).
416. Chikkanna-Gowda, C. P., Sheahan, B. J., Fleeton, M. N. & Atkins, G. J. Regression of mouse tumours and inhibition of metastases following administration of a Semliki Forest virus vector with enhanced expression of IL-12. *Gene Ther.* **12**, 1253–1263 (2005).
417. Jiang, T., Zhou, C. & Ren, S. Role of IL-2 in cancer immunotherapy. *Oncoimmunology* **5**, e1163462 (2016).
418. Quixabeira, D. C. A. *et al.* Oncolytic Adenovirus Coding for a Variant Interleukin 2 (vIL-2) Cytokine Re-Programs the Tumor Microenvironment and Confers Enhanced Tumor Control. *Front. Immunol.* **12**, (2021).
419. Ptacin, J. L. *et al.* An engineered IL-2 reprogrammed for anti-tumor therapy using a semi-synthetic organism. *Nat. Commun.* **12**, 4785 (2021).
420. Hamanishi, J., Mandai, M. & Konishi, I. Immune checkpoint inhibition in ovarian cancer. *Int. Immunol.* **28**, 339–348 (2016).
421. Park, J., Lee, J.-Y. & Kim, S. How to use immune checkpoint inhibitor in ovarian cancer? *J. Gynecol. Oncol.* **30**, (2019).
422. Chen, C.-Y., Hutzen, B., Wedekind, M. F. & Cripe, T. P. Oncolytic virus and PD-1/PD-L1 blockade combination therapy. *Oncolytic Virotherapy* **7**, 65–77 (2018).
423. Kowalsky, S. J. *et al.* Superagonist IL-15-Armed Oncolytic Virus Elicits Potent Antitumor Immunity and Therapy That Are Enhanced with PD-1 Blockade. *Mol. Ther.* **26**, 2476–2486 (2018).

424. Shi, G. *et al.* Oncolytic adenovirus inhibits malignant ascites of advanced ovarian cancer by reprogramming the ascitic immune microenvironment. *Mol. Ther. Oncolytics* **23**, 488–500 (2021).
425. Wellenstein, M. D. & de Visser, K. E. Cancer-Cell-Intrinsic Mechanisms Shaping the Tumor Immune Landscape. *Immunity* **48**, 399–416 (2018).
426. Gibney, G. T., Weiner, L. M. & Atkins, M. B. Predictive biomarkers for checkpoint inhibitor-based immunotherapy. *Lancet Oncol.* **17**, e542–e551 (2016).
427. Hugo, W. *et al.* Genomic and Transcriptomic Features of Response to Anti-PD-1 Therapy in Metastatic Melanoma. *Cell* **165**, 35–44 (2016).
428. Harel, M. *et al.* Proteomics of Melanoma Response to Immunotherapy Reveals Mitochondrial Dependence. *Cell* **179**, 236-250.e18 (2019).
429. Wang, J. *et al.* Proteome Profiling Outperforms Transcriptome Profiling for Coexpression Based Gene Function Prediction. *Mol. Cell. Proteomics MCP* **16**, 121–134 (2017).